Characterising the Quaternary stratigraphy of the paleovalley underlying Dunedin and Otago Harbour

Oliver W. Rees

A thesis submitted for the degree of

Master of Science

at the University of Otago, Dunedin,

New Zealand.

March 31st, 2020

Abstract

Beneath the surface of the low-lying densely populated suburbs of Dunedin and the adjacent Otago Harbour is an extensive record of past sea level change over the Quaternary. Prior research into the Quaternary stratigraphy of Dunedin and Otago Harbour is limited with only recent work including seismic lines collected in the harbour and gravity measurements and modelling only being completed in recent years. In this investigation, I use a combination of seismic and sedimentological techniques to identify and constrain paleo sea levels within the subsurface geology of Dunedin and Otago Harbour. This research aims to build a better understanding of near coast highstand environments in this uniquely preserved setting and using this knowledge to better understand the effects of future sea level rise.

Seismic imaging of sediments within Otago Harbour was used to track sea level highstand sedimentary units throughout the subsurface, identified by contrasts in the physical properties of the sediment, causing strong visible reflections. 42 seismic lines were collected in the harbour adjacent to Port Chalmers, imaging to a maximum of 140 m. The seismic images were used to propose and track representative sedimentary horizons, allowing comparison with the CE17/0106 sediment core which reached a depth of 20.7 m collected as part of the New Zealand SeaRise programme in early 2019 and from the Edgar Centre which reached a depth of 45.5 m in South Dunedin in 2016. This work maps five distinct horizontal sedimentary reflections observed within the paleovalley sediments, that coincide with observed changes in lithology within both the CE17/0106 and Edgar Centre cores. Elemental ratios such as Ca/Ti and Br/Inc produced from XRF measurements from core CE17/0106 are used to infer changes in the depositional environment as well as provenance. Radiocarbon ages from the CE17/0106 core provide an age model for the upper 12.4 m constraining it to the last 9 ka. The dated sediments can be tied to the shallowest horizon observed within the seismic record with similarities in the sediments between the CE17/0106 and Edgar Centre Cores.

Below the horizon recovered in core CE17/0106, several more distinctive horizontal sedimentary reflections were observed. These horizons were deposited during sea level highstand events, infilled from the initial erosion of the paleovalley. These horizons lack any signs of past tectonics; however, the deeper horizons show evidence of erosion between highstands, cutting channels through the Quaternary sediments.

Acknowledgements

I would like to thank my supervisors Andrew Gorman and Christina Riesselman for all the direction, advice and help over the last two years.

I would like to thank Phil Glassey and Simon Cox of GNS Science and Ben Mackey and Sharon Hornblow from the Otago Regional Council for including me in the core collection process as well as their ongoing support in analysing the core.

Many thanks to Chris Moy, Bob Dagg, Hamish Bowman, Gemma Kerr, Stephen Read, Julie Clark, Steve Little and Sean Heseltine for all the technical expertise and guidance throughout the project.

I would like to thank Otago Regional Council, OceanaGold, the MBIE-funded NZ SeaRise programme, the Dunedin City Council, GNS Science, and the University of Otago for funding the 2019 seismic survey, core collection and analysis and McNeill Drilling for collecting the cores.

Finally, a massive thanks to my parents Steve and Julie for their ongoing support throughout the last five years.

Table of contents

List of Figures

Chapter 1 Introduction

Chapter 2 Regional geology

Chapter 3 Methods

Chapter 4 Observations and initial interpretations

Chapter 5 Discussion

List of Tables

Chapter 3 Methods

Chapter 4 Observations and initial interpretations

Chapter 1 Introduction

As more attention is being drawn to climate change and natural hazards, the scientific community is increasingly interested in investigating the impact of these on our everyday lives. Research into the nature of the Quaternary sediments that make up much of the subsurface geology of housing and industrial real estate in Dunedin is becoming an increasing priority as local government agencies like the Otago Regional Council (ORC) and the Dunedin City Council (DCC) work to identify and mitigate hazards and future changes. Natural harbours like Otago Harbour and coastal settings like those found in South Dunedin are constantly being altered by environmental processes, being reshaped at a range of timescales from daily to geological. Otago Harbour formed as a result of erosion of the Miocene age Dunedin Volcano forming an extensive valley, which was subsequently infilled as a result of successive marine transgression (Fletcher, 2016; Glassey et al., 2003). An unusual aspect of Otago Harbour is that sediments are primarily sourced through longshore drift along the continental shelf from the south or from biogenic processes, with only a fraction of sediments delivered from the surrounding volcanic material (Glassey et al., 2003; Rees, 2018). As the sediments of Dunedin and the harbour can be attributed primarily to marine processes and less from proximal terrigenous sources/local erosion, the sediments provide a significant record of marine transgressions. Due to the dynamic nature of harbour systems, understanding the processes governing harbour infill as well as those currently acting on it is increasingly useful in predicting how these processes are likely to change in the future. The surface geology of Dunedin has been well documented for years; however, the variability of the Quaternary sediments of the harbour and Dunedin and their association with the underlying sediment stratigraphy are only now being investigated.

This thesis presents seismic data that were collected in the outer harbour to create cross-sectional images of the subsurface from the harbour floor to the basement of the eroded paleovalley. Data were collected by towing a controlled sound source known as a boomer (operating between 100-1000 Hz) and sound receivers known as a streamer behind a vessel along transects through the harbour. Reflections of the sound returning from features in the subsurface were recorded and used to construct composite images

of reflective features in the subsurface. Seismic imaging was used as a cost-effective method to provide coverage across a large area of the harbour in a way that drilling could not achieve. The variability of sediments in the harbour, as well as their modification from dredging, heavily impacted the quality and penetration of the data recovered. Unconsolidated sediments can absorb sounds differently and, in some instances, stop it completely from being transmitted, leading to acoustic wipeout where the sound waves have dissipated. The regular dredging of Otago Harbour to allow larger commercial ships to enter alters only a small portion of the harbour's sediments; however, the dredged channels, as well as shallow bathymetry in general, can have a significant influence in the quality of the seismic data. Reverberations within the channel walls as well as between the seafloor and the water's surface can create reverberating noise that can influence the quality of the images produced. Due to the harbour's shallow bathymetry, a small recreationally sized vessel (R/V *Tuhura*) was required to navigate the mudflats and sand bars.

Land-based drilling of the sediments of Dunedin has been used to add a geological context to the geophysical records. Drilling was undertaken in Dunedin in May of 2019 as part of the NZ SeaRise Programme, aimed at reconstructing the effects of past sea level changes to the sediments of South Dunedin. The sediments observed in the core can be used to ground-truth strong reflections observed in the seismic data, allowing the observations in the sediment stratigraphy to be inferred throughout the sediments of the harbour.

1.1 Location

The city of Dunedin, the centre of this research is located on the east coast of the South Island of New Zealand at -45.874°S 170.503°E. The research area of this project can be split into three distinct locations (Figure 1.1). The seismic data were collected in the outer basin of Otago Harbour, adjacent to Port Chalmers and Portobello in the southwest and Otakou and Waipuna Bay in the northeast (Figures 1.1 and 1.2). This area was selected based on previous seismic data collected by Fletcher (2016) and Rees (2018) where high-quality data collection was achieved.

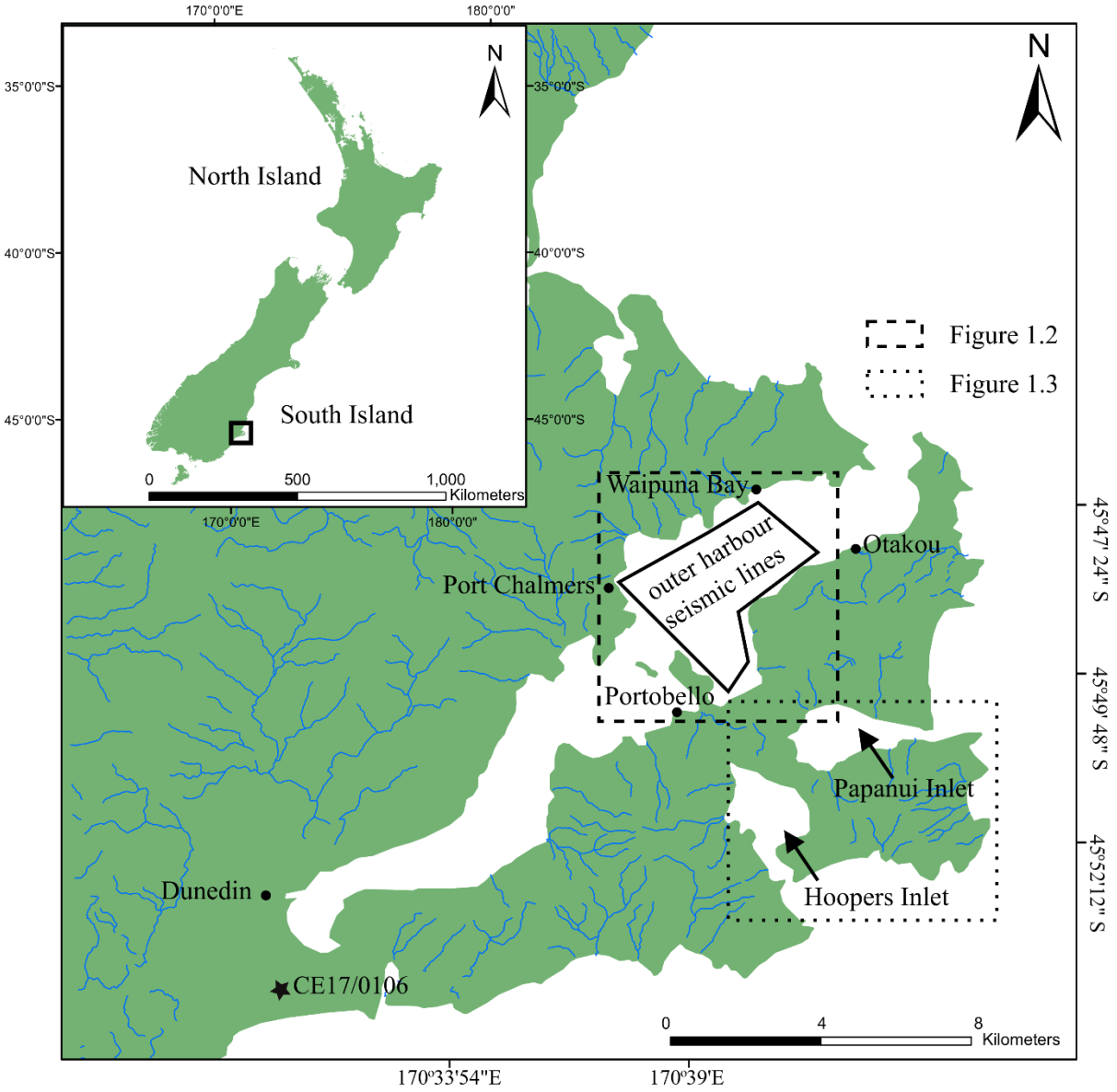

Figure 1.1: Location map of Otago Harbour in the South Island of New Zealand. Three main research areas outlined: outer harbour seismic lines, Hoopers and Papanui inlets on Otago Peninsula and the CE17/0106 core in South Dunedin. Figure 1.2 is outlined by a dashed square and Figure 1.3 is illustrated as a dotted square.

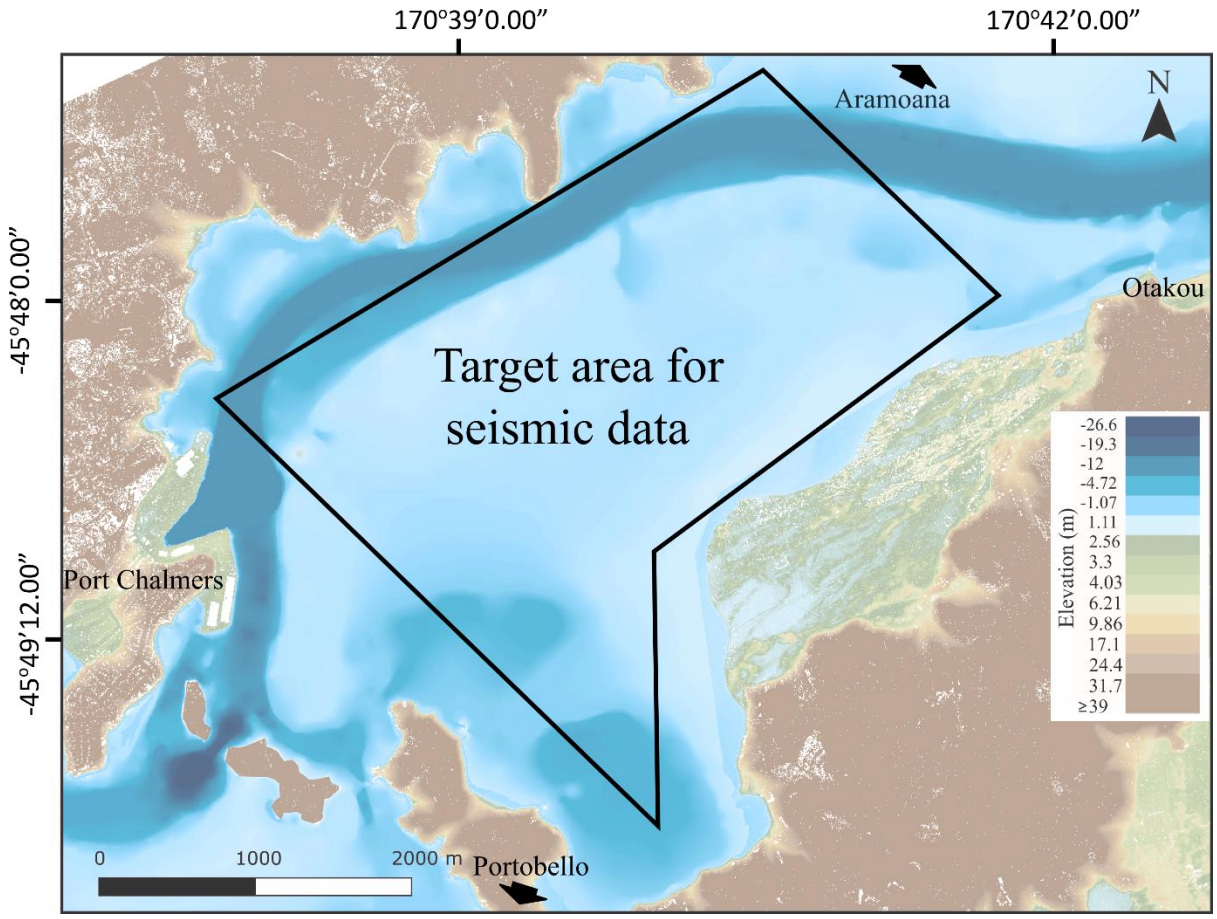

Figure 1.2: Outer harbour location map showing the target area of seismic lines collected as part of this investigation. Figure 1.2 is located within the dashed black box in Figure 1.1.

The second area of interest for this project is Dunedin. Eight land-based geotechnical cores were collected over several different Dunedin suburbs in 2019. Core CE17/0106, collected from De Carle Park, was selected as the core of focus for this research, although observations from cores collected in Tonga Park, Moana Rua Road and the Edgar Centre (collected in 2016 by the DCC via Tonkin and Taylor) were also utilised (Figure 1.1).

The third area was selected to present modern analogue environments of South Dunedin. Sediment samples were collected along transects from Hoopers and Papanui inlets on the eastern edge of Otago Peninsula (Figure 1.3). These inlets were selected as

modern estuarine sedimentary environments that could be compared to the sediments of the CE17/0106 core, to explore any similarities in the deposition. The proximity of Hoopers and Papanui inlets to South Dunedin coupled with their lack of major anthropogenic alteration made them ideal targets for exploring the processes that the sediments beneath Dunedin would have probably undergone prior to the arrival of humans (Figure 1.3).

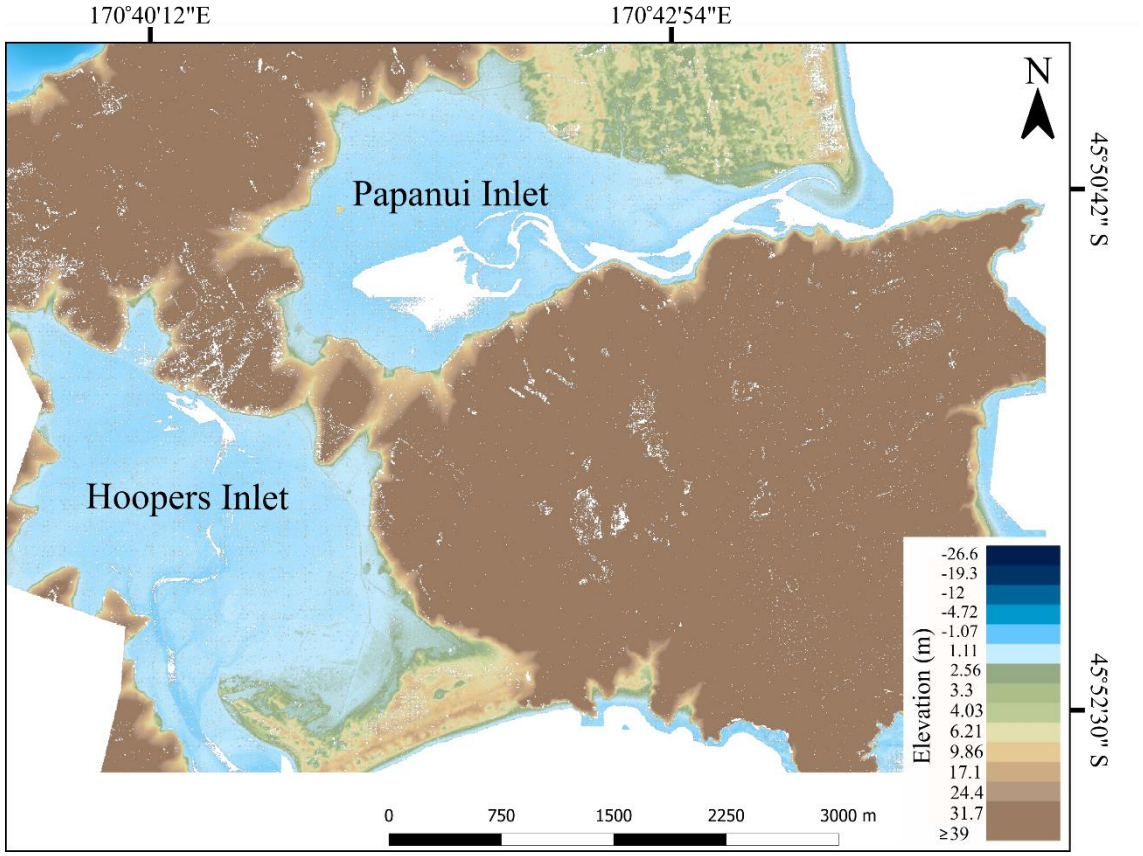

Figure 1.3: Location map for modern analogue samples collected in Hoopers and Papanui inlets. Figure 1.3 is illustrated as a dotted box in Figure 1.1.

1.2 Previous research

Until recently, our understanding of Otago Harbour was limited to extensive land-based observations; however, little research had been conducted into characterising the sediment stratigraphy of the harbour. Additionally, in recent years, there has been an

increasing emphasis on understanding natural hazards that could impact Dunedin, and in particular, the threat of sea level rise encroaching on South Dunedin.

Shears (2009) collected the first single-channel seismic reflection profiles in Otago Harbour and coupled these profiles with gravity transects in South Dunedin and Aramoana. Shears (2009) also produced a comprehensive sediment budget of Otago Harbour as well as the first geometric basement model, setting the basis for seismic reflection and gravity investigations.

In 2016, a regional-scale multichannel seismic investigation was conducted in the harbour by Fletcher (2016) as part of a BSc(Hons) degree. Fletcher (2016) aimed to place constraints on the harbour basement and sedimentary horizons as well as to investigate evidence of faulting which could prove or disprove previous theories of harbour infill and erosion. Fletcher's (2016) modelling produced depth-to-basement measurements throughout Otago Harbour. Rees (2018) increased the density of lines collected in the inner and outer harbour to enable the reconstruction of past sea levels from the stratigraphy of the harbour and to add ground-truthing from a geotechnical core collected from the Edgar Centre in South Dunedin. The data generated by Fletcher (2016) and Rees (2018) have been incorporated in the present study.

In recent years, interest in the sediments that constitute South Dunedin has grown. These include a gravity survey by Lutter (2018) and shear wave velocity investigation by Sangster (2019). Both aimed to constrain the depth to the basement in South Dunedin as well as the nature of the sediment that filled in the paleovalley, to allow a better understanding of the scale of sediment present.

Extensive research has been conducted into the Dunedin Volcanic Group (DVG) that forms the framework of the hills surrounding the basin and probably the basement beneath, focused mainly on constraining the age as well as the type and extent of volcanism (Baxter, 2019; Martin, 2000; Mcdougall & Coombs, 2012; Scott et al., 2020).

1.3 Aims

This investigation aims to characterise the Quaternary sediments of the Dunedin region, using a combination of marine seismic reflection profiling in the outer harbour and the stratigraphic and geochronological analysis of cores collected in South Dunedin. My research aims to build a more in-depth explanation for the processes that shaped the harbour into its current state.

Specific aims of this study:

- Constrain the geometry and geomorphology of the paleovalley that drained the harbour to the south, using a combination of cores and gravity measurements collected by Shears (2009) and Lutter (2018).
- Reconstruct the sediment infill history of core CE17/0106 through a combination of the geochemical and physical characteristics of the core, constrained by radiocarbon dates.
- Explore the anthropogenic influence on the immediate subsurface using heavy metal markers to explore the extent of anthropogenic contamination.
- Constrain the geometry and geomorphology of the deepest parts of the outer harbour paleovalley and sediment infill history for this region that appears to contain numerous cycles of deposition and erosion.
- Ground-truth the outer harbour seismic stratigraphy against the inner harbour sediments by comparing changes in lithology of the CE17/0106 and Edgar Centre cores to horizons identified in the harbour stratigraphy.
- Constrain basement geometry as an indicator of erosion history and key boundary conditions for basin infill.

1.4 Thesis outline

The rest of this thesis is laid out as follows. In Chapter 2, the regional geology and structures of Dunedin are explored to set the background for the seismic and stratigraphic investigations undertaken. Chapter 3 describes the methods followed for Otago Harbour seismic data collection as well as the collection and analysis of the

CE17/0106 core. Chapter 4 presents the observations and initial interpretations of the sediment stratigraphy of Dunedin and the outer harbour. Chapter 5 provides a discussion of the observations and initial interpretations and presents probable explanations for the processes involved in the infill and erosion of the Quaternary sediments. The thesis is concluded with Chapter 6, which outlines the main outputs of this investigation.

Chapter 2 Regional geology

2.1 New Zealand geological overview

A broad understanding of the regional geology and structures of the geology of Otago sets an important base for studying the formation and subsequent infill of Otago Harbour in detail. The geology of New Zealand can claim its origin from the supercontinent of Gondwana and its subsequent breakup (Mortimer, 2004; Waters & Craw, 2006). The majority of the continent of Zealandia is located below sea level with only 10% currently exposed as the islands of New Zealand (Mortimer, 2004). Zealandia is made up of a suite of terranes sourced from a combination of volcanism, sedimentation and metamorphism shaping it into the dynamic landscape present today.

Evidence of the breakup of Gondwana within the New Zealand geological setting can be observed through oceanic fracturing in the Tasman Sea (Mortimer, 2004). These oceanic fractures provide evidence for the relative orientation of the Pacific and Australian plates as they have moved apart over geological time. Much of Zealandia was submerged after the breakup of Gondwana; however, whether or not Zealandia was completely submerged is a topic of continued debate (Mortimer, 2004; Strogen et al., 2014). The maximum submergence of Zealandia is thought to have occurred between 25 and 21 Ma (Strogen et al., 2014). Only a fraction of Zealandia is currently exposed above sea level leaving most of the continent of Zealandia unexplored (Mortimer, 2004; Strogen et al., 2014).

Zealandia underwent both extension and rifting following the breakup of Gondwana and its subsequent separation from Australia about 80 Ma ago (Waters & Craw, 2006). A combination of faulting and uplift have contributed to extensive crustal thickening which is indicated by the formation of the Southern Alps of New Zealand's South Island (Kamp & Tippett, 1993). Once uplifted, New Zealand was exposed to extensive erosion and volcanism altering the already varied landscape.

2.2 Geological overview of Otago

The geological record of Dunedin and the wider Otago region has been extensively mapped. The basement of Dunedin consists of Otago Schist, a component of the Haast Schist constituting the basement of the wider Otago region. The Otago Schist is characterised by quartzofeldspathic and micaceous foliations and exhibits a metamorphic textural zone IV (Mortimer, 2004; Turnbull et al., 2010) (Figure 2.1). The Otago Schist formed through the metamorphism of mud and sandstone protoliths that are Permian to Triassic in age (Turnbull et al., 2010). Exhumation of the schist occurred from 110 Ma from its parent terrane the Caples and Rakaia terrane (Gray & Foster, 2004).

Of the three subcategories of the Haast Schist, the Otago Schist is the most extensive. These categories are distinguished predominantly by textural appearance (Turnbull et al., 2010). The Haast Schist makes up a large proportion of the basement geology of the South Island of New Zealand. The Otago Schist is expected to form the basement geology of Otago Harbour; however, it is not directly observed in this region. Rather, it is important due to it being the most likely source of much of the terrigenous sediment found in the Dunedin area.

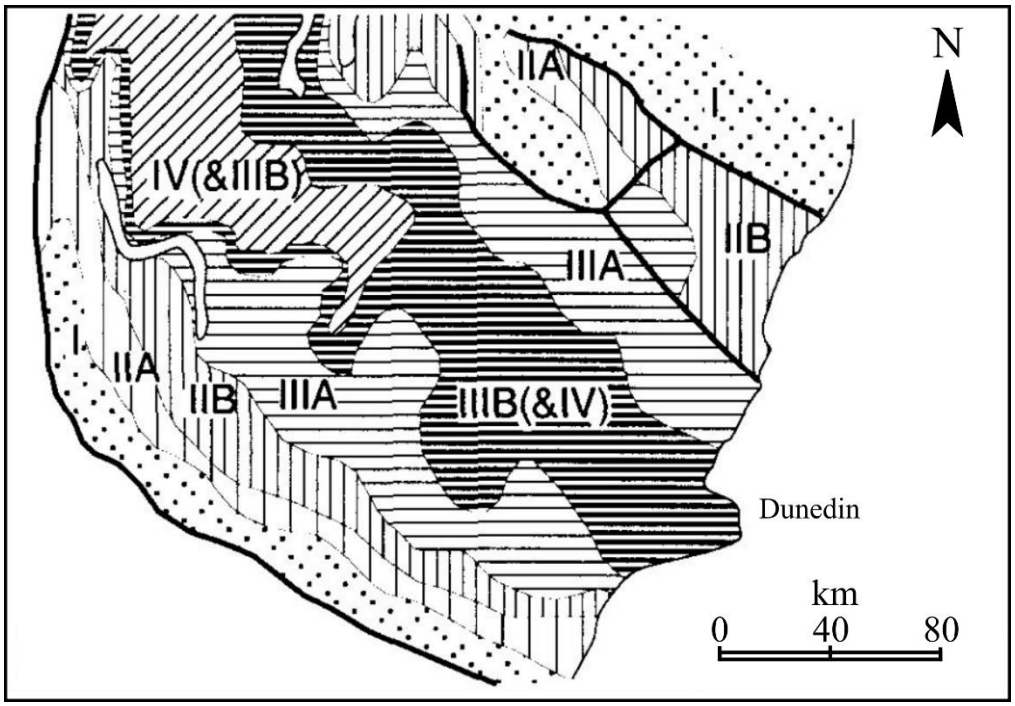

Figure 2.1: Textural zones of schist in the Otago region, adapted from Turnbull et al (2001). The Roman numeral refers to the number of the textural zone, with each zone distinguished by a different pattern.

Deposited directly above the schist is an up-to 500 m thick suite of Cretaceous aged non-marine sedimentary rocks separated from the basement by an unconformity (Martin, 2000; Mcdougall & Coombs, 2012). The unconformity known as the Waipounamu Erosion Surface is a low-relief surface carved from the marine transgression between the Cretaceous and the Oligocene (100-25 Ma) getting younger as the surface extends inland (Landis et al., 2008). Situated directly on top of the non-marine sediments, and separated in most places by a disconformity is an up-to 400 m thick suite of marine sedimentary rocks, Cretaceous to Paleogene in age (Mcdougall & Coombs, 2012).

Following the deposition of the marine sedimentary suite was the Dunedin Volcanic Complex. The Dunedin Volcano erupted through several distinct eruption phases between 16 and 11 Ma. Erupted material varied across the landscape, including lava flows, tuffs and breccias (Scott et al., 2020) (Figure 2.2). Since the eruptive sequence ceased at 11 Ma, erosion has subsequently carved a NE-SW orientated valley which

due to changes in sea level and subsidence has filled in with Quaternary aged estuarine and marine sediments (Glassey et al., 2003).

The orientation of Otago Harbour matches many of the nearby NE-SW trending faults, including the Titri and Akatore Faults (Figure 2.2). The trigger for erosion that formed the harbour is yet to be conclusively determined. Although several theories could explain the harbour's location, the most plausible involves erosion from a central catchment situated at the centre of the volcano near Portobello. This theory suggests two rivers drained from centralised catchments with one draining northeast and the other southwest along a possible fault allowing an area of weakness for the rivers to exploit. Previous seismic work by Fletcher (2016) and Rees (2018) identified a basement high near the volcano's centre in Portobello, deepening in both directions. The exploitation of a fault to facilitate erosion is consistent with the proximity and orientation of the Akatore, Titri and Green Island Faults; however, no conclusive evidence of faulting has been observed within the rock record or previous geophysical investigations.

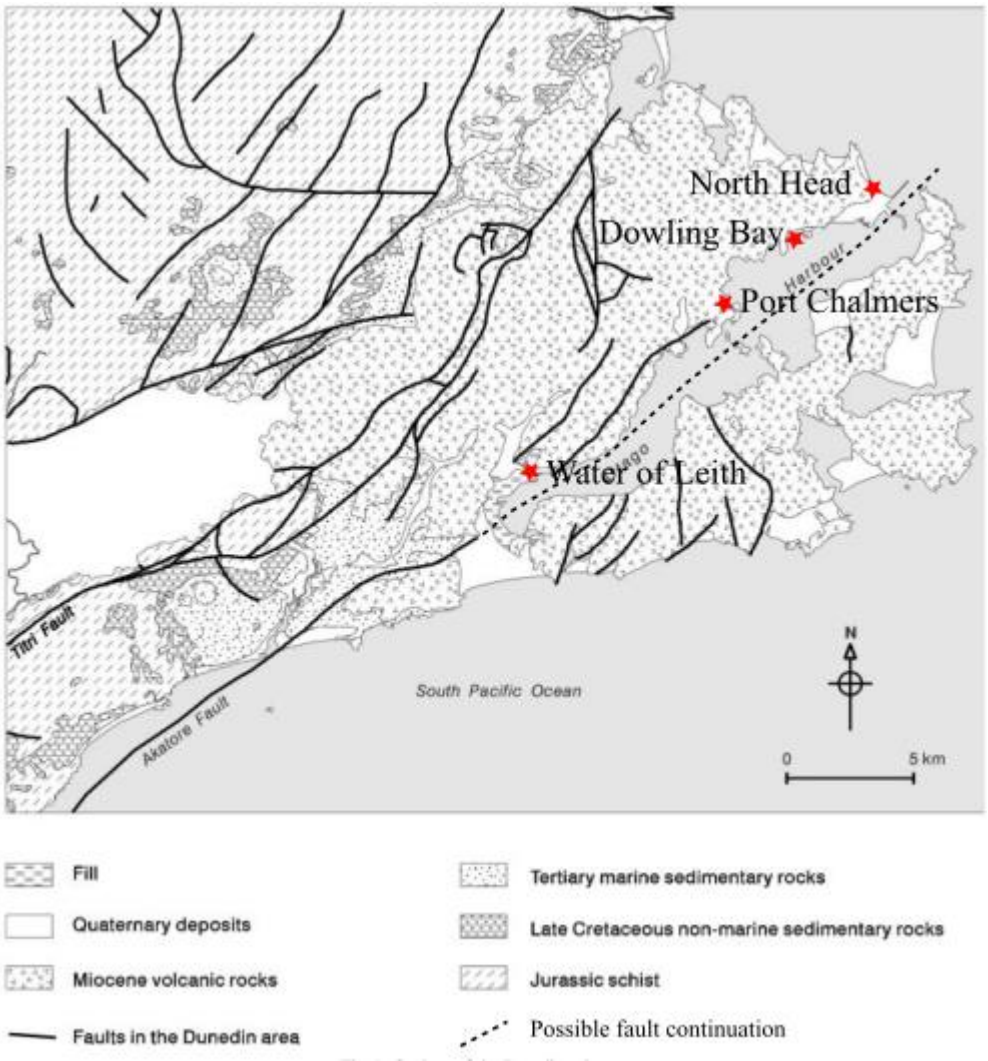

Figure 2.2: Map of the geology of Dunedin, indicating faults present and the theorised extension of the Akatore Fault through the harbour. Adapted from Glassey et al (2003). The Titri and Akatore Faults are the only known faults to be currently active in the area.

2.3 Dunedin geology

2.3.1 Late Cretaceous-aged sedimentary rocks

Deposited on top of the Otago Schist basement is a package of late Cretaceous aged non-marine sedimentary rocks. The Otago Schist has undergone extensive faulting and uplift since its initial metamorphism in the Jurassic (Bull & Cooper, 1986). Exposure of the schist from uplift allowed it to undergo extensive erosion setting the base of

deposition for terrestrially sourced sedimentary units. Two main rock units have been observed in this Late Cretaceous sedimentary sequence: Taratu Formation and the Henley Breccia.

2.3.2 Paleogene aged marine sedimentary rocks

The coast of New Zealand underwent marine transgression during the Paleogene. This marine transgression formed a suite of marine sedimentary rocks on top of the previously deposited non-marine sedimentary rocks. This suite of rocks can be split into four main units starting with the oldest; Abbotsford Formation consisting mainly of clay-rich glauconitic sandstone and mudstone; Green Island Sandstone, rich in glauconite and ranging from fine to medium sand; Burnside Mudstone predominantly clay-rich calcareous mudstone and the Caversham Sandstone consisting of cemented calcareous sandstone (Glassey et al., 2003; McKellar et al., 1990; Price & Chappell, 1975).

2.3.3 Dunedin Volcanic Group

The Dunedin Volcanic Group (DVG) covers an area 30 km in diameter, with both its eruptive and geographic centres located between Portobello and Port Chalmers (Price & Chappell, 1975; Reichgelt et al., 2016; Reilly, 1972). The DVG formed due to the eruption of the Dunedin Volcano between 16 and 11 Ma (Scott et al., 2020). The DVG covers an area of nearly 300 km^2 with the volume of erupted material estimated to be as much as 150 km^3 (Reilly, 1972). The process of eruption and subsequent formation of the Dunedin landscape can be attributed to four main eruptive phases (Figure 2.3). Initially, the Dunedin Volcano formed in a shallow coastal marine setting, but due to a long eruption period, later phases erupted above sea level as a result of coincident marine regression (Coombs et al., 2010). The four distinctive eruptive phases formed a range of distinct volcanic lavas ranging from trachytes in the initial phase to phonolites in the later phases (Martin, 2000) (Figure 2.3).

The initiation of volcanism instigating the initial eruptive phase is characterised by anorthoclase trachyte tuffs and flows (Allen, 1974). Localised outcrops of the initial eruptive phase lavas are observed adjacent to Port Chalmers and at North Head, additionally, a minor occurrence is seen at Dowling Bay (Coombs et al, 1960) (Figure 2.2 and 2.3).

Sitting atop the initial phase trachytes is the first eruptive phase. The first eruptive phase is made up predominantly of kaiwekites (Ti-augite and anorthoclase rich) and basalts forming from erupted flows (Benson & Turner, 1989) (Figure 2.3). Explosively erupted feldspar-rich tuffs formed through magmatic differentiation followed by kaiwekite and basalt flows, concluding the first eruptive phase (Lutter, 2018; Martin, 2000).

Following the initial and first eruptive phases, alluvial deposits of eroded volcanic clasts formed. These clasts are primarily sourced from explosively erupted feldspar-rich clasts formed through magmatic differentiation, that deposited in areas of naturally low relief, such as floodplains or river valleys (Baxter, 2019; Martin, 2000).

The lava flows of the second eruptive phase immediately followed the formation of the older floodplain conglomerates. Lava flows were extensively deposited around their respective source vents (Martin, 2000) (Figure 2.3). Initially, the flows consisted of basalt but progressed to phonolites as they became more feldspathic and alkaline (Martin, 2000).

The third and final eruptive phase of the DVG was comprised mainly of cossyrite bearing lavas (Martin, 2000). This was followed by further emplacements of phonolite (Baxter, 2019) (Figure 2.3).

Finally, vents of the complex were filled by the Port Chalmers Breccia (Allen, 1974). The breccia contains a variety of clast sizes ranging from as large at 2 m down to ash sized particles, forming an unsorted, massive volcaniclastic deposit (Martin, 2000). The unsorted, massive nature of the breccia is thought to be caused through the blocking and subsequent explosive eruption of vents depositing the clasts atop the previously deposited third eruptive phase phonolites (Martin, 2000). The Port Chalmers Breccia was formed in at least four separate vents controlled from faulting, these were situated

between current day Port Chalmers and Hoopers Inlet (Allen, 1974). These vents varied in size from as small as 160 m in diameter to 650 m (Price & Chappell, 1975).

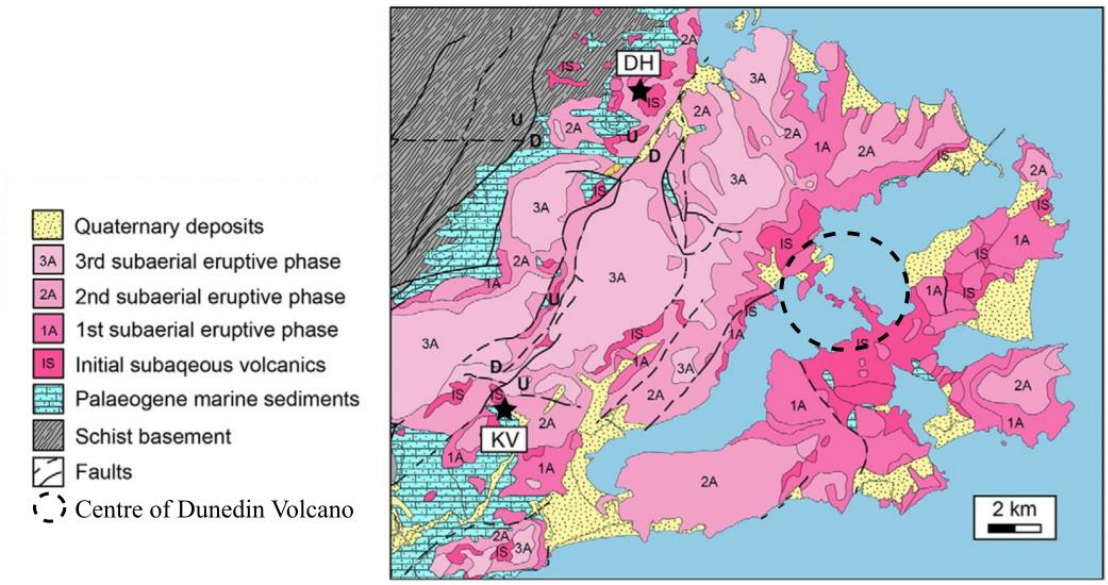

Figure 2.3: Map outlining the extent of different eruptive phases of the Dunedin Volcanic Group. Adapted from Reichgelt (2016).

2.3.4 Quaternary sediment infill

Once the eruptions of the Dunedin Volcanic Group ceased, subsequent erosion carved out the northeast-southwest orientated harbour. Erosion of a valley well below current sea level was facilitated by a base level during the glacial states of the Quaternary that was about 120 m lower than today's sea level. Fluctuations in sea level resulting from glacially controlled eustacy then allowed sediment infill to begin. The sediment package of Otago Harbour varies across its length. Harbour sediments can be differentiated into two main types: fine to medium-grained quartz-rich sand (Glassey et al., 2003; Shears, 2009) in the higher energy environments (more commonly towards Taiaroa Head in the outer harbour) and the significantly finer-grained black mud and

silt that make up the low energy tidal mudflats at the extremities of the harbour and are most commonly seen in the inner harbour (Fletcher, 2016; Rees, 2018; Shears, 2009).

The sediment infill of Otago Harbour is primarily attributed to the transport of sediments along the coast via longshore drift (Carter, 2010; Smith et al., 2010). The main sediment source of Otago Harbour has been attributed to the Clutha River, which provided sediments rich in quartz to be transported by the northbound current (Carter, 2010). Although the Water of Leith is the main source of eroded volcanic material into the harbour system, volcanic material only contributes a very small amount of the total sediment input (Rees, 2018) (Figure 2.2). The precise volume of sediment within the harbour is still unknown despite past attempts at modelling. A larger portion of the harbour including the South Dunedin Tombolo is made up of longshore drift sourced sediment infill (Smith *et al.*, 2010). The tombolo formed from an influx of sediment that sealed off the southwestern harbour entrance, forming a sediment bridge facilitating the connection to the current day Otago Peninsula.

The age range of sediment infill is the focus of ongoing research but is probably Quaternary; radiocarbon dating has constrained the shallowest 20 m of sediment in geotechnical cores collected at Portsmouth Drive to be <50 000 years in age (Rees, 2018).

2.3.5 Regional structures

The greater Dunedin area has been influenced by several faults, some of which are still active (Figure 2.2). The Dunedin area has experienced gradual tilting as a result of this faulting, imposing a 3^{o}-7^{o} dip to the southwest (Glassey et al., 2003). Several of these faults run in a parallel orientation to the larger Alpine Fault at the convergence of the Pacific and Australian plates. The larger local faults, including the Akatore and Titri Faults, have this northeast-southeast strike and are situated west of Dunedin (Glassey et al., 2003) (Figure 2.2). Exposures of basement Otago Schist have been uplifted locally by the Titri Fault (Glassey et al., 2003). The Akatore Fault possibly extends from offshore, cutting through Dunedin city beneath Holocene cover and extending up the harbour; however, its presence has only been inferred (Frank, 2016; Glassey et al., 2003) (Figure 2.2). As mentioned, the presence of the Akatore Fault

extending through the harbour has been theorised as a zone of weakness that facilitated the harbour's erosional formation (Fletcher, 2016).

The Alpine Fault, one of New Zealand's largest and most active faults was formed as a result of tectonic stress from the initiation of spreading between the Antarctic and Australian plates at the end of the Oligocene (Kamp & Tippett, 1993).

Chapter 3 Methods

3.1 Pre-survey planning

Extensive planning was done before the survey started. In particular, permission from both the Geology and Marine Science departments was required to comply with the University of Otago vessel bookings and health and safety procedures.

Seismic equipment used is as follows:

- R/V *Tuhura* – Primary vessel for all harbour seismic work. It measures 6.5 m in length and is propelled by a single 150 hp engine. The R/V *Tuhura* is operated by the University of Otago's Marine Science Department.
- Boomer power source – Honda EU20i generator, producing 8 amps and 2.2 kW.
- Geometrics MicroEel streamer – 24 channel streamer consisting of 72 individual hydrophones (24 groups of 3). Hydrophone groups are distributed along the streamer at a spacing of 3.125 m for a total length of 75 m.
- Seismic source – Ferranti boomer catamaran which operates between 100 – 1000 Hz from 213-230 db.
- Capacitor Box – Geopluse capacitor, producing between 105 and 455 J with a maximum shot rate of 8.5 times per second.
- Geode – A Geometrics 24 channel geode seismograph was used to collect data received off the streamer.

Planning documentation involved establishing routes, the details of the people on board, and safety procedures. When work on the R/V *Tuhura* started, everyone present was taken through the onboard safety induction, indicating hazards and the location and proper use of personal protective equipment.

Seismic survey cruise tracks were designed based on preliminary interpretations of lines collected in 2016 by Fletcher (2016) and in 2018 by Rees (2018). 2019 surveys targeted areas off Port Chalmers between Careys Bay and Lower Portobello in the southwest to Waipuna Bay and Otakou in the northeast. Lines were planned before the start of the survey to maximise coverage of the harbour. Seismic grids were planned using the OPENCPN software package, and cruise tracks with start and endpoints for

each line entered into shipboard GNSS unit. The shallow bathymetry of Otago Harbour played a significant role in the planning process as large areas of interest in the harbour are only accessible at high tide.

3.2 Seismic equipment

Due to accessibility issues within the harbour, the seismic data collection required an agile and shallow hulled vessel; for this, the R/V *Tuhura* was used. The R/V *Tuhura* allowed access to most of the harbour, unreachable by Otago University's primary vessel the R/V *Polaris II;* however due to the R/V *Tuhura's* size it did not have enough onboard power to operate the seismic equipment so an external generator was required.

The boomer and streamer were tethered to the stern of the vessel and towed in parallel. The distances between these tether points were measured and recorded in relation to the shipboard GNSS equipment. These distances could be used in the processing stages to correct the geometry of the lines (Figure 3.1 and 3.2).

Set up parameters for lines collected in 2019 mirrored those of lines collected in 2018 (Rees, 2018). The hydrophone array (length of 73.525 m) started at 27.3 m from the stern of the vessel (Figure 3.1 and 3.2). The maximum angle of movement from the stern of the vessel for the Boomer was 15.5^{o} (Rees, 2018). The GNSS recording of each shot location was positioned in the wheelhouse of the R/V *Tuhura*, 3.2 m in front of the Boomer tether point, with a further 24.84 m to the boomer (Rees, 2018) (Figure 3.1).

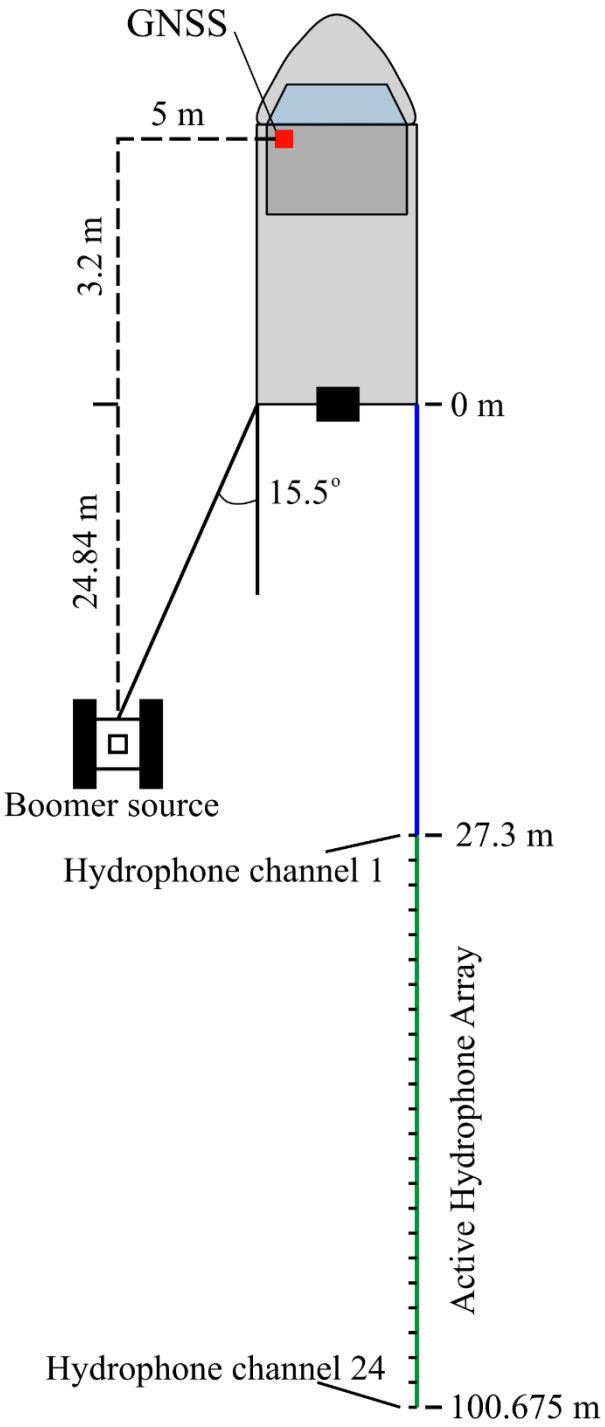

Figure 3.1: Equipment setup parameters on the R/V *Tuhura.*

Data quality from channel 1 was monitored in real-time on a Panasonic Toughbook, to show a real-time plot of one of the 24 channels being recorded to assess data quality as well as allowing collection parameters to be adjusted on the fly.

Figure 3.2: Seismic gear deployed off the stern of the R/V *Tuhura. The acoustic boomer source can be seen breaking the surface on the right.*

3.3 Seismic data collection

Seismic data were collected in 2019 over five days, split into two separate collection windows. The first half of the survey was conducted on the 9th and 10th of January and it was completed on February 11th to 13th. In total, the survey includes 42 seismic lines collected, these were spaced between 100 – 150 m apart (six were not processed as they lacked location measurements) (Table 3.1) (Figure 3.3). The main aim of the data collection was to image the subsurface while maintaining consistency throughout the survey which was a key challenge. The R/V *Tuhura's* ideal speed for data collection was four knots; however, several factors including the shallow bathymetry caused the boat's speed to vary between 2 and 5 knots.

Table 3.1: Table of processed lines collected as part of the 2019 outer harbour seismic survey.

Line Number	Start Point	End Point	Orientation	Length (km)
19_6	Portobello Bay	Deborah Bay	SE-NW	4.28
19_7	Deborah Bay	Portobello Bay	NW-SE	2.87
19_9	Harwood	Dowling Bay	NW-SE	2.14
19_10	Harwood	Dowling Bay	NW-SE	1.93
19_11	Dowling Bay	Harwood	SE-NW	1.98
19_12	Harwood	Dowling Bay	SE-NW	1.97
19_13	Harwood	Dowling Bay	SE-NW	2.17
19_14	Harwood	Waipuna Bay	SE-NW	1.82
19_15	Waipuna Bay	Mid harbour	NW-SE	0.94
19_16	Careys Bay	Aramoana	SW-NE	2.64
19_17	Portobello Bay	Deborah Bay	SE-NW	2.66
19_18	Portobello Bay	Hamilton Bay	SE-NW	2.54
19_19	Hamilton Bay	Harwood	NW-SE	2.43
19_20	Harwood	Hamilton Bay	SE-NW	2.46
19_21	Hamilton Bay	Harwood	NW-SE	2.36
19_22	Harwood	Hamilton Bay	SE-NW	2.25
19_23	Hamilton Bay	Harwood	NW-SE	2.28
19_24	Harwood	Hamilton Bay	SE-NW	2.16
19_25	Port Chalmers	Aramoana	SW-NE	4.45
19_26	Aramoana	Port Chalmers	NE-SW	4.3
19_27	Port Chalmers	Mid harbour	SW-NE	1.3
19_28	Mid harbour	Aramoana	SW-NE	3.62
19_29	Aramoana	Quarantine Island	NE-SW	5.1
19_30	Quarantine Island	Aramoana	SW-NE	5.43
19_31	Aramoana	Harwood	NE-SW	1.8
19_32	Hamilton Bay	Harwood	NW-SE	2.08
19_33	Harwood	Dowling Bay	SW-NE	2.06
19_34	Dowling Bay	Harwood	NW-SE	2.1
19_35	Harwood	Dowling Bay	SE-NW	2.11
19_36	Dowling Bay	Harwood	NW-SE	2.1
19_37	Harwood	Dowling Bay	NW-SE	2.08
19_38	Harwood	Dowling Bay	NW-SE	2.22
19_39	Harwood	Dowling Bay	NW-SE	2.12
19_40	Tayler Point	Harwood	NW-SE	2.04
19_41	Harwood	Tayler Point	SE-NW	2.19
19_42	Waipuna Bay	Harwood	NW-SE	2.02

The water depth of the survey area at high tide ranged from as shallow as 0.5 m to as deep as 14 m in the dredged channel (Figure 3.3). The addition of a float to the end of the streamer, in 2018, minimised instances of the streamer dragging along the seafloor.

This proved beneficial in the post-processing direct arrival picking, as well as mitigating any potential damage from seafloor contact to the towed array. Differences in the conditions during data collection were accounted for during the processing and analysis stages to minimise their impact on data quality.

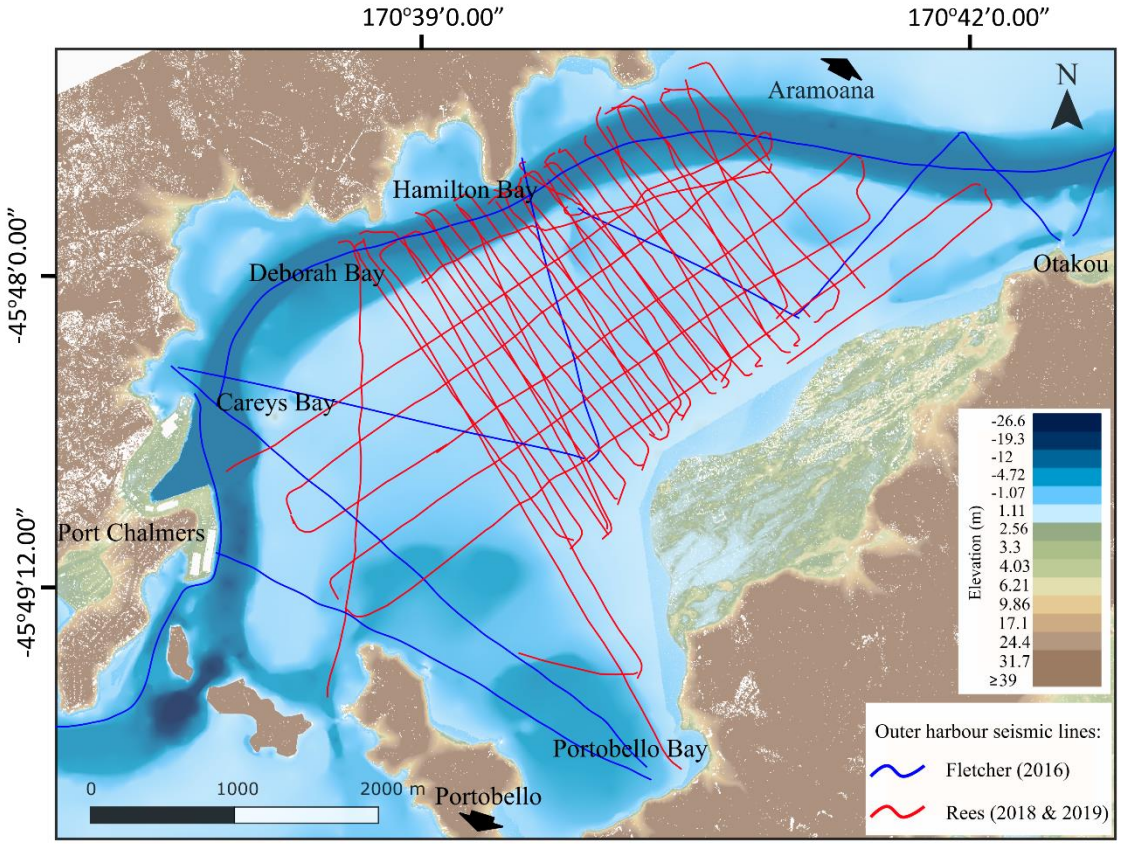

Figure 3.3: Map of outer harbour line locations.

3.4 Seismic processing steps

3.4.1 Reading in field data

Field data were recorded as separate SEG-D formatted files by the Geometrics software. These files are consecutively numbered and file names ending in ".dat". The first Claritas module applied to the data simply reads in a list of SEG-D files (Claritas Module: READSEGD) and writes out a merged SEG-Y formatted raw shot file to disc (Claritas module: DISCWRITE) using a naming convention consisting of the line

number followed by “rawshots.csgy”, where the “.csgy” extension refers to an SEG-Y file that has been output by the Claritas software with an extended set of headers that Claritas can use to aid in reading the file for subsequent processing steps.

3.4.2 Job Control System (JCS)

A JCS master spreadsheet was formed using relevant information for each line. During the seismic collection, all shots from each day were collected as a single continuous line and subsequently split into individual lines post-survey in Claritas. Included in this spreadsheet was the line name (e.g., 19_10 where 19 refers to the year the line was collected and 10 is the 10^{th} line collected that year), the starting and ending shots and the total shots in each line. The JCS file is interactively used throughout the different job flows to manually select the lines and associated parameters needed for the job to run (refer to appendix E).

3.4.3 Updating Geometry

During data collection, both the streamer and boomer are continuously moving relative to the boat’s standard configuration as a result of currents and minor course adjustments. To accurately map the subsurface locations of reflections, the geometrical configuration of the equipment needs to be updated and corrected in the SEG-Y headers to account for the irregularities in the boat’s course. The Claritas geometry application is used to plot each shot position (.sht file) which allows the manual reviewing of shots and the removal of any sharp or abrupt bends. This tool allows the reselection of the start and end of each line as well as transitions between lines, generally smoothing their shape. It is important to remove or mitigate these transitions as the position of the streamer can change dramatically when making turns, and potentially result in the equipment dragging on the seafloor. Once the lines were clipped, the survey geometry from the R/V *Tuhura* including the position of the streamer and boomers tether points at the stern of the vessel, their maximum offset angles as the equipment travels through the water as well as their relative position to the laptop and the GNSS receiver were added.

3.4.4 Direct arrival calculations (source-receiver offset determination)

Once the geometry of each seismic line was updated, a preliminary assessment of the seismic data could be made by examining shot records interactively (Rees, 2018). Several different aspects of the data collection could impact the quality of the data, particularly the movement and position of the towed streamer. Streamer feathering resulting in an inaccurate normal moveout correction could be observed in later stacking of the data. Streamer feathering occurs when the position and orientation of the streamer gradually changes during data collection, particularly during the transitions between lines, where the vessel velocity and heading can change leading to the streamer dragging on the seafloor. If feathering is not considered when establishing geometric assumptions, it will negatively affect stacking. Changes in the distance (offset) between the boomer (sound source) and the streamer (sound receiver) alters the two-way return time for sound and affects their positions relative to the GNSS receiver.

The processing software initially assumes a predictable arrival time for a reflected soundwave based on a hyperbolic moveout geometry; This determination can be improved by measuring the direct arrival times between source and receiver and using those times to calculate the actual offset distance (Figure 3.4). A .pic file was produced for each shot record using a subset job of the previous UPDATEGEOM job flow in Claritas (Figure 3.4). A file of these travel time picks (.pic file) was produced for each shot record using an interactive facility within the Claritas SV (seismic viewer) utility.

Each .pic file was converted into a .ahl format using the “pic2offset” routine so that the true offset between the boomer and streamer could be calculated and added to the header file in the UPDATEGEOM job flow. This updated distance for each shot gave a much more realistic offset which aided in the clarity of the seismic data.

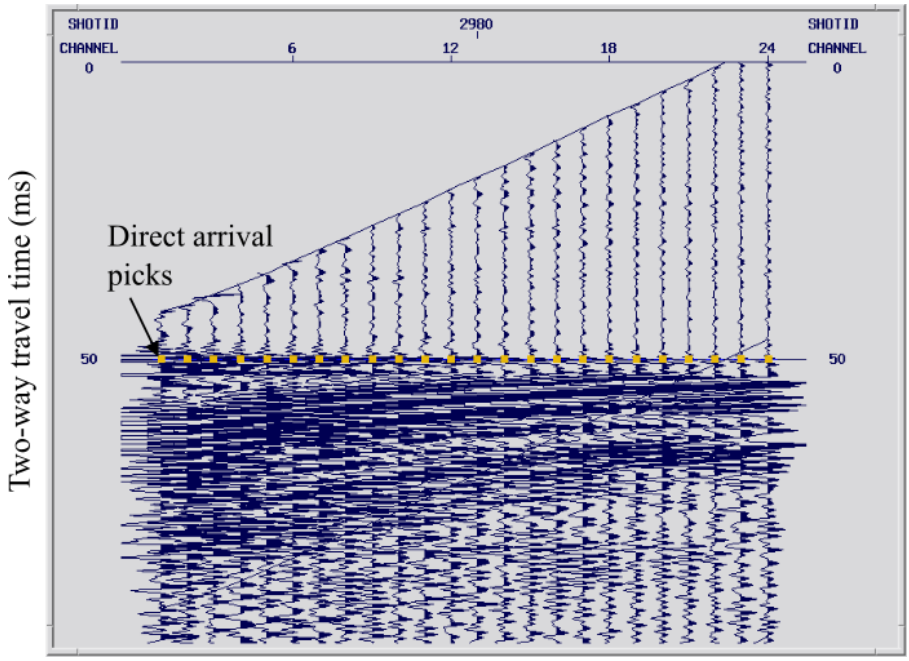

Figure 3.4: Direct arrival selection example, with picks indicated in yellow, plotted with reduction velocity. This is used to improve the distance calculation for the boomer and streamer.

3.4.5 Bandpass filtering

Bandpass filtering is a way of excluding both high and low frequencies from the seismic data. Processing software enables the addition of a variety of filters during both pre- and post-stack processing. One bandpass filter used by Claritas is a finite-difference filter routine (FDFILT). For this filter, four frequencies are selected to form the corners of a trapezoid, filtering out any frequencies outside of the outer two frequencies, and allowing all frequencies to pass between the middle frequencies (Figure 3.5). Filtering is ramped linearly at frequencies between the first, second, third and fourth points to exclude any noise in the field data post-processing. These frequencies are selected based on identifying frequencies that are likely to be produced by the boomer. The frequencies used for the lines presented here were 150, 250, 1000 and 1250 Hz (Rees, 2018) (Figure 3.5).

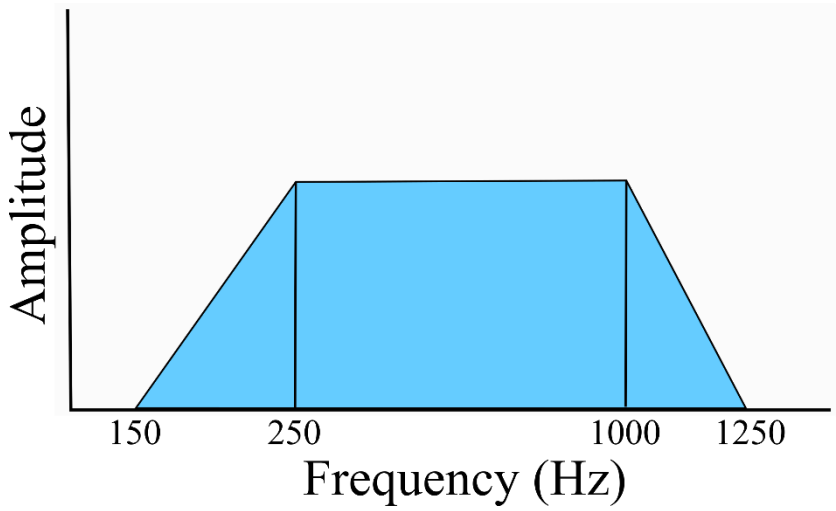

Figure 3.5: Bandpass filter parameters used to exclude frequencies not expected from the seismic equipment.

3.4.6 Raw stack

Running the raw stack job created an initial stack of the common-midpoint-gathers, prior to the velocity analysis. The raw stack job flow allows initial quality control of the data as well as an assessment of the efficacy of velocity corrections (described below) and geometry updates (based on the direct arrivals as described above). The initial velocity model used for the raw stack consists of a constantly increasing velocity from the velocity selected for the water to seafloor boundary at 1500 m/s.

3.4.7 Velocity analysis and NMO corrections

Sound travels at different velocities through media with different physical properties. For example, P-waves travel through water at about 1500 m/s but in near-surface saturated sediments usually travels between 1500 and 1800 m/s (Chong & Ni, 2009; Han et al., 2012). If these varying velocities are not accounted for, then poor stacking will result. Even though velocities generally increase with depth, this increase is seldom linear and changes throughout the subsurface as a function of geology, therefore

requiring the velocity model to be interactively updated. The Claritas Velocity Analysis (CVA) tool was used to do this (Figure 3.6). Within CVA, velocities were adjusted in the constant velocity CDP gathers window to produce flat horizons at particular travel times (Figure 3.6). When a flat horizon is obtained, this can be selected to produce a time – velocity pair at that horizon. This was repeated down through the CDP gather to produce the "columns" in the velocity model and laterally at a regular interval (100 CDPs in this case) (Figure 3.6) to produce the "rows". The selected velocity model for each line is saved as a file (formatted appropriately for Claritas with the file name appended by the extension ".nmo") which can be applied to CDP gathers through the Normal Moveout (NMO) correction before stacking. The velocity analysis step is critical for later steps that convert travel time to depth.

Two related velocity concepts, root-mean-square (RMS) velocity and interval velocities are considered in the velocity analysis to achieve realistic stacking velocities. RMS velocity refers to a calculated velocity travelling down and back through a specific set of layers (or intervals), each with a known velocity (Sheriff, 1994). Individual interval velocities, constant velocities that can be assigned to an individual layer, provide quantitative information that is related to the physical nature of the rock layer. If the stacking velocity, determined by the velocity analysis procedure described above, is assumed to be the equivalent of RMS velocity, then component interval velocities can be calculated to provide constraints on rock properties.

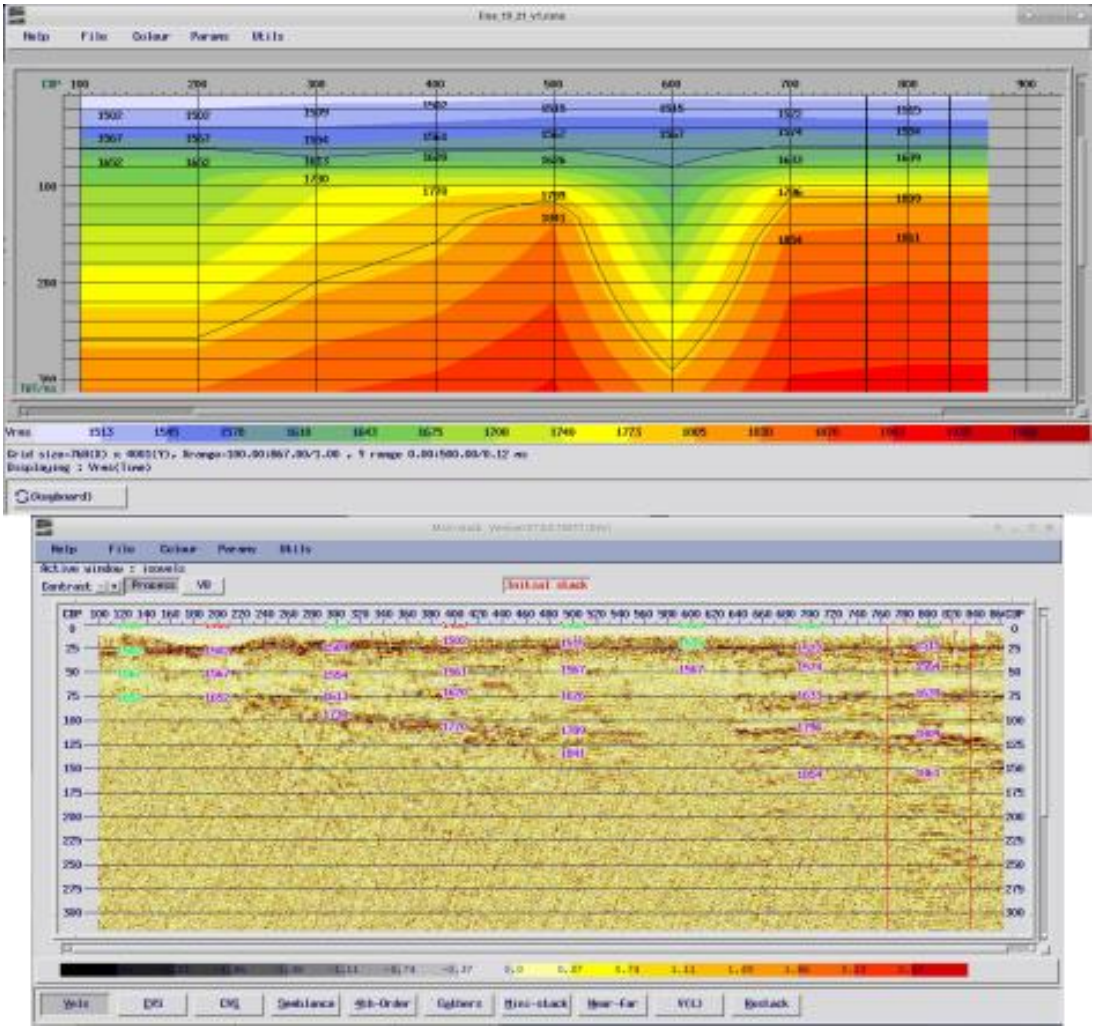

Figure 3.6: Manual velocity selections used to make NMO corrections.

3.4.8 Improving signal resolution

Two separate deconvolution methods were applied to the data in an attempt to enhance the clarity of data while minimising both coherent and incoherent noise unrelated to the boomer seismic source (Haldorsen et al., 1994). The processes used were a trace-by-trace Weiner deconvolution (DECONW) and a spatial deconvolution filter (sometimes referred to as a coherency filter) (FXDECON). Deconvolution processes were applied poststack. Deconvolution filters or operators are designed to improve the resolution (e.g., bandwidth) and general quality of data; this process can reduce the effect of signal loss that can occur due to the physical limitations of the sources or receivers

(Sheriff, 1994). In general, the Weiner deconvolution helps remove background noise recorded during the survey whereas the spatial deconvolution tends to emphasizes lateral horizons in the seismic profiles (Rees, 2018).

3.5 Seismic analysis

3.5.1 Kingdom import

Processed seismic lines were exported as SEG-Y files that could be plotted in the University of Otago's primary seismic analysis program: Kingdom (from Market IHS). The exported SEG-Y files were all spatially located in relation to the New Zealand Transverse Mercator (NZTM) map projection. Kingdom enables the interpretation of individual lines in relation to adjacent lines within a single map system. This allows interpretations to be extended throughout the subsurface and permitting gradual changes in the subsurface sediment to be identified.

3.5.2 Basement selection

The main aim for the seismic investigation of Otago Harbour was to better constrain the suite of sediments that makes up the harbour. Seismic imaging provides the ability to identify the regional basement/ bedrock as a high contrast reflection underlying the sedimentary units deposited in the harbour (Figure 3.7). The topographic relief of the basement and the way it changes along the harbour is especially important for understanding the history of sediment infill as well as understanding the processes involved. Basement reflections were identified within each seismic cross-section and marked in blue to stand out from the sedimentary record (Figure 3.7). The same colour coding system for basement and sedimentary horizons was used from previous surveys conducted by Rees (2018) and Fletcher (2016) (surveys 18TU283 and 16PL165) to keep observations consistent within the Kingdom project (Figure 3.7).

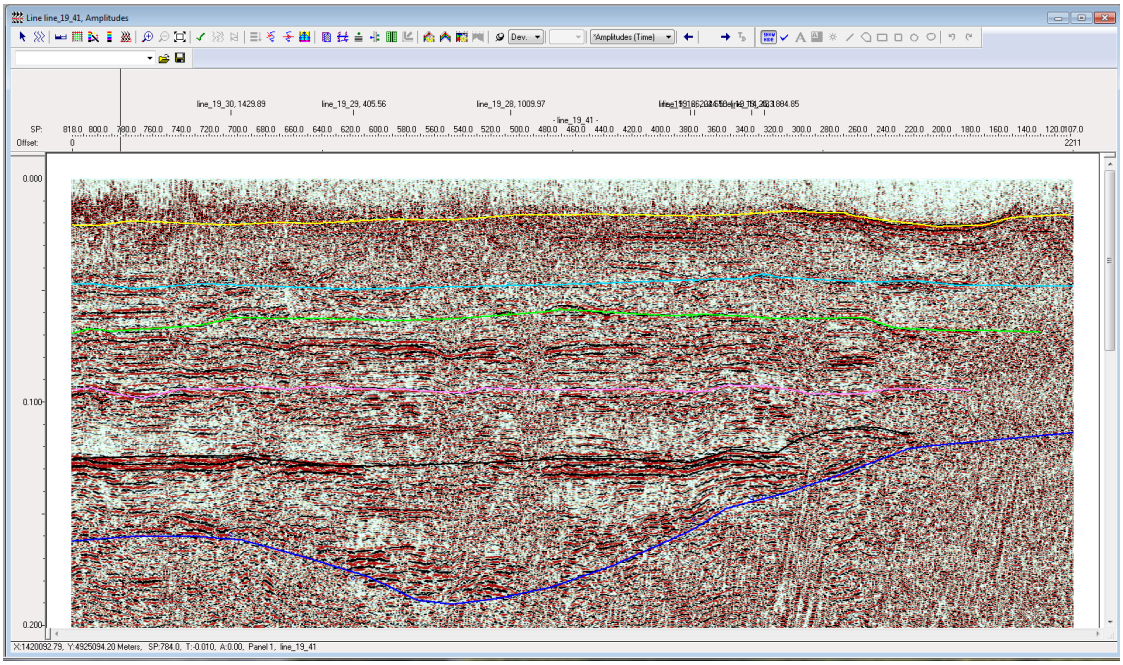

Figure 3.7: Horizons and basement reflections identified and selected in the seismic analysis program Kingdom (from Market IHS).

3.5.3 Horizon selection

In addition to basement reflections, another important result from seismic imaging is the ability to identify surfaces within the subsurface sediments represented as sedimentary horizons in the seismic data (Figure 3.7). Five distinct sedimentary horizons were interpreted across the outer harbour seismic lines (Figure 3.7). These were colour coded by depth with the shallowest in yellow, followed by light blue, green, pink and black. Horizons were tracked across multiple lines allowing the orientation and dip of horizons to be identified and mapped. Horizons were tracked using their position within the subsurface, considering two-way time as well and distinctive reflection characteristics. The five horizons selected were not the only observed horizons, but they are the most significant and frequently observed throughout the subsurface (Figure 3.7). Several less continuous horizons were observed but were not selected as key horizons due to their discontinuous nature. The horizons were

selected from the peak waveform observed which remained constant across all the observed horizons.

3.6 New Zealand SeaRise core collection

The South Dunedin SeaRise drilling was conducted from the 20th of May to the 5th of June 2019. A total of eight bores were drilled (Figure 3.8). The shallowest five (CE17/0100 to CE17/0104) were drilled to 15 m and were used primarily for the installation of piezometers for groundwater measurements (Figure 3.8). The deeper three cores (CE17/0105 to CE17/0107) were designed to produce a complete geological record to the basement of South Dunedin. The location of cores was based on past land geophysics, gravity modelling and cone penetration tests (CPT) in order to best constrain the Quaternary sediments in South Dunedin (Figure 3.8).

Drilling was funded by the Otago Regional Council, Oceana Gold, Dunedin City Council (DCC) and GNS Science and completed by McNeill Drilling. The cores were collected using a FRASTE Sonic Samp Drill in 1.5-3 m runs with varying core recovery.

Sonic drilling was conducted by a team of three (one driller and two offsiders). The core was recovered in a steel core barrel with a drill bit and a plastic core catcher at its end. Two primary drill bits were used; the soft sediment bit and the rock bit which uses more drilling fluid to cool, each with varying recovery. The core was recovered in 1.5 or 3 m runs with the shorter length used when the material was harder.

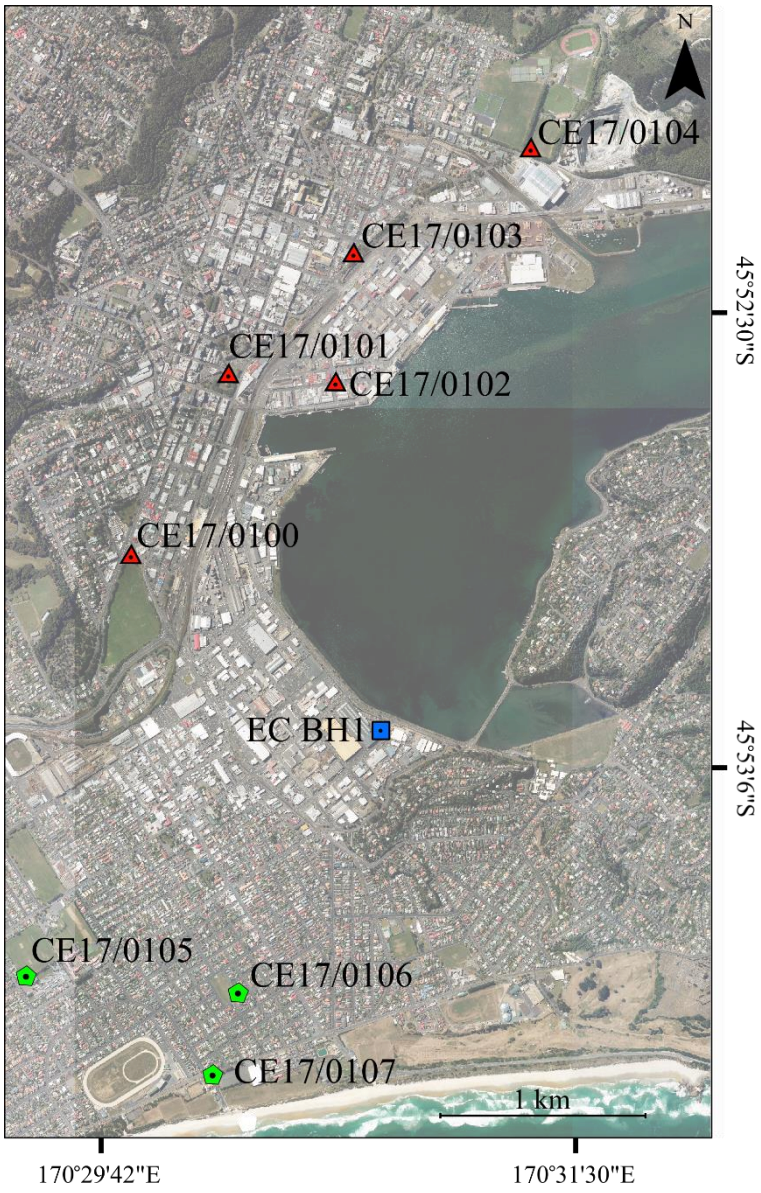

Figure 3.8: Location map of all cores collected as part of the NZ SeaRise programme in Dunedin as well as the Edgar Centre core. The Edgar Centre core is marked by a blue square, New Zealand SeaRise cores in South Dunedin by green pentagons and New Zealand SeaRise cores in Central and North Dunedin by red triangles.

Initially, the core collection barrel was rotated and vibrated into the subsurface for the length of the core barrel. A protective steel casing that protected the integrity of the core was then drilled into place, matching the depth of the collected core. The core section was then extracted from the hole leaving the protective core casing in place to allow the next section to re-enter and be drilled past it. Once above ground the core

barrel was angled, the core catcher removed and bagged, and the barrel vibrated while a drilling offsider collected the recovered core in a split PVC tube. Split PVC core liners were then placed on the core with the orientation marked and rotated removing the initial PVC split tube. Next, the core was logged and cut into 60 cm sections. Each section was enclosed by a second split PVC tube and sealed in lay-flat plastic, and placed in corrugated PVC core boxes with four lengths per box. On reaching a perceived basement or the desired drill depth the core was reviewed to select the best sedimentary horizon in which to install the piezometer for water table measurements. The core barrel was removed leaving the protective core casing in place. The bore was then "developed" by placing lengths of interlocking PVC tubing into the bore including a 3 m section of slotted PVC to allow water in. Once the PVC pipe was installed bags of silica granules were poured into the free space between the PVC and the core casing to provide a filter to stop the PVC pipe filing with fine silt and sand, prolonging its usability. The protective core casing was then removed leaving the PVC and silica shield in place, which was then pumped out by the evacuation truck to allow *in situ* groundwater to fill in. The top of the pipe was then concreted into the ground and sealed, ready for the installation of the remote measurement piezometer.

3.6.1 Initial core logging

Before the core was sectioned, boxed and sealed, an initial geotechnical sediment log was produced. Primary observations recorded in this log include colour, grain size, structure, and preservation. Observations were made along with continuous logging sheets and measurements for the start and end of core lengths obtained from the driller's recorded depths. The start of the core collection was offset from ground level due to the soft layers of grass and dirt that are difficult to core. Ground-level was recorded as the top (0 m) of the core but the first 30 – 100 cm was not recovered. Prior to drilling, a high-pressure water blaster was used in conjunction with an evacuation truck to wash away and pump out the top of the borehole providing a more consolidated start to the sediment core. The sediment recovered in the core catcher at the base of each run was bagged, logged and stored with the relevant core (Figure 3.9).

Figure 3.9: Image of ideal core recovery where the core was extracted smoothly and in a single continuous section.

The process of sonic drilling can have a lot of influence on the core, and recovery quality varied greatly across the eight boreholes, and from driller to driller as well. Sonic drilling does not collect the core in a core liner but rather in a steel core barrel, requiring the core to be removed from the barrel after each core run (Figure 3.9). The core is vibrated out of the core barrel into a split core liner; this process coupled with the vibration during drilling leaves a >1 cm liquefaction rind on the circumference of the core (Figure 3.9). The consistency of the core being extracted from the core barrel also greatly impacted core quality. The vibrations sometimes made the core flow out of the tube into the collection split core, being easily stretched and shrunk depending on the speed of the offsider collecting it. This allowed the core to be stretched or shrunk in some extreme cases by as much as 1 m. In other instances, rocks got stuck in the core catcher allowing the high-pressure drilling fluid to escape and washing away much of the finer sediment in the vicinity of a stuck rock. Additionally, well-lithified sediments

sometimes got stuck in the barrel, requiring the drillers to apply force via a sledgehammer to coax the core to move (Figure 3.9). This often resulted in the complete fracturing of the core, obscuring primary structures or features.

Figure 3.10: Core being extracted from the core barrel with a sledgehammer, where the core was stuck in place.

The consistency of sediment also contributed to blowouts from the core barrel, which occurred when the pressure of the drilling fluid caused the sediment to explode out of the core barrel onto the ground. Blowouts were recorded on the log and the core was reorganised as accurately as possible. Core loss was common and not always limited to the top or bottom of the run. If no field description was recorded, the loss was assumed from the top of the run and was recorded in the log and on markers within the core boxes.

‘Extra’ core material was also recovered where the water table was high, and sediment flowed into the protective core casing between runs. This sediment was recovered as fall-in at the top of the next core, but as most of the sediment was very soft and unconsolidated, it was sometimes difficult to distinguish between the primary core and the fall-in.

Once logging was completed and the core was sealed and boxed, the cores were transported to the Otago Repository for Core Analysis (ORCA) where it was placed in a refrigerated shipping container to await analysis (Figure 3.11).

Figure 3.11: Image of core logging process where 1.5 -3 m lengths were split into 0.6 m section and boxed. Initial log involved scrapping the drilling core rind which was leftover disturbance from the sonic drilling process.

3.6.2 Core splitting and secondary logging

On completion of the core collection, the CE17/0106 core was selected for further analysis based primarily on the recovery and preservation of sediments. A second, more detailed, core log was completed after splitting and resurfacing for the length of the core. Due to the varying lithologies recovered in the core, which influenced preservation and recovery, much of the core could be split while harder sections had to be resurfaced with metal spatulas and wire to expose a surface unaltered by drilling disturbance. Sections of the core that were relatively soft could be split using piano wire, creating flat surfaces ideal for major and trace element analysis using an ITRAX X-ray fluorescence (XRF) core scanner. After splitting the best-preserved half was saved as the archive half for use with non-destructive analysis, while the other was designated as the working half and sampled for destructive tests such as radiocarbon dating and grain size analysis.

The newly resurfaced and split-core was logged, with focus on colour (using the Munsell colour chart), grain size, primary structures, and intervals of drilling disturbance. The logged information was digitised using the logging software PSICAT, allowing the original digital core log to be refined with more detailed observations.

3.6.3 ITRAX core scanner

Split archive sections of the CE17/0106 core were run in succession through the ITRAX core scanner. The ITRAX core scanner collected three data sets along the core: high-resolution core image, radiographic image and x-ray fluorescence. The ITRAX is versatile in its ability to scan for elemental counts, as the x-ray source is replaceable allowing a wider range of elements to be targeted. For this investigation, a Molybdenum (Mo) tube was selected in order to obtain the largest range of elements present within the 13.5 m of the core.

3.6.4 Core scanning flow

At the beginning of each analytical day, the X-ray tube was warmed up by incrementally increasing tube voltage to 60 kV. Once warmed up, a reference glass, Q-spec provided by Cox Analytical, was measured to evaluate instrument performance using the same configuration as the downcore analysis. Core CE17/0106 was resurfaced prior to scanning, core gaps and areas of irregular topography were identified in an initial surface scan and removed from the run, and elemental data were collected at 2.5 mm resolution using a voltage of 30 kV and a current of 55 mA for 6 seconds per spot (Figures 3.12 and 3.13). X-radiographic parameters were set at 60 kV and 50 mA and scanned at the same resolution as elemental data. Downcore data are presented as elemental ratios or normalised by the degree of incoherent scattering to enable comparison between different elements and account for changes in water content downcore (Davies et al., 2015).

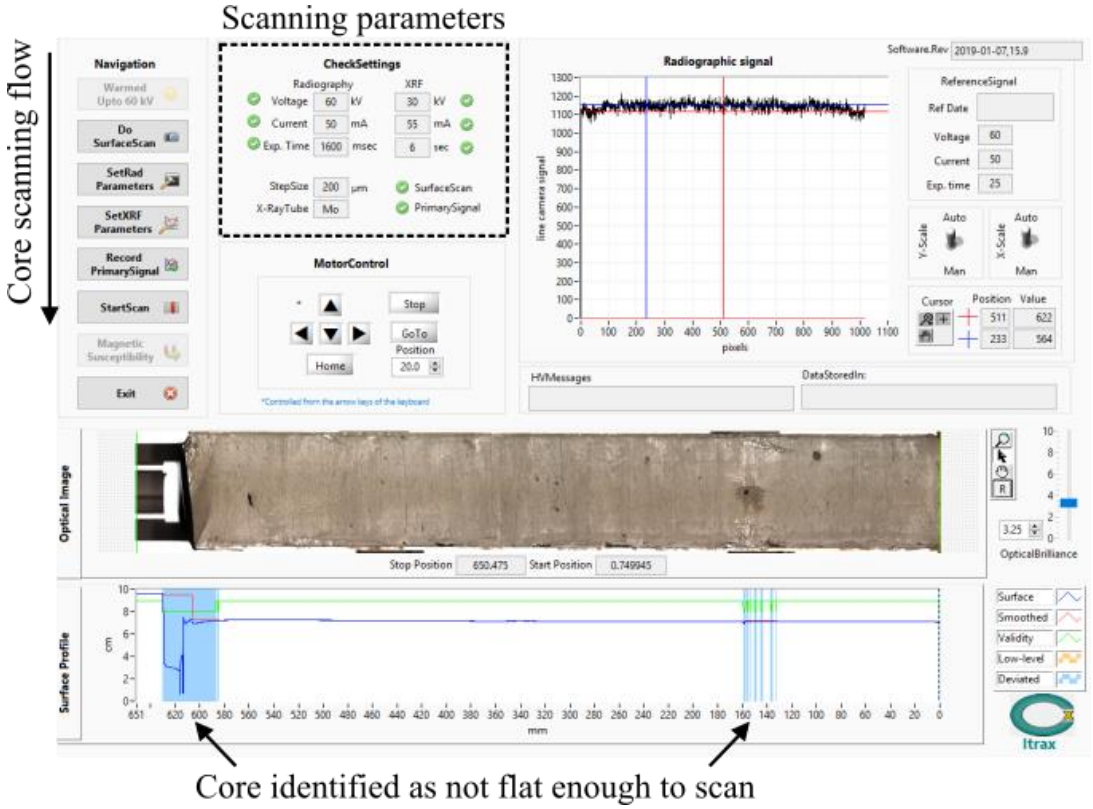

Figure 3.12: Core scanner setup with voltages and currents set. Blue sections are identified on the surface profile where changes in the surface topography could impact data collection.

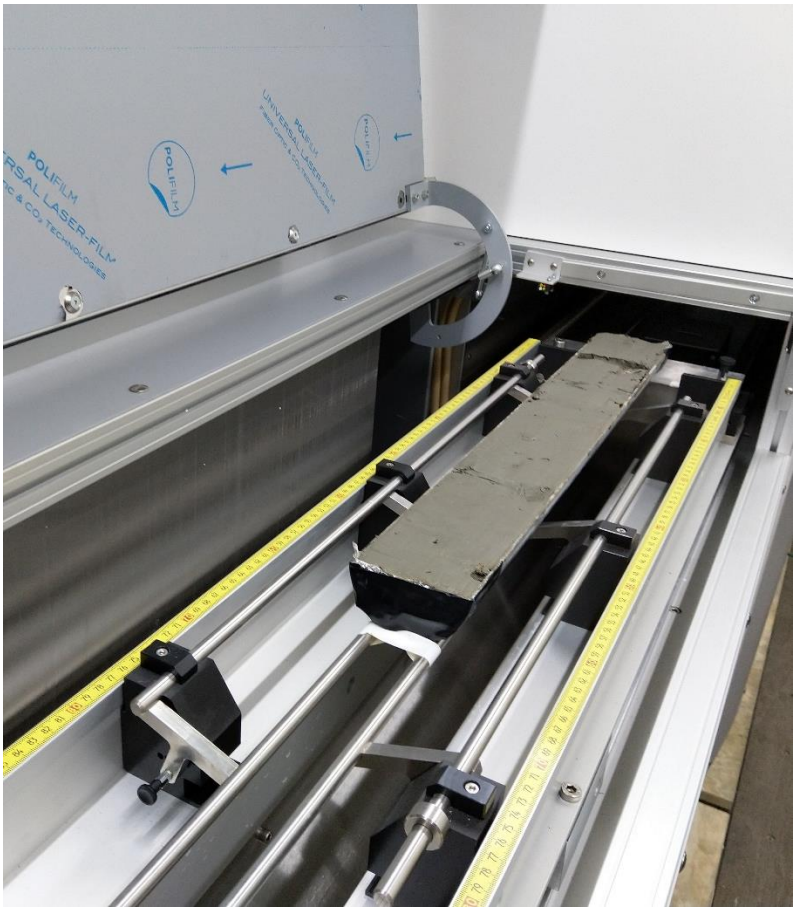

Figure 3.13: Core section prepared for running through the Itrax.

3.6.5 Grain size analysis

Samples for grain size analysis of core CE17/0106 were collected at 0.5 m intervals down to 10.5 m, then increasing to 0.125 intervals to a depth of 13.25 m. Data were collected from these samples using a Mastersizer particle analyser housed in the University of Otago School of Geography. Each of the 42 samples was pre-treated with hydrogen peroxide (H_2O_2) to remove organic matter and sodium hydroxide (NaOH) to remove biogenic silica. 0.6-0.8 g was weighed into a 50 ml centrifuge tube. 10 ml of 30% H_2O_2 was added to each sample then the tubes were placed in a water bath overnight at 50°C with loosened lids. After reacting for a minimum of 8 hours, samples were topped up to 50 ml with Elix water (type two purified water), centrifuged for 10 minutes at 3000 rpm, decanted, and rinsed two additional times with Elix water to remove residual H_2O_2. Next, 10 ml of 1M NaOH was added to each sample, heated for

four hours at 50° C, shaken, heated for an additional 30 minutes and triple-rinsed with Elix water as described above. Finally, 5 ml of 5% sodium hexametaphosphate added to each sample and samples were gently shaken for two hours to disperse particles.

Following pretreatment, samples were loaded into the Mastersizer automatic sampler and analysed following the University of Otago, School of Geography's Westland Lakes protocol (Figure 3.14). Each sample was measured three times and values were averaged. A master data file including all the grain size data was exported from the Mastersizer into the Excel plug-in GRADISTAT, a grain size analysis program that quickly processes and plots grain size statistics including mean, mode, sorting, kurtosis and grain size distribution in both metric and phi units (Blott & Pye, 2001).

Figure 3.14: Mastersizer grain size analysis, samples could be run one at a time or loaded into the automatic sampler on the right to run autonomously.

3.7 Modern environmental analogue

Modern sediment samples were collected from two estuaries on the Otago Peninsula for comparison to the grain size data collected from core CE17/0106. Six locations each from Hoopers Inlet and Papanui inlet were targeted to provide representative environments observed in the CE17/0106 core record.

Sampling was undertaken on the 12$^{th\ of}$ September 2019. Each sample was collected using a set of metal spatulas, from a depth of 10 cm. The environment was then described, and the location recorded on a handheld GNSS. The modern analogue samples were prepared and analysed following the same protocols as the CE17/0106 core samples.

Discrete modern samples were pressed into discs for Itrax analysis of major and trace element chemistry. First, sediments were oven-dried, homogenized using an agate mortar and pestle, and approximately 5 g of homogenized material was mixed with 0.5 ml of polyvinyl alcohol. Next, the mixture loaded into a steel compression cylinder, placed in a hydraulic press, pressed under 5-6 tons of pressure for 30 seconds, removed and placed in an oven at 30° C for 24 hours to cure. The cured discs were then placed in a plastic sample tray and run through the Itrax using the same settings as the CE17/0106 core.

3.8 Radiocarbon dating

During the assembly of the initial geotechnical log and subsequent secondary log, sections of core rich in terrestrial organic material like wood or charcoal were identified for potential radiocarbon sampling.

Horizons for radiocarbon dating were selected based on the abundance of terrestrial organic material identified during logging with samples collected at 1m intervals or where visible changes occurred. Samples were pre-treated at the University of Otago and dated at the GNS Rafter Isotope Laboratory using the Accelerator Mass Spectrometer (AMS) in early 2020. Samples were normalised against a blank sample known to be older than 50 ka; for these samples, a “Queets A” blank was used. Discrete

samples with a maximum thickness of 2 cm were placed in beakers of Elix water on a shaker table to disaggregate the sediment. Sediment in solution was then washed through 250- and 500-micron sieves to isolate larger wood fragments for dating. The 250-500 μm fraction was transferred to a petri dish and smaller wood fragments were picked under a binocular microscope. Wood fragments were washed and scraped clean in Elix water to remove residual sediment or other contaminants. Once clean, samples were transferred into glass test tubes on a 40° C block heater set until completely dry.

Dry samples were weighed, and samples larger than 2 mg were selected for dating. A room temperature acid-alkaline-acid (AAA) pre-treatment was completed in the University of Otago Department of Geology, following the GNS Science Rafter Radiocarbon Laboratory standard operating procedure (SOP). The Rafter AAA room temperature method was selected due to the small size of organic fragments in core CE17/0106, to minimise loss of mass during acid washes which can occur at higher temperatures. A radiocarbon dead (>50 000-year-old) wood standard, 'Queets A', was processed in parallel with the unknowns for use in a blank correction.

AAA pre-treatment required three successive washes in acid, base and acid. For this 0.5 M, HCl was used for both acid steps and 0.1 M NaOH was used for the alkaline wash.

Each sample is placed in a labelled centrifuge tube and dried from the previous Elix washing. 5-8 mL of 0.5 M HCl is added to each tube using a pipette. The samples were then sealed in the tubes and agitated every few minutes for 30 minutes. Any colour change in the solution or sample was recorded. The excess acid was pipetted off and the sample was neutralised to a neutral pH, this was done by diluting the acid with Elix water and centrifuging the samples.

After the neutralisation of the acid, an alkaline wash of 0.1 M NaOH was done. Like the previous acid, wash samples were left for 30 minutes with regular agitation. Any colour change in the solution or sample was recorded. If the solution was not close to clear and colourless, the alkaline wash could be repeated to remove any residual humic acid. The alkaline sample was then neutralised using dilution and the centrifuge.

A final acid wash was done to remove any residual carbonate left on the samples. Any colour change in the solution or sample was recorded. Like the first acid wash, 0.5 M HCl was used. The sample was washed for 15 minutes then neutralised.

Once the final wash was completed, all samples were dried on a digital block heater at 40^{o}C for several hours until the samples were completely dry. Samples were then left to return to room temperature, then sealed to stop condensation occurring in the vials. Samples were then dry weighed to ensure they were large enough samples for combustion. Each sample was then transferred into a glass vial, sealed with foil and lids and shipped to GNS Science Rafter Radiocarbon Laboratory for dating.

Chapter 4 Observations and initial interpretations

4.1 CE17/0106 core logging observations

As part of the NZ SeaRise program, eight cores were collected from strategic locations in low lying areas of Dunedin to increase our understanding of the Quaternary sediments (Figure 3.8). This work also involved the installation of a network of autonomous piezometers for groundwater management. For the purpose of this thesis, based on core recovery and preservation the second core collected for the program (CE17/0106) located in De Carle Park was selected for a detailed sedimentary analysis. CE17/0106 reaches a total depth of 20.7 m where it enters a basement unit of volcanic material, deemed too hard for the sonic drill rig to push through. CE17/0106 can be split into four distinct units (Figure 4.1). These units are distinguished by any structures, grain size, colour or organic material present.

4.1.1 Unit 0 Anthropocene

Unit 0 (U0) is defined by mixed grain sizes and high terrestrial organic content consisting predominantly of roots. The upper metre of this unit was not recovered as a result of the drilling process, only the bottom 1-1.15 m drilling depth was preserved. The 15 cm of U0 that was successfully recovered has been extensively altered by anthropogenic processes and includes hard fill, characterised by brick, concrete mixed with silt and sand (Figure 4.1).

4.1.2 Unit 1

Unit 1 (U1) is the largest unit within the CE17/0106 core, observed between 1.15-11.4 m. U1 exhibits a predominantly silt grain size with some minor fine-medium sand in the deeper sections as well as at the top sharp transition from U1 to U0. The colour of U1 ranges from light to dark grey (Munsell colours 2GLEY3/1 to 1GLEY4/1).

Complete (between 2-4 cm) and fragmented shells are common through the first 4 m of U1 and decrease in abundance with depth. Due to the drilling process, no structures were preserved within U1 (Figure 4.1). Terrestrial organic material such as wood and charcoal fragments are abundant down the length of U1 and foraminifera were identified at 2.35, 3.45 and 8.4 m.

4.1.3 Unit 2

Unit 2 (U2) is observed between 11.4 and 13.3 m. U2 exhibits fine to coarse sand with abundant small wood fragments like the two shallower units. Some larger clasts between 2-5 mm were present in U2; however, no large shell fragments were observed (Figure 4.1). U2 is predominantly light grey to brown (Munsell colours 1GLEY4/1 to 2.5Y4/3). Like U0 and U1, any structures that may have been present in U2 have been obscured by drilling disturbance.

4.1.4 Unit 3

Unit 3 (U3) spans from 13.3 m to the base of the core at 20.7 m. The upper contact between U3 and U2 is gradational from the coarse sand of U2 to weathered volcanic granules. The weathered volcanic material was recovered in a matrix of clay and sand, possibly added as a result of the drilling process. At 17.8 m the core progresses into unaltered crystalline basalt. The basalt was heavily fractured from the drilling process but does not show any evidence of weathering. As the core terminated at this three-metre section of basalt, it was not possible to determine whether it was an *in situ* basaltic flow or a large boulder. The colour for the weathered basalt section of U3 ranged from grey to red (Munsell colours 5YR3/1 to 2GLEY5/1); the basalt itself was black. No shell fragments were present within U3 and little to no wood fragments or charcoal were observed.

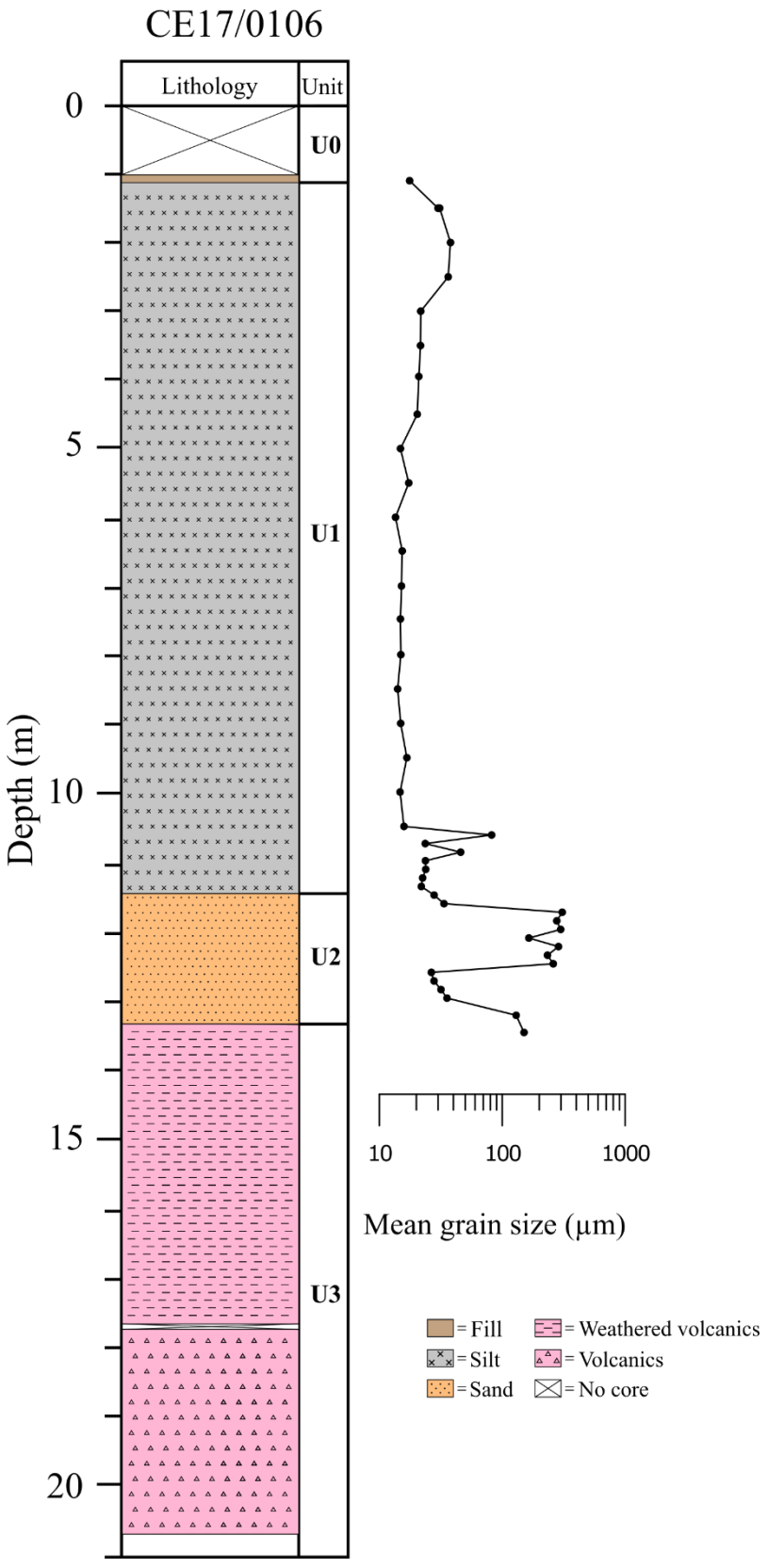

Figure 4.1: Down core plot of mean grain sizes.

4.2 Grain size analysis

Each sample collected from the CE17/0106 core was run through the Mastersizer particle size analyser, producing am individual grain size distribution for each sample (Figure 4.1). The resulting grain size data were input to the Excel plugin GRADISTAT. GRADISTAT was produced by Kenneth Pye Associates Ltd. to rapidly analyse grain size data using both logarithmic and Folk and Ward graphical methods (Blott & Pye, 2001). GRADISTAT then calculated the mean, sorting, skewness and kurtosis of each sample as well as producing grain size distribution histograms.

The CE17/0106 core has several distinct variations in grain size down the core. This variation is represented as the geometric mean within each interval. From 1.1 – 2.5 m (U1) the mean grain sizes increase from 17.6 to 30.9 μm (Figure 4.1). From 2.5 to 4.5 m (U1) the mean grain size remains largely constant at 20 μm. At 4.5 m the mean grain size decreases to 14.8 μm and remains largely constant till 11 m (U1), where it sharply increases to 298.8 μm at 12 m (U2). There is a noticeable drop in the mean grain size at 13 m to 35.50 μm, where it then begins to increase again to 178.1 μm at 13.5 m (Figure 4.1).

4.2.1 Modern analogue sediments

Two tidal inlets on the Otago Peninsula were targeted as modern analogues for the depositional environments observed in the CE17/0106 core (Figure 4.2). Papanui and Hoopers inlets were selected as representative inlets because they exhibit all of the environments inferred from the core record, from a high-energy beach to a low-energy estuarine environment (Table 4.1).

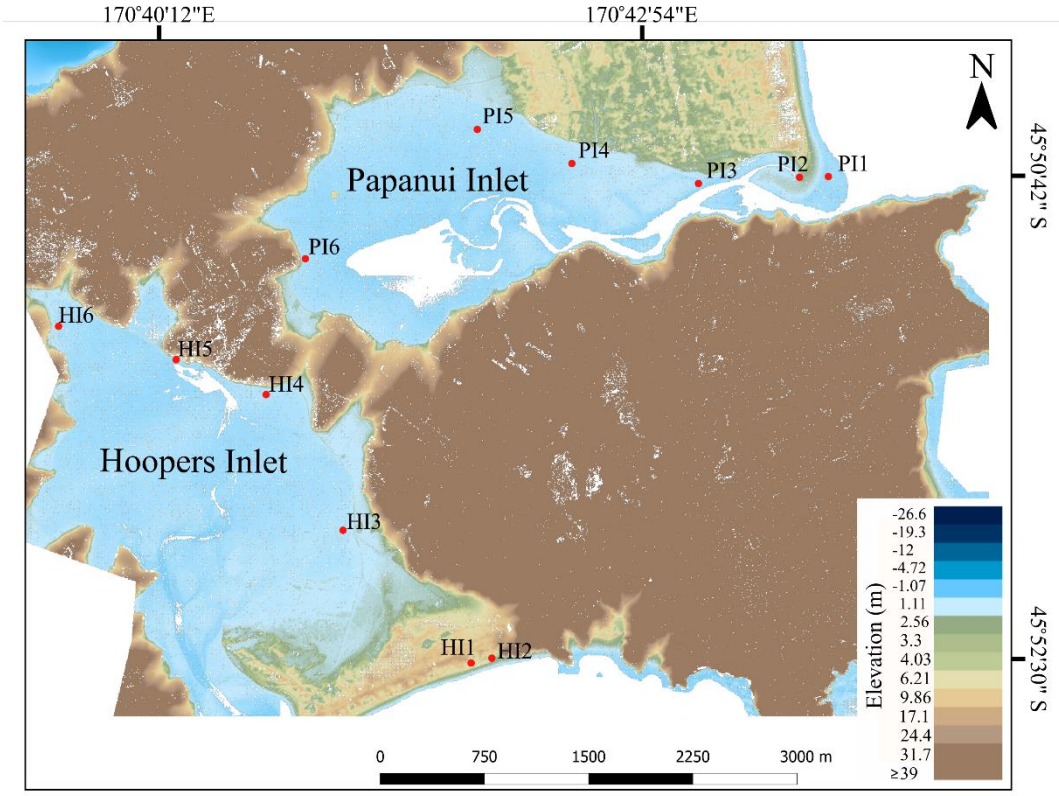

Figure 4.2: Location map of sediment samples collected from both Papanui and Hoopers Inlet.

Table 4.1: Papanui and Hoopers Inlet samples and their description.

Sample ID	Easting	Northing	Sample collection description
HI1	E1421372	N4917214	Middle of sand dune
HI2	E1421522	N4917249	Beach
HI3	E1420450	N4918169	Easutary on leeward side of dunes
HI4	E1419896	N4919146	Mud flat
HI5	E1419249	N4919397	Mud flat
HI6	E1418402	N4919637	Mud flat
PI1	E1423944	N4920715	Sand dune from the mouth of the estuary
PI2	E1423736	N4920709	Leward side of the dune system
PI3	E1423008	N4920665	Sand bar located within the estuary
PI4	E1422097	N4920808	Sandy mud flat
PI5	E1421416	N1421416	Mud flat
PI6	E1420179	N4920123	Mud flat

4.2.2 Grain size distribution

The samples from CE17/0106, as well as the modern analogue samples, were grouped based on their grain size distribution using the location, size and number of peaks to differentiate samples. Six groups were identified and plotted as volume % versus particle diameter in μm. Grain size classification was done using an adapted Wentworth grain size scale (Blott & Pye, 2001) (Figures 4.3 to 4.8).

- Group 1 shows characteristics of a lagoon environment, where shallow bodies of water are protected from a large tidal/wave influence by a beach barrier (Nichols, 2009). The relatively low energy environment of a lagoon allows finer clay- and silt-sized particles to deposit while introducing sand through aeolian sources or through wave action causing washover deposits (Boggs, 2006; Nichols, 2009) (Figures 4.3).

- Group 2 grain size distribution suggests a very low energy depositional environment, where wave influence is minimal (Nichols, 2009). The small fraction of sand can be attributed to aeolian transportation from a surrounding beach or dunes (Figures 4.4).

- Group 3 shows characteristics of intertidal mudflats, likely on the extremities of an estuarine environment, where the energy is low enough to allow silts and clays to deposit but with enough energy from tidal influences to introduce sand (Nichols, 2009). The presence of minor amounts of sand, but predominantly silt and clay, suggests an environment with tidal influence (Figures 4.5).

- Group 4 particles are predominantly fine to medium sand forming the largest peak, with a secondary peak of fine to coarse silt grain sizes. Group 4 exhibits characteristics of a tidal sand bar, where there is a moderate amount of energy to move larger sand particles, but in places, the energy was low enough to allow silt to deposit (Boggs, 2006; Nichols, 2009) (Figures 4.6).

- Group 5 distribution is consistent with a lagoon environment, like Group 1; however, the sand fraction is smaller. Group 5 would require a predominantly low energy environment to facilitate the deposition of silt and clay and has

likely gained its sand fraction from aeolian deposition from the sand barrier enclosing the lagoon or a nearby beach (Boggs, 2006) (Figures 4.7).

- Group 6 samples were collected from a moderate energy intertidal zone towards the mouth of the estuary where tidal influence is most prevalent (Figures 4.8).

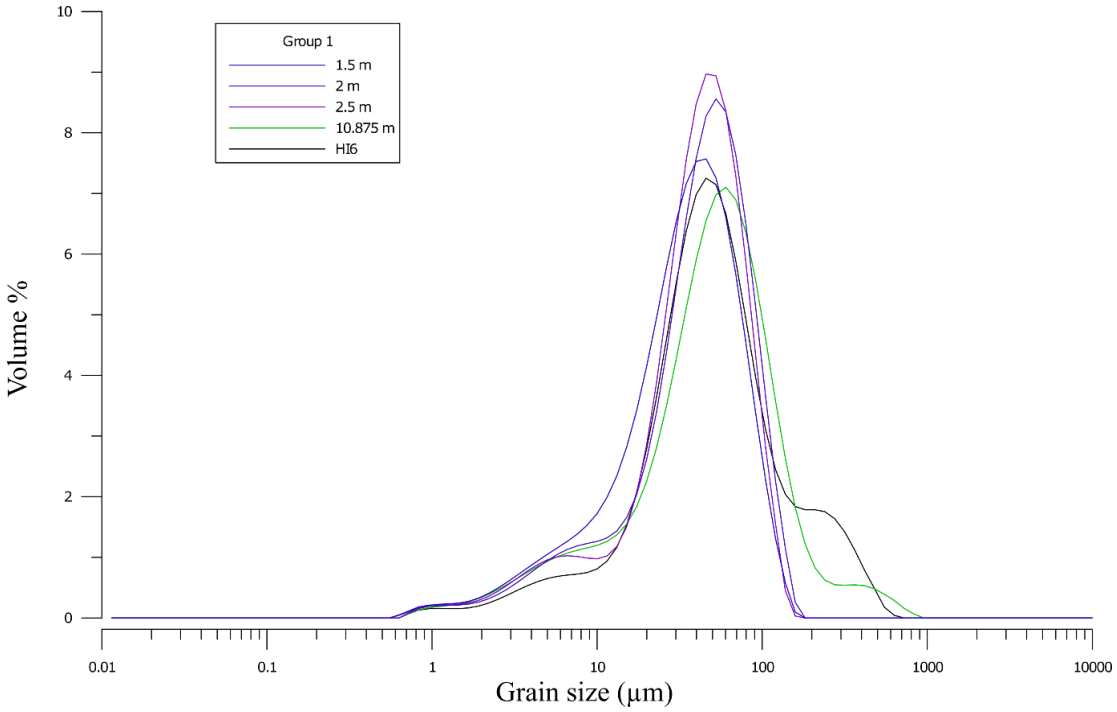

Figure 4.3: Group 1 exhibits a left-skewed normal distribution with the main peak occurring at 60 µm. The majority of particles in Group 1 samples fall in U1, between fine silt and very fine sand; however, fine to coarse sand, as well as clay-sized particles, are also present.

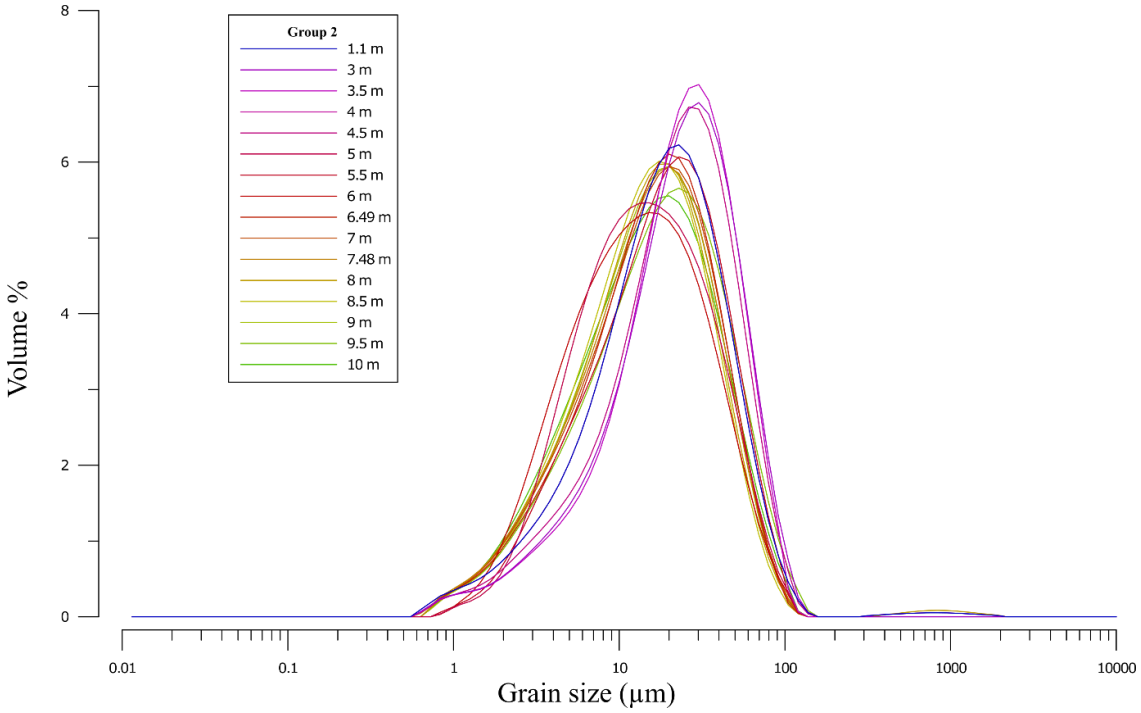

Figure 4.4: Group 2 has a unimodal distribution, peaking at 20 µm. The majority of particles in Group 2 samples encompass U1 and span very fine to medium silt with a minor sand fraction.

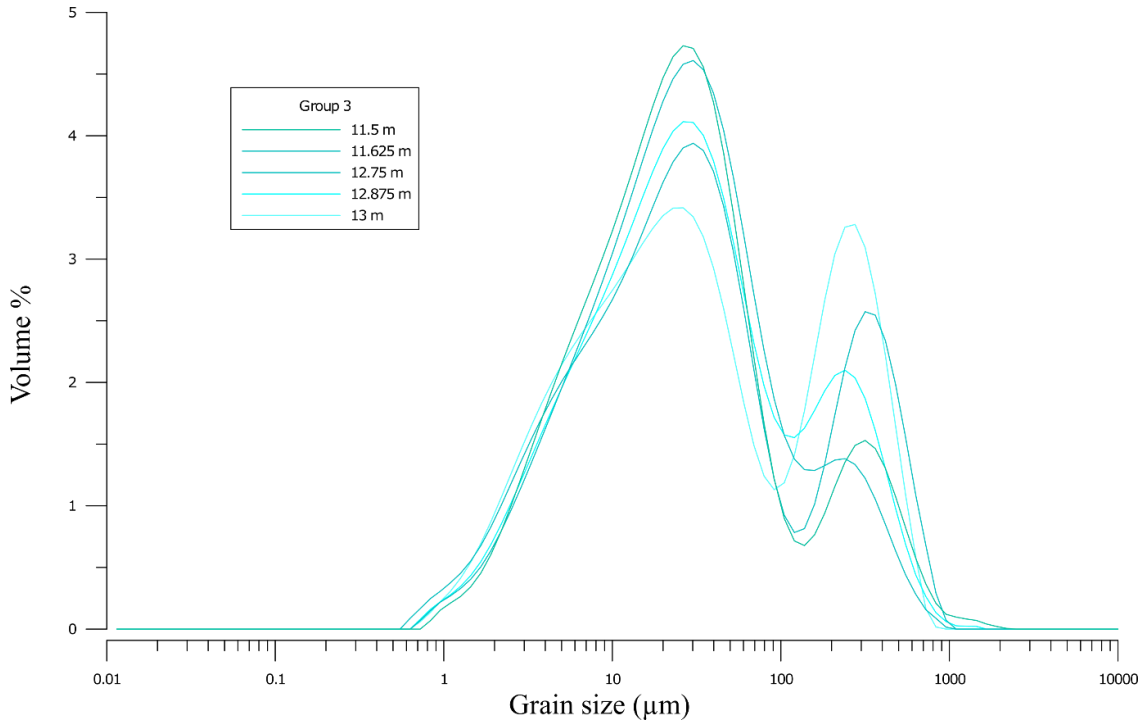

Figure 4.5: Group 3 has a right-skewed bimodal distribution with the largest peak at 20 µm and a secondary peak at 120 µm making up mainly U2. Group 3 particles range in size from clay to very fine sand.

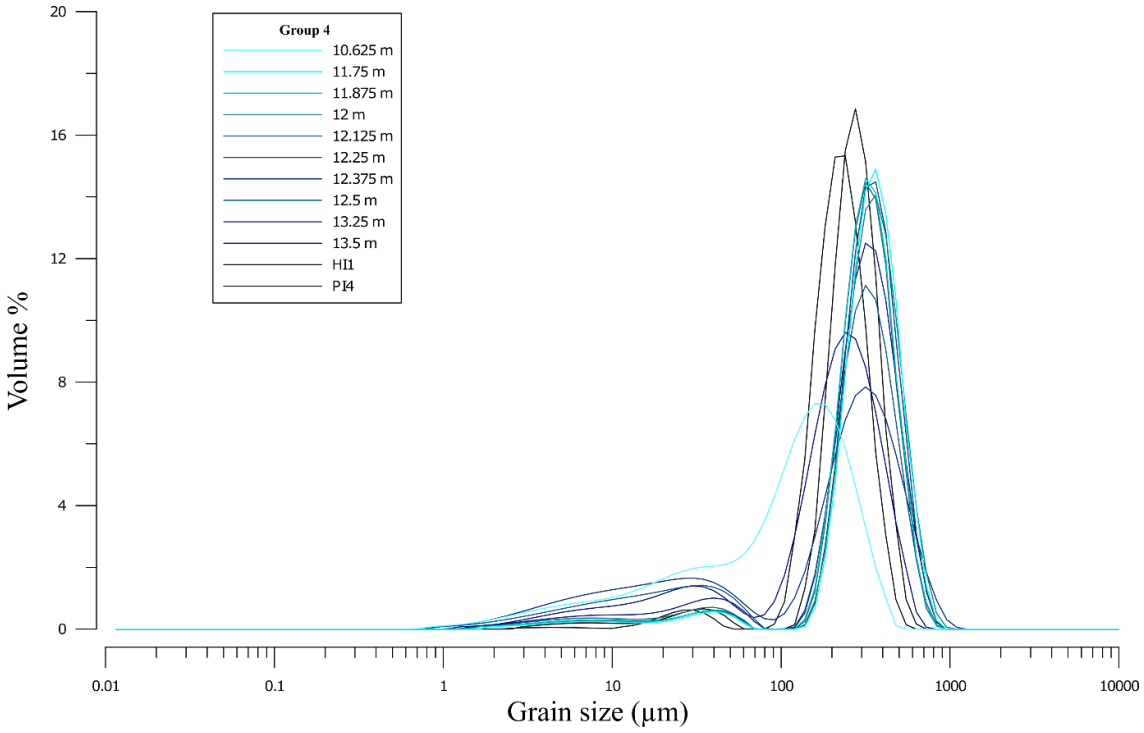

Figure 4.6: Group 4 has a right-skewed bimodal distribution, with the largest peak occurring at 300 µm and a significantly smaller one between 5-40 µm and is mainly U2. Group 4 particles are predominantly fine to medium sand forming the largest peak, with a secondary peak of fine to coarse silt grain sizes.

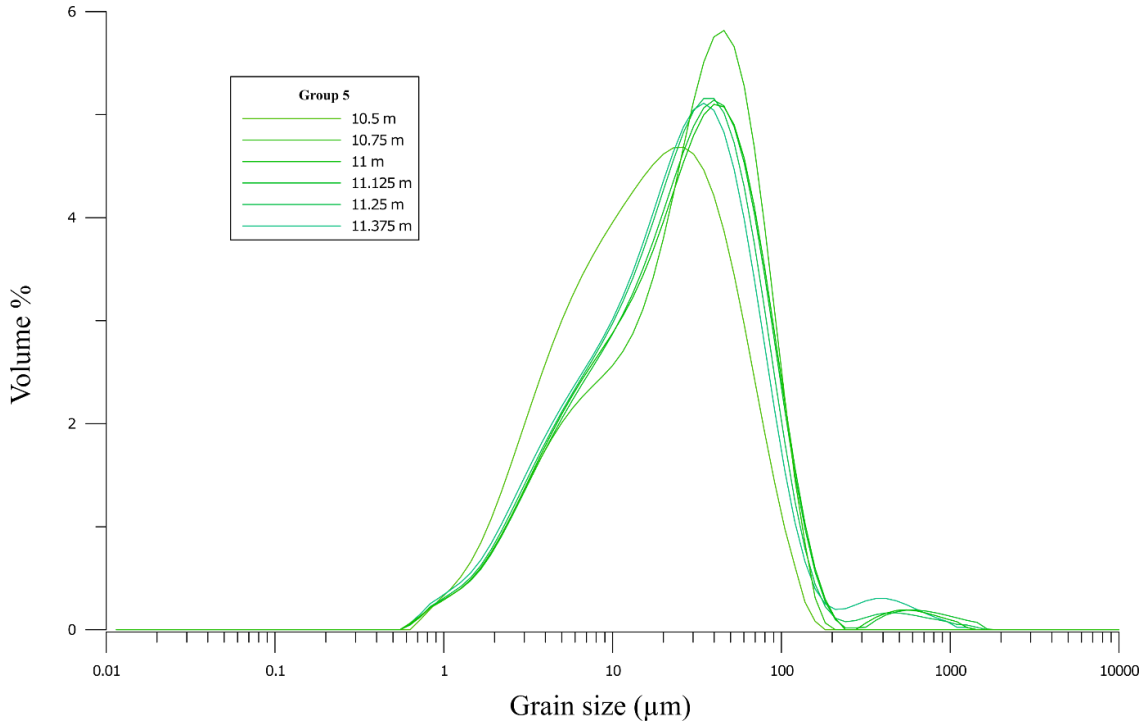

Figure 4.7: Group 5 has a right-skewed bimodal distribution and is predominantly U1. The largest peak occurs at 50 µm and ranges from clay to very fine sand. A secondary smaller peak is seen at 500 µm and is made up of medium to coarse sand.

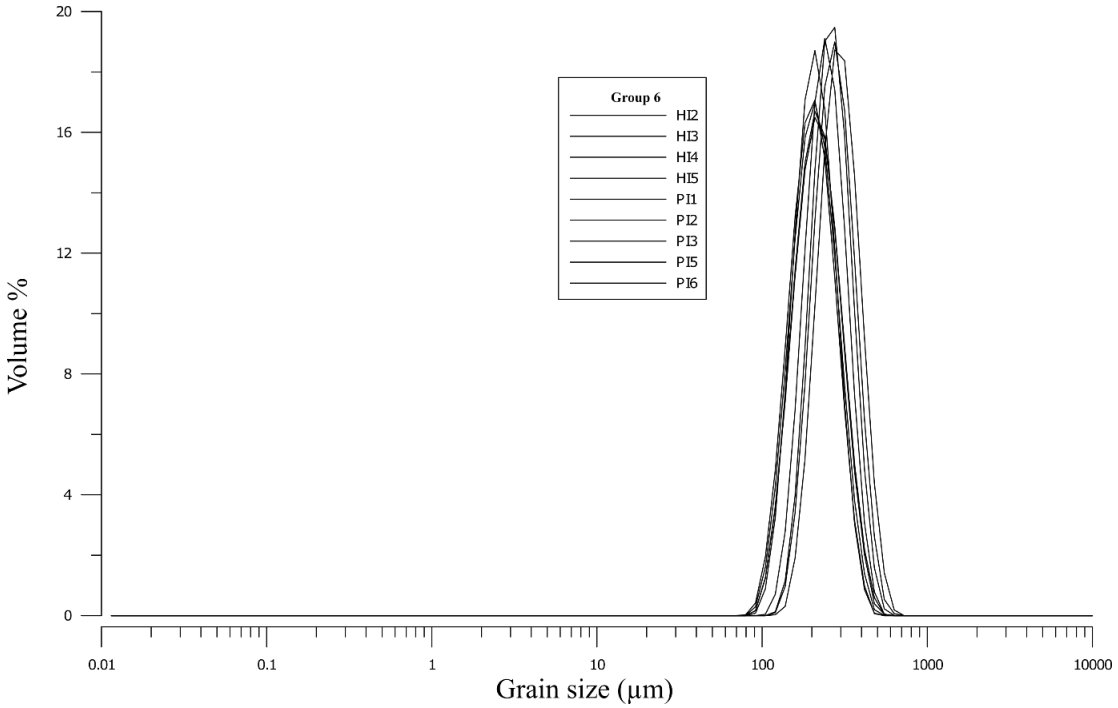

Figure 4.8: Group 6 consists entirely of modern samples. Particles have a unimodal distribution, with a peak at 300 µm and a range from very fine to coarse sand.

4.3 Itrax core scanner results

Reconstructing past environments using elemental ratios often involves assessing a site-specific relationship between elements. A range of elemental ratios were used to discern changes in sedimentation processes, provenance and environmental changes. For this reason, multiple ratios were used to infer similar types of environmental changes, to strengthen interpretations made from the CE17/0106 core Spikes were identified when the scanner directly landed on shell fragments, fragments of terrestrial organic matter or water. These spikes could be removed by analysing core images collected during the scanning process and removing the corresponding data adversely impacted by the core surface.

To minimise the influence of variations in water content or amorphous organic matter, Itrax counts per second (cps) for each element of interest were normalised against either

the incoherent scatter or the cps for another element from the same XRF measurement spot (Löwemark et al., 2011).

4.3.1 Organic abundance ratios

Bromine/incoherent scatter (Br/Inc) and incoherent scatter/coherent scatter (Inc/Coh) ratios are used to show relative levels of organic material within the core. The first 0.15 m of core encompassing U0 (from 1-1.15 m) exhibits a very low Br/Inc ratio value <0.015. This rapidly increases to a peak of 0.09 at 1.23 m and then decreases gradually to 2 m where it levels out (Figure 4.9). The relative abundance of organic material indicated by the Br/Inc ratio shows a gradual increase in organic content with several small peaks throughout U1. It then begins to decrease to background levels from 9 m, with two distinct peaks at 11.8 m and 12.2 m. Br/Inc broadly indicates an overall decrease in organic abundance with depth (Figure 4.9).

The Inc/Coh ratio is the amount of incoherent vs. coherent scatter within the core and can be used to indicate the relative abundance of the organic material present (Croudace & Rothwell, 2015). The Inc/Coh ratio much like the Br/Inc indicates an initial high abundance of organic material gradually decreasing at 2 m (from U0 transitioning to U1) (Figure 4.9). The relative abundance of organic material then gradually increases until 8.5 m where it begins to decrease till the transition from U1 to U2. A large multipeak interval between 11.8 and 12.2 m coincides with the two peaks observed in the Br/Inc (Figure 4.9).

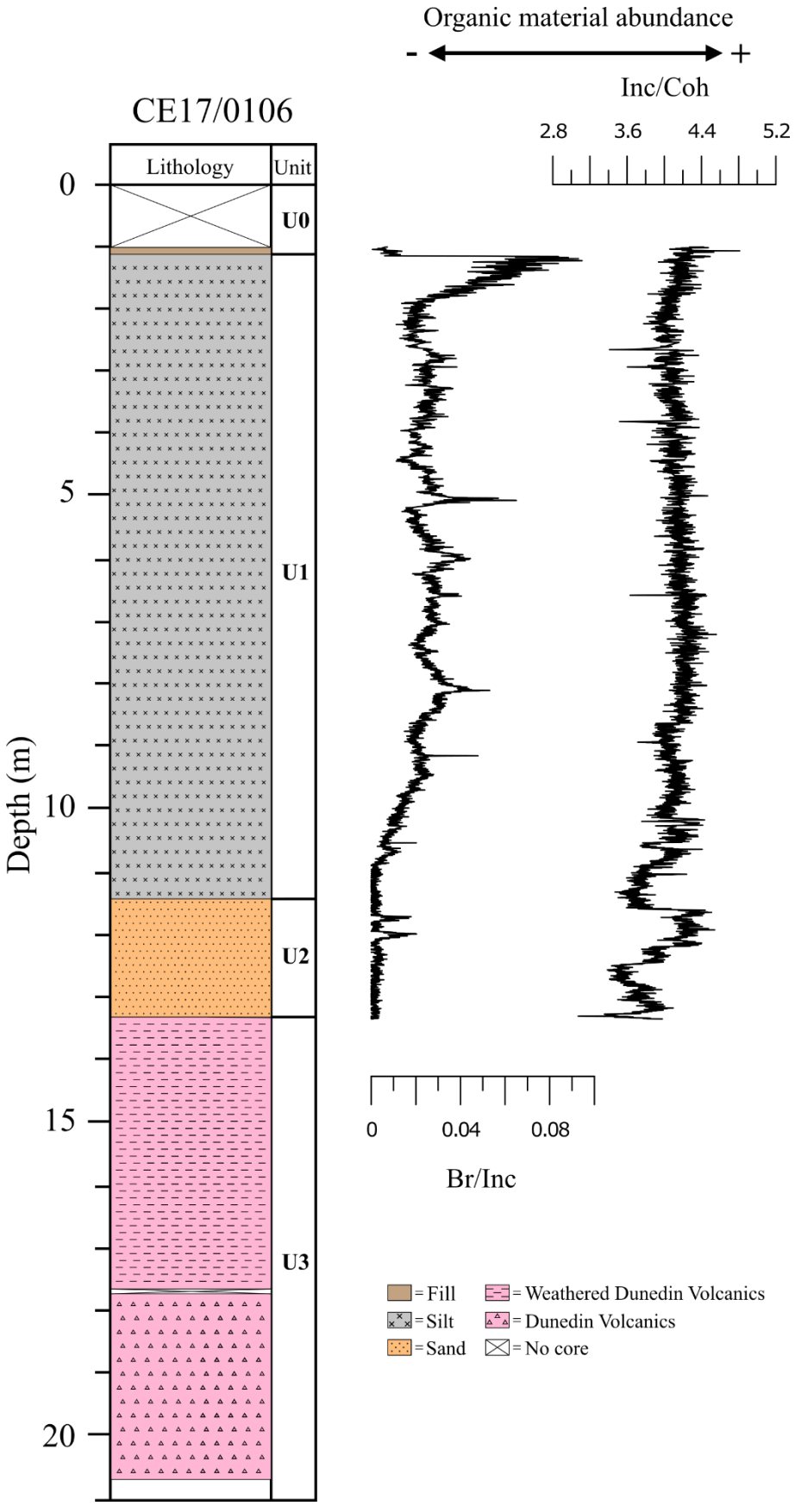

Figure 4.9: Itrax organic proxy ratios.

4.3.2 Terrestrial versus marine ratios

Distinguishing the provenance of sediment within the core record can be achieved through numerous elemental ratios, including both Ca/Ti and Sr/Ti (Croudace & Rothwell, 2015). Both calcium (Ca) and strontium (Sr) are attributed to biogenic marine biogenic carbonates such as plankton and foraminifers (Ingram et al., 2010). Ca/Ti and Sr/Ti are plotted to indicate relative changes in biogenic- to terrigenous-sourced sediments. Potassium is normalised against the incoherent scatter (K/Inc) and is used to indicate changes in the sediment supply (Croudace & Rothwell, 2015; Hepp et al., 2006).

Multiple elemental ratios are used as proxies for similar environmental changes to provide a more robust interpretation than would be possible from a single ratio. For example, some extreme peaks in Ca/Ti can be attributed to spot measurements of shell fragments, leading to a peak in the Ca count. The initial 0.15 m of the core (U0) exhibits relatively high peaks for Ca/Ti and Sr/Ti, which decrease across the U0 to U1 transition then increase again, peaking at 2 m (Figure 4.10). Below the peak, all three proxies gradually decrease to 6 m where they level off. This indicates a high input of biogenic material, gradually decreasing with depth. From 6 to 10.1 m (U1) the ratio values remain low, indicating a decrease in biogenic input and an increase in terrestrial sourced material (Figure 4.10). As the core transition into U2, there are several larger peaks than U1 suggesting episodic increases in biogenic input followed be terrestrially sourced material.

The K/Inc ratio indicates an initially low input of terrestrial material, coinciding with the increase in biogenic material inferred from the other three proxies, followed by an increase in terrestrial material at the bottom of U0 (Figure 4.10). Following this increase K/Inc then abruptly drop at 2 m, gradually increasing again till 3 m and then decreasing slightly to 4 m. A period of increasing terrestrial input is observed between 4 and 9.5 m, mirroring the decrease in biogenic material observed in the other proxies. K/Inc values then broadly decline as the core transitions from U1 into U2, K/Inc covaries with the previous proxies and indicating alternating periods of increased terrestrial input followed by periods of increased biogenic input (Figure 4.10).

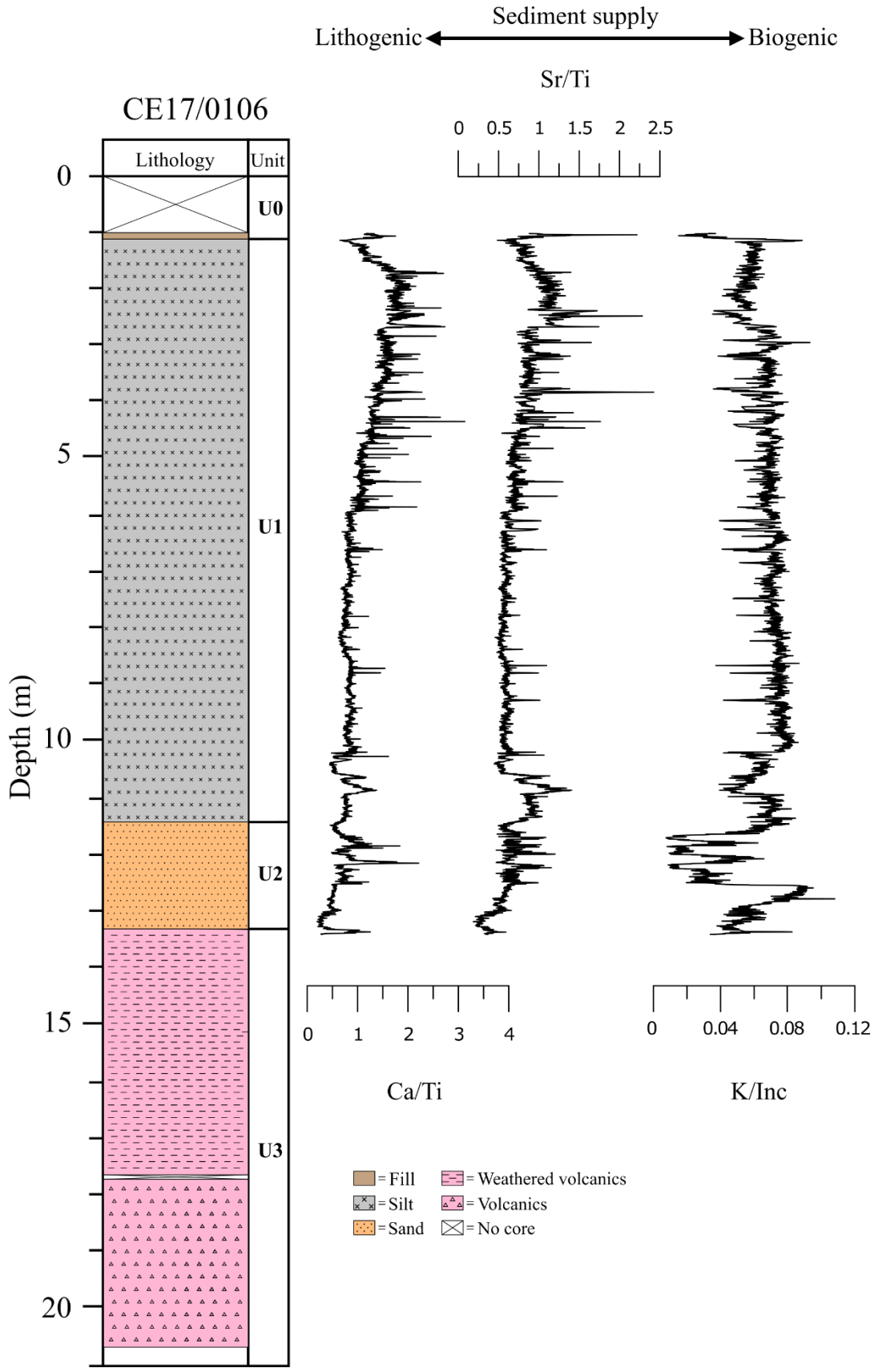

Figure 4.10: Lithogenic versus biogenic sediment supply Itrax proxies.

4.3.3 Grain size ratios

Elemental ratios can be coupled with discrete grain size measurements to identify downcore changes in particle size. Because zirconium (Zr) more common in coarse-grained sediments and rubidium (Rb) is more common in clays, the Zr/Rb ratio can be used as a grain size proxy (Croudace & Rothwell, 2015; Liu et al., 2006; Minjie et al., 2011). In CE17/0106, the Zr/Rb ratio coincides well with discrete mean grain size measurements down to 10.5 m. The coarse spacing of grain size samples does not allow direct comparison below 10.5 m where the frequency of Zr/Rb variations is higher; however, it does indicate rapid changes in grain size throughout U2, also seen in the mean grain size data (Figure 4.11).

Higher values of the titanium (Ti) to aluminium (Al) ratio can be attributed to coarser-grained sediments and can be used in conjunction with other proxies to infer rapid particle size change (Croudace & Rothwell, 2015). The initial Ti/Al ratio was adjusted using a 5-point moving average to remove the extreme peaks and troughs. The first 11.5 m maintains consistent values mirroring the Mastersizer mean grain size (Figure 4.11). Values increase past 11.5 m till 13.5 m where they decrease to the level of the first 8.5 m with only two minor peaks (Figure 4.11).

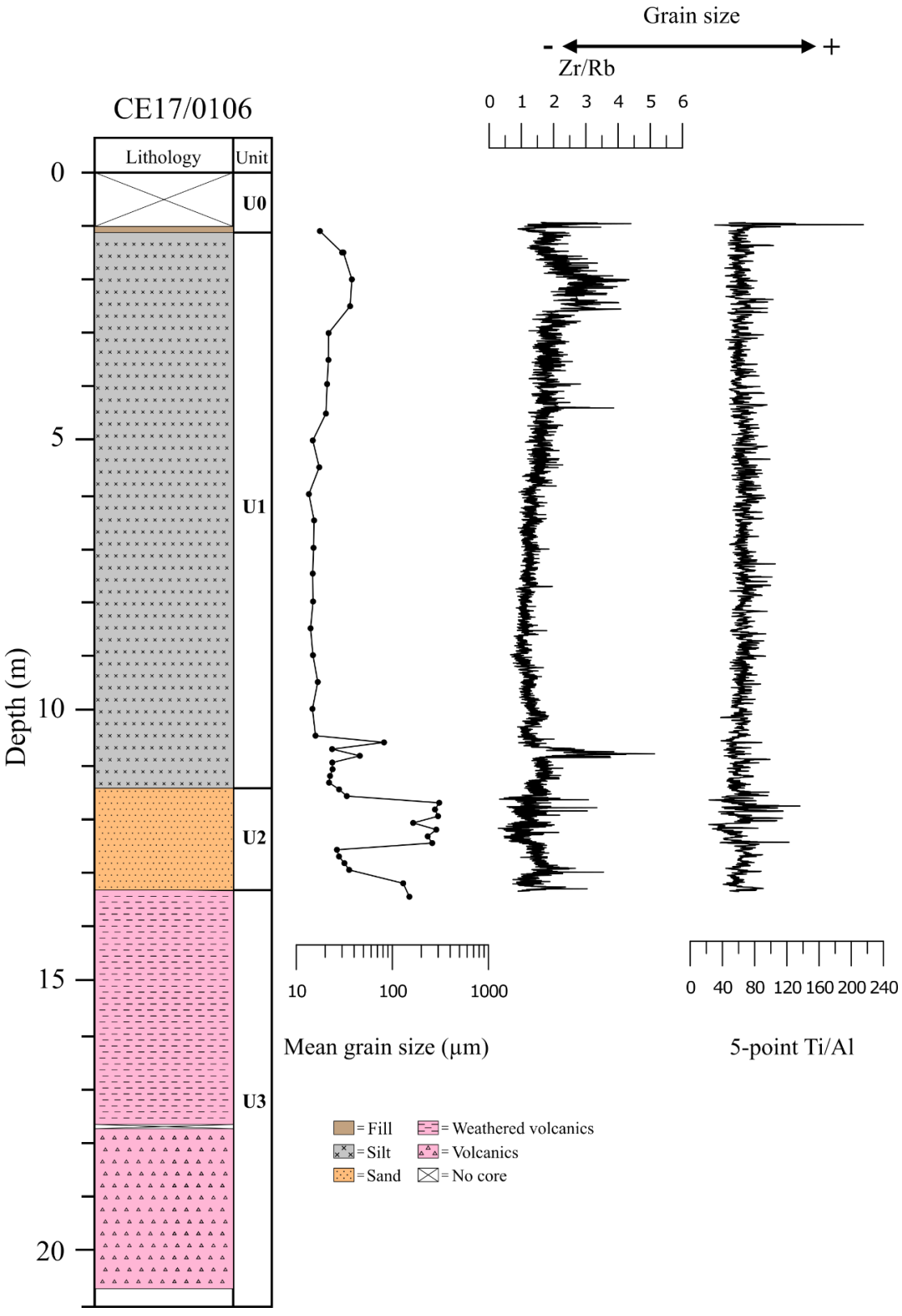

Figure 4.11: Grain size proxies plotted against average grain size measurements down core.

4.3.4 Anthropogenic markers in the sediment record

The impact of the anthropogenic activities on sediments in South Dunedin is evident within the CE17/0106 core. Two heavy metal indicator elements used to illustrate the pollution on the sediment record, arsenic (As) and lead (Pb) (Molamohyeddin et al., 2017), were compared in shallow and deeper intervals of the sedimentary column by plotting downcore As/Inc and Pb/Inc ratios. Due to drilling disturbance, only 0.15 m of anthropogenic material in U0, (from 1-1.15 m drilled depth) was recovered. As the Itrax measured in counts per second and not parts per million (ppm) these ratios are not concentrations but still quantitative measures to illustrate the comparative difference between core sections (Figure 4.12). Pb/Inc indicates large peaks from 1-1.15 m then drops off to background levels where the core transitions from U0 to U1 (Figure 4.12). As/Inc indicates large peaks from 1-1.125 m then drops abruptly with a slight increase from 1.15 to 1.2 m, then dropping down again (Figure 4.12).

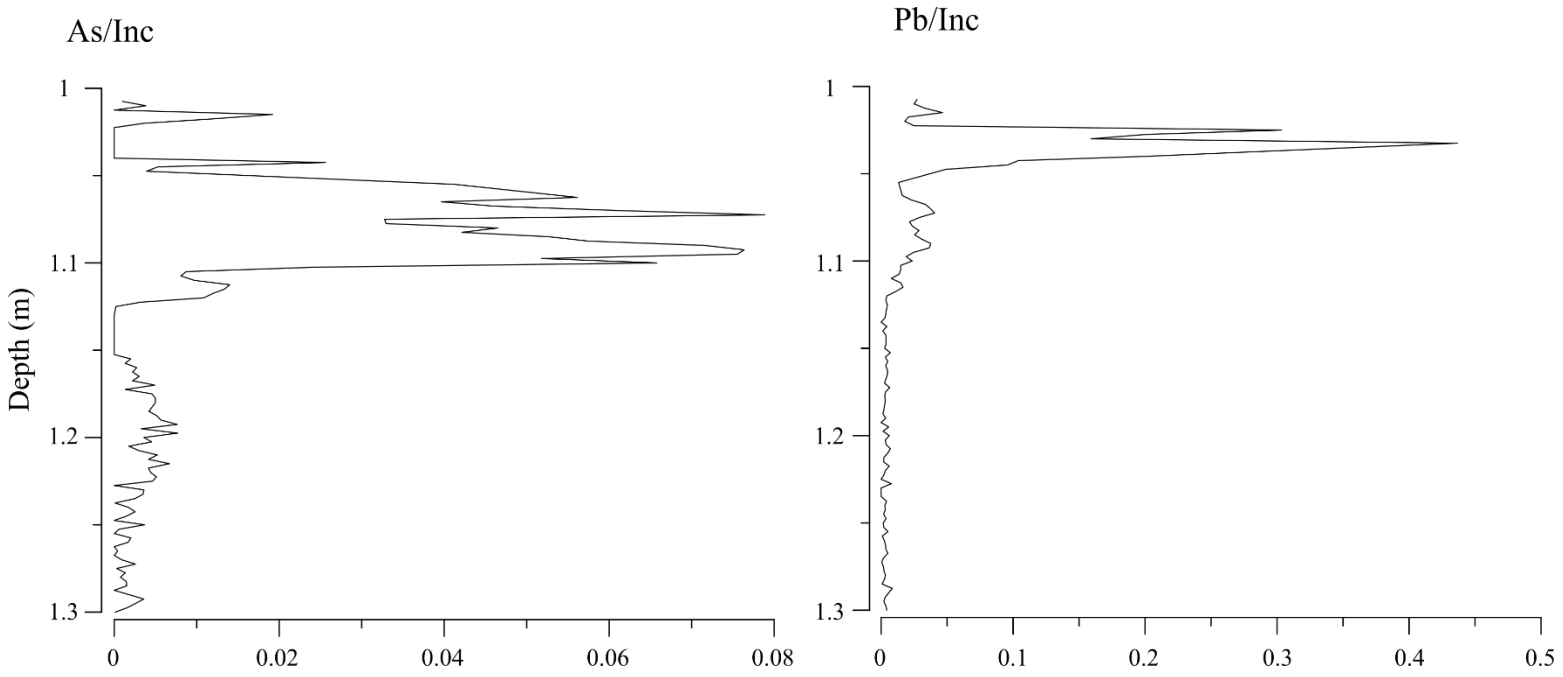

Figure 4.12: As/Inc ratio for 1-1.3 m core depth. From 1-1.15 m it shows comparatively extreme levels of As/Inc when compared to 1.15-1.3 m of the core which shows background levels. Pb/Inc indicates large peaks from 1-1.15 m drops off to background levels abruptly.

4.4 Facies differentiation

Based on the range of proxies outlined above, five facies were differentiated in core CE17/0106. Each facies has unique characteristics not identifiable during the visual inspection and initial logging, which indicate different environments of deposition. These differ from the units which were differentiated from just the drill logs and visual descriptions.

4.4.1 Facies 0

Facies 0 (F0) encompasses the first 0.15 m of core recovered from 1-1.15 m drilled depth (Table 4.2). F0 exhibits low organic material abundance as well as a primarily lithogenic sourced sediment (Figures 4.9 and 4.10). F0 also has comparatively high arsenic and lead concentrations attributed to anthropogenic influences on the immediate subsurface which then dropped off to background levels (Figure 4.12). Building materials such as brick and concrete were observed in the initial log of the core throughout F0, which can be attributed to the land reclamation process where foreign materials were introduced to raise ground levels. Only one-grain size measurement was collected from F0 which returned a predominantly medium to coarse silt, with some minor very fine sand (Figure 4.1).

4.4.2 Facies 1

Facies 1 (F1) spans from 1.15 – 3 m depth. F1 has a comparatively high wood and charcoal fragment abundance as well as a high biogenic sediment supply (Table 4.2). From the base of F0, the mean grain size increases downcore to approximately 40 μm then abruptly decreases across the F1/F2 transition (Figure 4.1). Grain size samples collected from F1 fall into group 1 of the grain size distribution graphs, with a grain size range of medium silt to very fine sand (Figure 4.3).

Secondary occurrences of F1 can be observed from 10.5 – 10.62 and 10.7-11.4 m. An increase in the mean grain size can be observed from F2, which is mirrored by the

Zr/Rb grain size proxy (Figure 4.11). A temporary increase in the biogenic sediment supply is also seen, which coincides with the previous occurrence of F1. The depositional environment of F1 would require a moderate amount of energy to move larger sand particles, but it would be predominantly low energy to allow silts to deposit, suggesting an intertidal mudflat paleoenvironment (Boggs, 2006; Nichols, 2009).

4.4.3 Facies 2

Facies 2 (F2) makes up the largest section of the core spanning from 3 – 10.5 m (Table 4.2). The mean grain size of F2 ranges from 20-30 μm with all the grain size distribution samples falling into group 2 (Figure 4.4). The grain size proxies mirror this minimal change in grain size down the core (Figure 4.1). Terrestrial versus biogenic sediment supply proxies indicate a general decrease in biogenic sediment contribution from the overlying facies, moving towards a more terrestrially dominated sediment supply (Figure 4.10). Despite minor peaks in organic material abundance ratios, these proxies remain relatively invariant through F2, then begin to decline again at the transition to back to F1 at 10 m (Figure 4.9). The dominance of silt-sized grains suggests a very low energy depositional environment, where wave influence is minimal (Nichols, 2009). The small fraction of sand present could be attributed to aeolian transportation from a surrounding beach or dunes.

4.4.4 Facies 3

Facies 3 (F3) spans 10.62-10.7 and 11.4-13.3 m and exhibits that largest grain size in the CE17/0106 core, with most samples falling into group 4 (Table 4.2). Some of the samples; however, fall into group 3, which also had a bimodal distribution. Both peaks of group 3 coincide with group 4, with group 3 having higher silt proportion and group 4 higher sand. Both group 3 and 4 have a greater proportion of >100 μm grains than any other grain size distribution group; this is mirrored in the grain size proxy ratios (Figure 4.11). Multiple peaks of high organic abundance are observed within F3; however, these decrease to the lowest values observed in the core as it progresses to F4. Terrestrially sourced material is dominant in F3, except for a few distinct peaks that

coincide with peaks in organic abundance ratios, attributed terrestrial organic materials (Figures 4.9 and 4.10). The depositional environment for F3 was probably influenced heavily by tidal cycles, introducing the larger sands; however, the presence of finer silts requires periods of very low energy to allow deposition (Nichols, 2009).

4.4.5 Facies 4

Facies 4 (F4) encompasses the volcanic section of the CE17/0106 core from 13.3 to the end of the core at 20.7 m. Due to the inability to split F4 and run it through the same XRF analysis as the previous sections, its differentiation is based on visible observations. F4 consists of heavily fractured basalt (fracturing caused by the drilling process). At the top of F4, the basalt appears weathered but progresses downcore to un-weathered material (Table 4.2).

Table 4.2: CE17/0106 facies descriptions

Facies	Depth occurrences	Physical descriptions	XRF/Grain size properties	Paleoenvironmental interpretations	References
Facies 0	1-1.15 m	Hard fill material, including brick and masonry. Dark brown colour with some minor silt and sand present.	High As and Pb counts. High wood fragment abundance.	Anthropogenic hard fill deposited during land reclamation.	(Molamohyeddin, Ghafourian and Sadatipour, 2017)
Facies 1	1.15-3 and 10.5-11.4 m	Structureless dark grey silt with some fine sand.	High wood fragment abundance. Mean grain size of 40 µm.	Estuarine, low energy environment	(Anthony and Héquette, 2007) (Croudace and Rothwell, 2015)(Nichols, 2009)
Facies 2	3-10.5 m	Structureless dark grey silt, with minor very fine sand.	Mean grain size from 20-30 µm. Increasing terrestrial sediment supply. Decreasing wood fragment abundance.	Estuarine, low energy environment	(Anthony and Héquette, 2007) (Croudace and Rothwell, 2015)(Nichols, 2009)
Facies 3	11.4-13.3 m	Structureless grey sand with silt.	Low wood fragment abundance, dominantly terrestrially sourced material. Greatest >100 µm grainsize volume of all facies.	Tidal zone, high energy environment	(Anthony and Héquette, 2007) (Croudace and Rothwell, 2015)(Nichols, 2009)
Facies 4	13.3-20.7 m	Initially weathered, but predominantly unaltered basalt.		Erupted volcanic material from the Dunedin Volcanic Group	(Martin, 2000)

4.4.6 Environmental comparisons between CE17/0106 and modern estuarine environments

Discrete modern samples collected from Hoopers and Papanui inlets were analysed on the Itrax core scanner and Mastersizer particle size analyser for comparison to measurements made on the core. Grain sizes from 9 of 12 modern samples fell into group 6 (Figure 4.8) with the remaining three, HI6 (Group 1), PI4 and HI1 (both group 4) falling into grain size distributions observed in the core. Down core plots of both Ca/Ti (lithogenic versus biogenic sediment sources) and Zr/Rb (grain size variation) plotted with modern samples on top illustrate similarities and differences (Figures 4.13 and 4.14). Sample HI6 coincides with the Ca/Ti proxy, intersecting values in F1, as do Group 1 grain size values (Figures 4.3 and 4.13). The HI6 Zr/Rb ratio again plots within both occurrences of F1 in core CE17/0106. Both Ca/Ti and Zr/Rb values for HI1 are elevated in comparison to downcore measurements. The Ca/Ti value of PI4 is higher than any values measured in the core; however, it does intersect values at the top of F1 and the top of F2, coinciding with grain size measurements from Group 4 (Figure 4.6). All the Papanui Inlet samples indicate a greater biogenic sediment source with high Ca/Ti values (Rothwell & Croudace, 2015). All inlet samples except for HI1 intersected the downcore Zr/Rb curve; however, a comparative relationship between modern samples and the core, when there is no correlation with grain size measurements, does not create a strong analogue (Figure 4.14).

The narrow range of lithologies represented by the modern samples limits their potential for direct comparison to core CE17/0106. Despite this, samples HI6 and PI4 could offer modern analogues for depositional environments represented core.

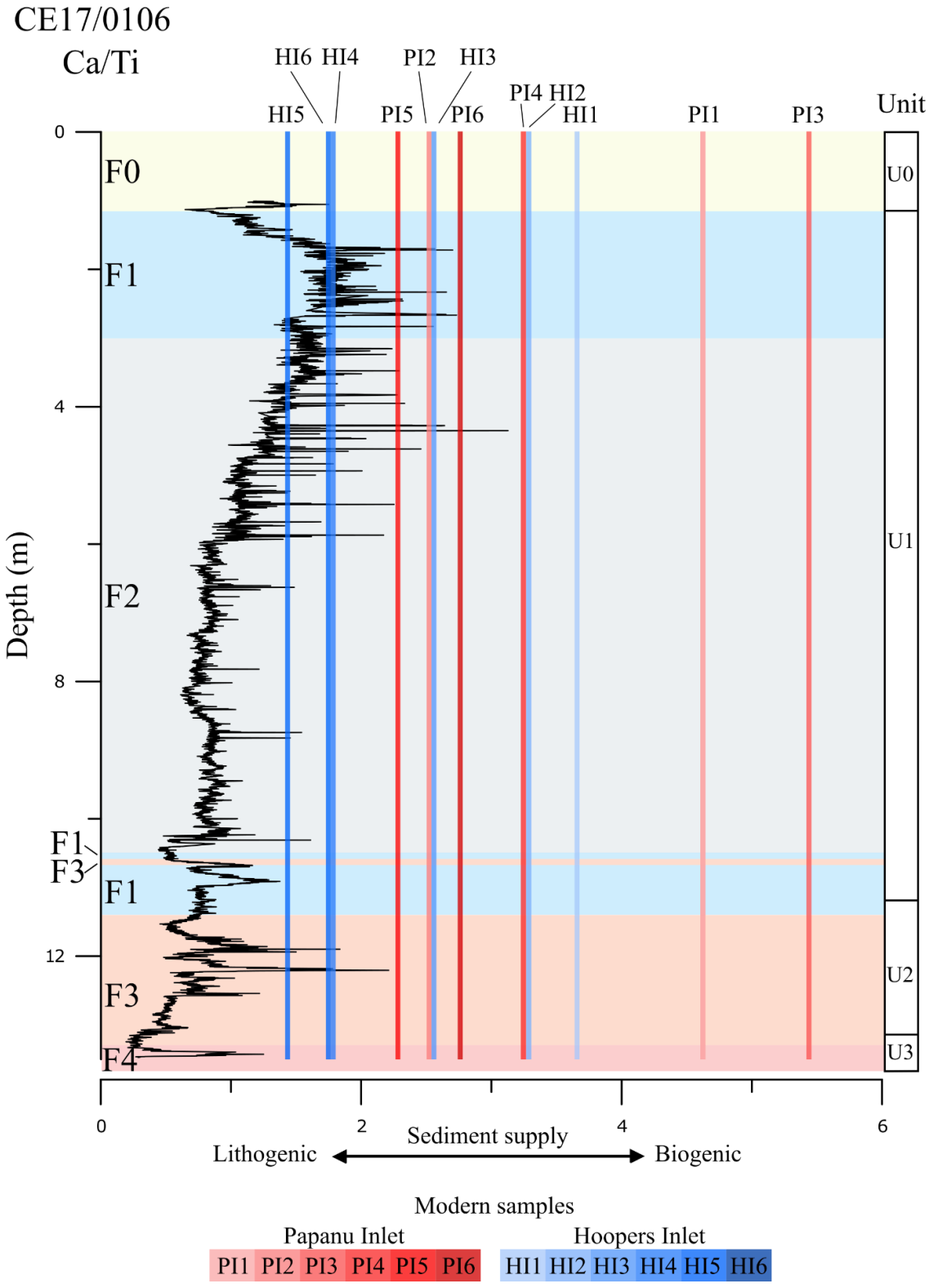

Figure 4.13: Down core Ca/Ti proxy measurements collected from the CE17/0106 core, with modern samples collected from Hoopers and Papanui inlets plotted on top.

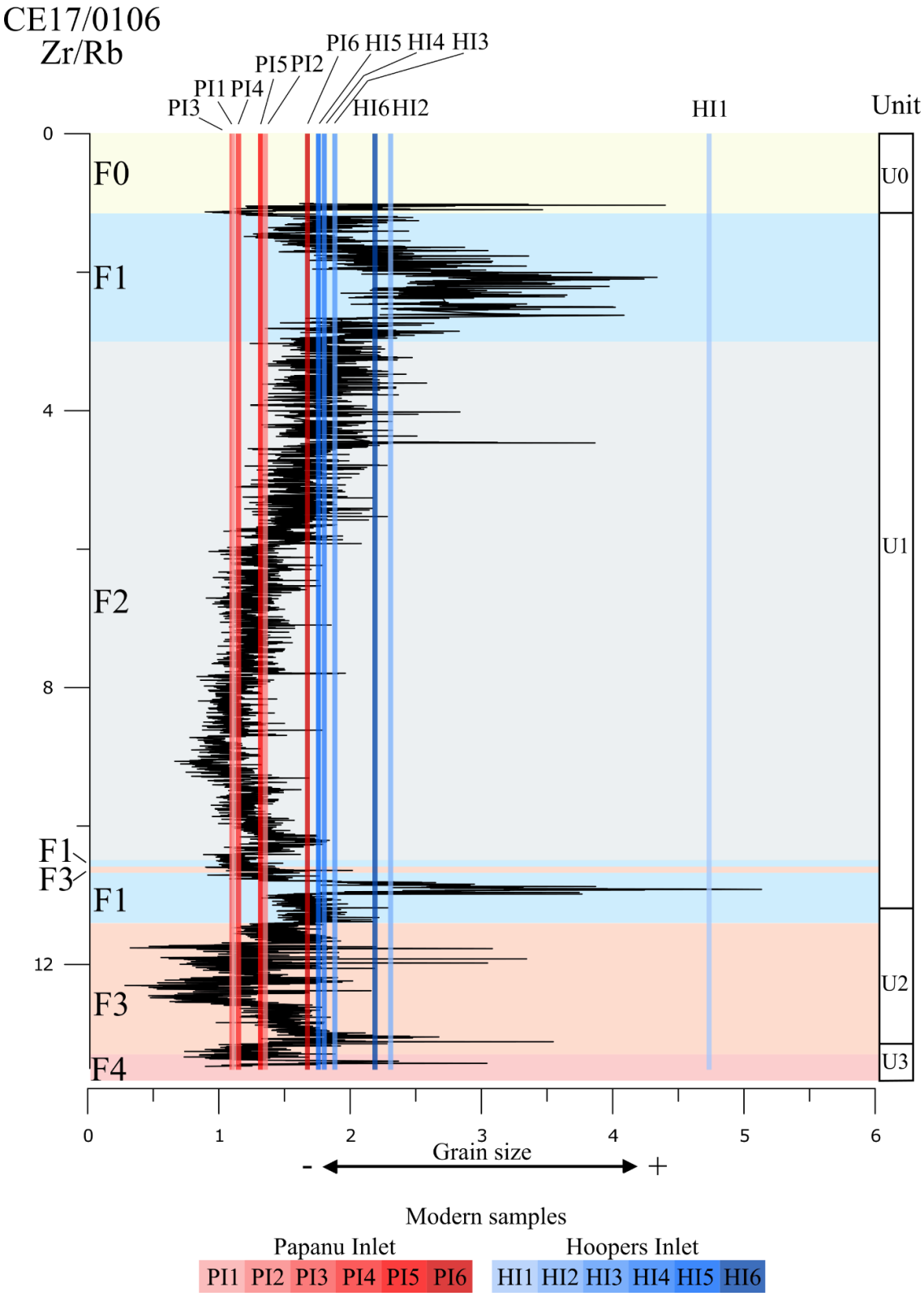

Figure 4.14: Down core Zr/Rb proxy measurements collected from the CE17/0106 core, with modern samples collected from Hoopers and Papanui inlets plotted on top.

4.5 CE17/0106 age model development

Radiocarbon dating on wood fragment samples along the length of the core was used to produce an age-depth model for the CE17/0106 core. Duplicate wood samples were processed from the same sieved fractions to evaluate the influence of reworking. Radiocarbon samples for both the CE17/0106 and Edgar Centre cores were calibrated against the SHCal13 Southern Hemisphere calibration (Hogg et al., 2013), a Southern Hemisphere calibration curve constructed from New Zealand and Australian dendrochronological records, to reduce sample age errors and allow the conversion from a conventional radiocarbon age to a calendar age in years before present (Cal yr BP), where present is the year 1950 (Hogg et al., 2013) (Table 4.3).

Table 4.3: Radiocarbon dates collected from wood fragments found in the CE17/0106 core. Each sample is presented with a Conventional Radiocarbon Age (CRA) and 1 and 2 sigma confidence intervals for the calibrated age (Cal yr BP).

OU_ID	Rafter ID	Depth (cm	CRA	CRA error	1 sigma calibrated age	2 sigma calibrated age	Calibrated age (Cal yr BP)	Cal yr BP error
OU_2019_44	R 41390/2	140	3727	23	4083.0 BP to 4025.0 BP (62.4% of area)	4142.0 BP to 4125.0 BP (3.2% of area)	4020.5	53.5
					4013.0 BP to 3976.0 BP (37.6% of area)	4093.0 BP to 3914.0 BP (96.8% of area)		
OU_2019_45	R 41390/3	525	5901	26	6727.0 BP to 6650.0 BP (100% of area)	6750.0 BP to 6601.0 BP (95.4% of area)	6688.5	38.5
						6589.0 BP to 6564.0 BP (4.6% of area)		
OU_2019_46	R 41390/4	525	5926	25	6735.0 BP to 6669.0 BP (100% of area)	6781.0 BP to 6761.0 BP (5.8% of area)	6702	33
						6758.0 BP to 6639.0 BP (94.2% of area)		
OU_2019_47	R 41390/5	755	6311	95	7279.0 BP to 7149.0 BP (62.7% of area)	7417.0 BP to 7346.0 BP (7.0% of area)	7148.5	130.5
					7125.0 BP to 7018.0 BP (37.3% of area)	7342.0 BP to 6948.0 BP (93% of area)		
OU_2019_48	R 41390/6	1045	7182	28	7995.0 BP to 7988.0 BP (10.4% of area)	8018.0 BP to 7928.0 BP (94.4% of area)	7967	28
					7983.0 BP to 7939.0 BP (89.6% of area)	7893.0 BP to 7873.0 BP (5.6% of area)		
OU_2019_49	R 41390/7	1130	8150	29	9085.0 BP to 9050.0 BP (41.5% of area)	9123.0 BP to 8994.0 BP (100% of area)	9043	42
					9033.0 BP to 9001.0 BP (58.5% of area)			
OU_2019_50	R 41390/8	1130	8074	30	9011.0 BP to 8970.0 BP (39.2% of area)	9021.0 BP to 8770.0 BP (100% of area)	8897.5	113.5
					8917.0 BP to 8893.0 BP (13.8% of area)			
					8886.0 BP to 8863.0 BP (15.1% of area)			
					8830.0 BP to 8784.0 BP (31.9% of area)			
OU_2019_51	R 41390/9	1240	8164	36	9112.0 BP to 9107.0 BP (3.9% of area)	9243.0 BP to 9216.0 BP (2.9% of area)	9048.5	42.5
					9091.0 BP to 9006.0 BP (96.1% of area)	9207.0 BP to 9174.0 BP (3.7% of area)		
						9138.0 BP to 8991.0 BP (93.4% of area)		

Both conventional radiocarbon and calibrated ages are reported for all samples (Table 4.3). The conventional radiocarbon age is a radiometric age using the Libby half-life and expressed in an age before present (BP) ± the 1-sigma error (Libby, 1961), while the calibrated age, as described above, is presented in Cal yr BP with 1- and 2-sigma confidence intervals. When the conventional radiocarbon age intersects the 1-sigma confidence interval of the calibration curve multiple times, that single conventional radiocarbon age can yield multiple possible calendar ages represented as multiple peaks (Figure 4.15). To provide a useable calibrated radiocarbon age, the maximum and minimum ages for the 1-sigma value were selected and the age was placed at the median value between these two. In the example shown in (Figure 4.15), the age was placed between 9011 BP and 8784 BP giving an age of 8897.5±113.5 Cal yr BP. This provides an age with a smaller error than the 2-sigma age of 8895.5±125.5 Cal year BP.

All of the CE17/0106 samples returned ages within the radiocarbon datable range (<50,000 Cal yr BP). The first age at 1.4 m returned an age of 4020.5±53.5 Cal yr BP followed by two ages at 5.25 m (6688.5±38.5 Cal yr BP and 6702±33 Cal yr BP). The average of these two ages (6695 years) yields a sedimentation rate of 1.4 mm/yr, with 3.85 m of sediment deposited over 2675 years. At 10.45 m the age was 7967±28 Cal yr BP, which using the previous averaged age produced a sedimentation rate of 4 mm/yr over the 1272 years. Two ages were returned at 11.3 m when averaged produced an age of 8970 Cal yr BP. This produced a sedimentation rate of 0.8 mm/yr over the 1003 years. The final date at the base of the core at 12.4 m was 9048.5±42.5 Cal yr BP. This equated to a sedimentation rate of 14 mm/yr over the 78 years, the highest rate observed in the core. These calculations are based on the assumptions that sedimentation is constant between dated horizons, that absolute ages are accurate, and in the cases where duplicate ages for a single horizon have been averaged, that the age errors are not consequential.

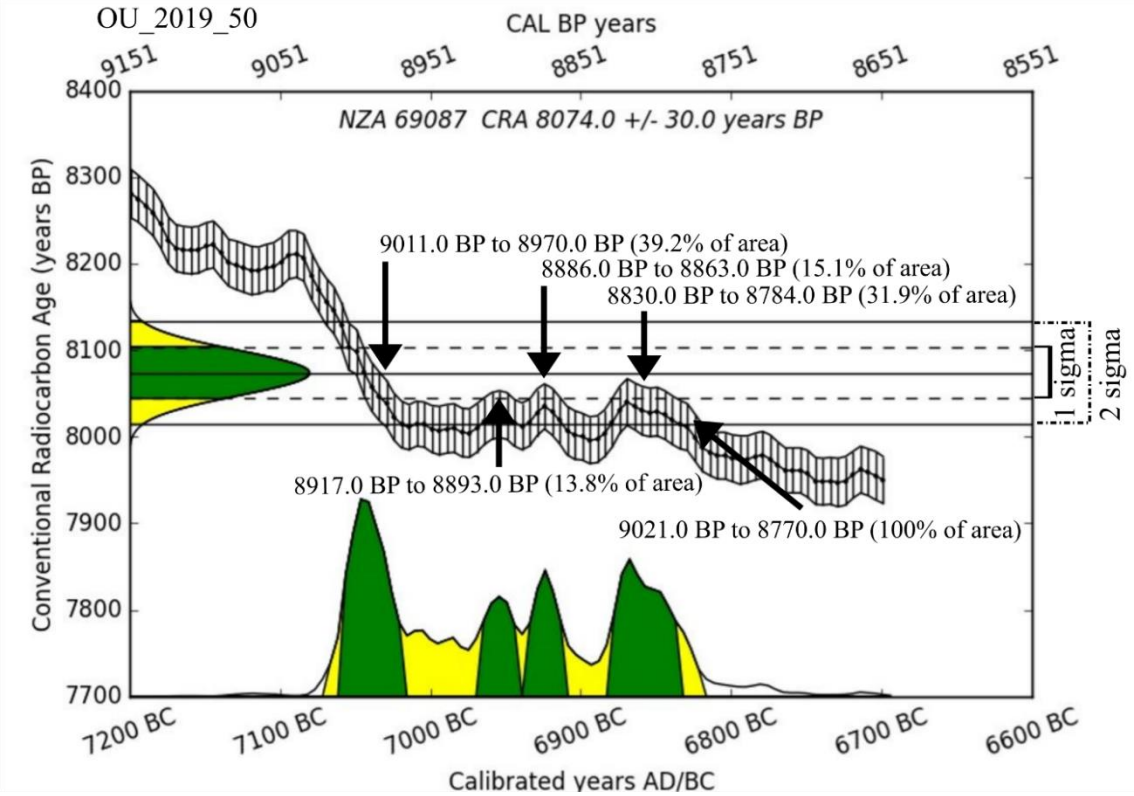

Figure 4.15: Annotated calibration report for radiocarbon sample. Three separate instances of the calibration curve entering the 1 sigma confidence interval, providing four potential ages ranging from 9011 BP to 8784 BP.

4.5.1 Age model

The R-based radiocarbon modelling software Clam was used to produce an age-depth model for core CE17/0106. This method takes conventional radiocarbon ages, calibrates them against the regional SHCAL13 curve, and plots the calibrated ages with their associated errors against depth. Robust age modelling requires that age increase with depth, which did not happen for the Edgar Centre core in South Dunedin. Instead, some sections of the Edgar Centre core returned a mix of ages with multiple age reversals between 7and 12 m, indicating the likely reworking of material, introducing older material into younger sediments (Rees, 2018). The increasing age with the depth of the CE17/0106 core suggests that reworking is not significant in the pre-Anthropocene interval below 1.15 m.

Two hiatuses in the age model were placed at 1.15 m, below the anthropogenic section of sediment, and at 10.62 m, where a probable erosional surface was identified between radiocarbon dates at 10.45 and 11.3 m (Figure 4.16). This hiatus was positioned at the top of the first occurrence of F3 when, at ~9000 ka, the core site would have been up to 10 m above sea level and the rate of sedimentation would have been low (Dlabola et al., 2015) (Figure 4.16). The clear anthropogenic sediment illustrated in F0 helped to place a chronostratigraphic constraint on the upper 1.15 m of the core. Industrialization of Dunedin began in the 1850s, which allowed the age of ~1850 ka to be placed at 1.15 m with the rest of F0 covering <170 years (Morris, 2008) (Figure 4.16).

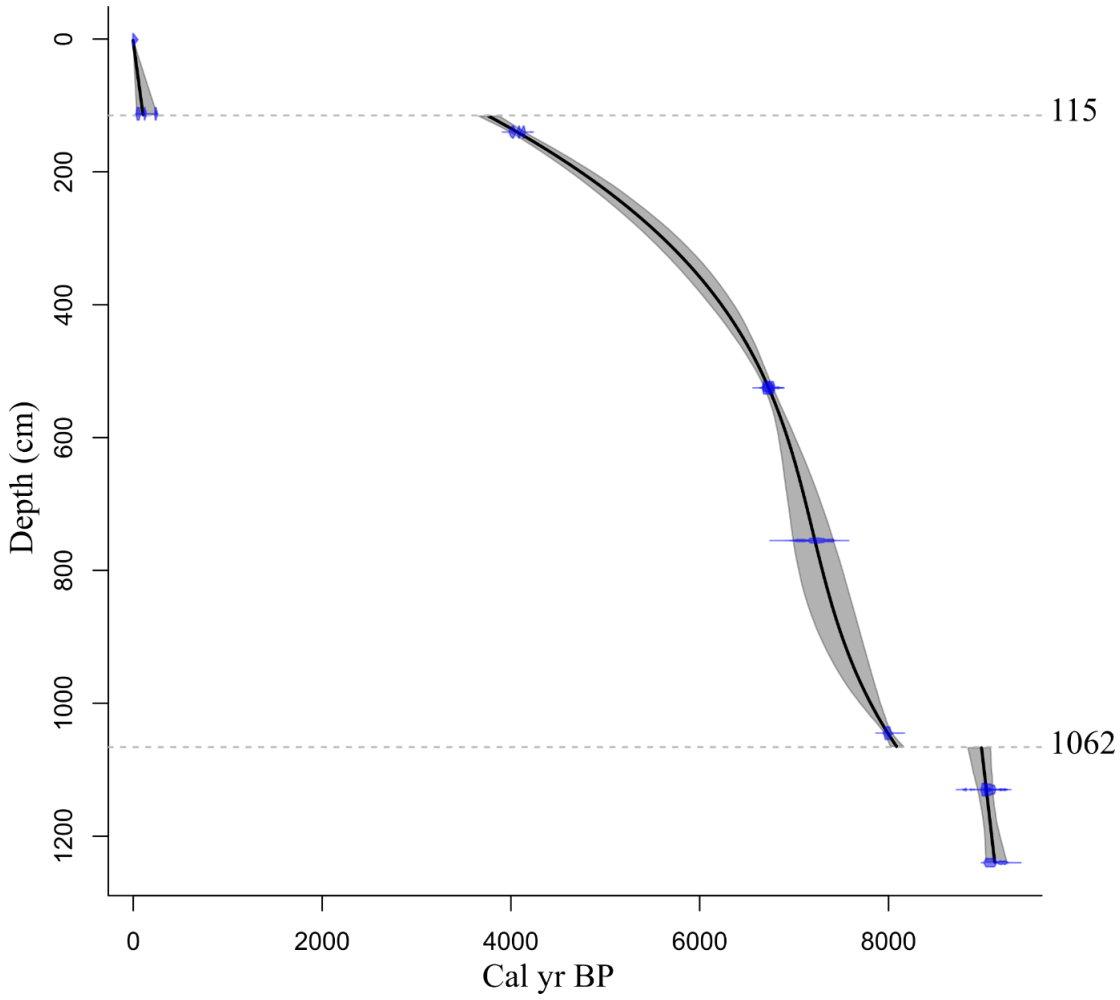

Figure 4.16: Clam radiocarbon age-depth model, each age is presented as a distribution plot, not a singular point to represent the range of ages it could be.

4.6 Outer harbour seismic reflection data

Based on seismic reflection data collected by Fletcher (2016) and Rees (2018), the area of the outer section of Otago Harbour adjacent to Port Chalmers was selected as an ideal area for a high-density seismic reflection investigation. 42 additional seismic lines were collected in an overlapping grid spanning from Port Chalmers and Portobello in the southwest to Waipuna and Otakou in the northeast (Figure 4.17).

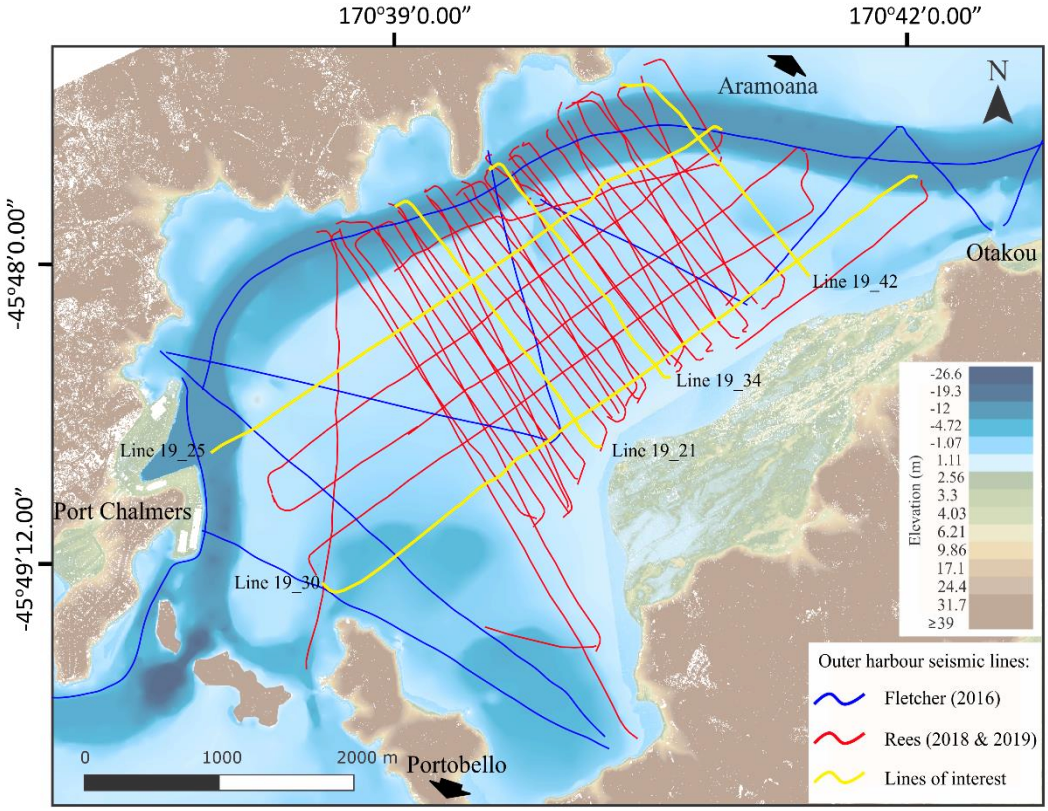

Figure 4.17 Location map of harbour seismic lines with lines of interest marked.

The surface sediment of the outer harbour primarily consists of sand and mudflats that are constantly reworked by tides. The average water depth for the outer harbour survey area ranged from 0.5-2 m at high tide, making access either side of high tide logistically difficult. The lines were collected to increase the density of previously collected lines in the area, allowing more precise constraints to be placed on observed sedimentary horizons within the subsurface. The variability of the outer harbour environment had a

noticeable impact on the quality of data collected and had to be considered during the processing stages. The lithology, water depth and swell all potentially impact the quality of data. The biggest impact is attributed to the shallow water depth, which in places resulted in the towed seismic gear coming in contact with the seafloor, and probably had a significant impact on the imaging capabilities of the immediate subsurface.

Due to the regular movement of commercial vessels in the harbour, the shipping channel is dredged to >14 m's deep, significantly deeper than the rest of the outer harbour (Figure 4.17). As in previous surveys by Shears (2009), Fletcher (2016) and Rees (2018) the dredged channel in almost all circumstances produced wipeout as the reverberations of sound within the channel restricted further penetration into the subsurface. Additionally, large tracts of the shallower survey area also had areas of minimal penetration, which was attributed to the previously mentioned environmental factors and equipment limitations.

4.7 Basal reflection

A significant capability of seismic imaging is the ability to constrain the contact between a sedimentary basin and the underlying basement geology. This allows the vertical and lateral extent of sediment fill within the paleovalley to be constrained. The lithology of the basement underlying the outer Otago Harbour is yet to be directly sampled; however, the strong reflectivity observed in nearly all the seismic cross-sections clearly indicates the transition from sediment to the basement. Basal reflections can be identified across most seismic lines collected in the outer harbour with varying strengths and depths, although due to environmental limitations, the basal reflection is not always continuous across the entirety of the line and is susceptible to wipeout caused by lack of penetration. On lines collected in close proximity to the shore, the basement can be tracked onshore to volcanic outcrops, indicating that basement may in part be of volcanic origin. A main identifiable characteristic of the basal reflection is its undulating morphology, easily distinguished from the planar sub-horizontal sedimentary horizons observed in the stratigraphy above the basement.

Basal reflections are common throughout the outer harbour survey area, coinciding well with reflections observed by both Fletcher (2016) and Rees (2018). Wipeout has occurred across Shears (2009), Fletcher (2016) and Rees (2018) and is observed across lines collected in 2019, and could have several sources; including shallow gas, organic material on the seafloor or the general characteristics of the sediment which causes acoustic blanking, stopping the acoustic source penetrating the subsurface (Kim et al., 2004) (Figure 4.18).

Due to the presence of wipeout within the data, the basement depth of Otago Harbour sometimes had to be inferred between observed reflections. Although nearly all lines possess a certain level of wipeout, some only show a minor degradation on the data quality. One example is line 19_42 (Figure 4.18), which lost resolution only below the dredged channel. In contrast, line 19_34 is an example of extensive wipeout, where over 50% of the line has been lost (Figure 4.19).

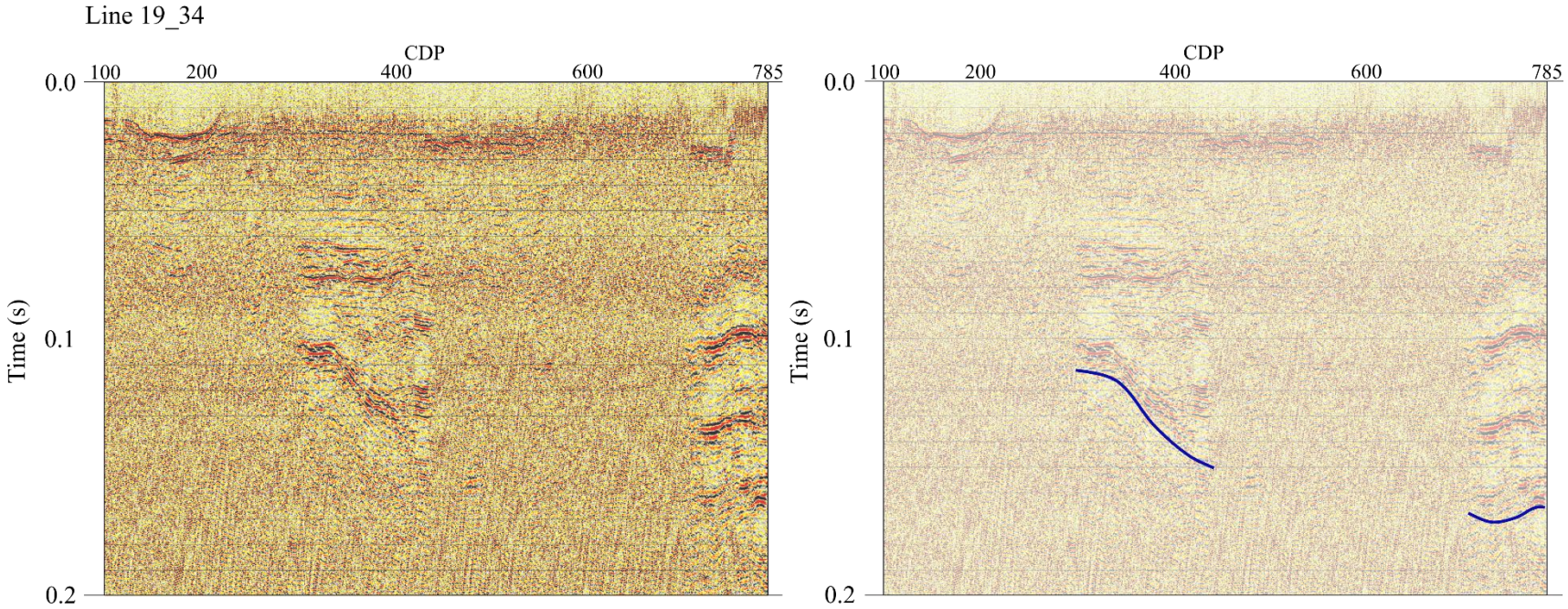

Figure 4.18: Basal reflection observed in Line 19_34, represented as a blue line. Basal reflection is split due to wipeout in the cross-section.

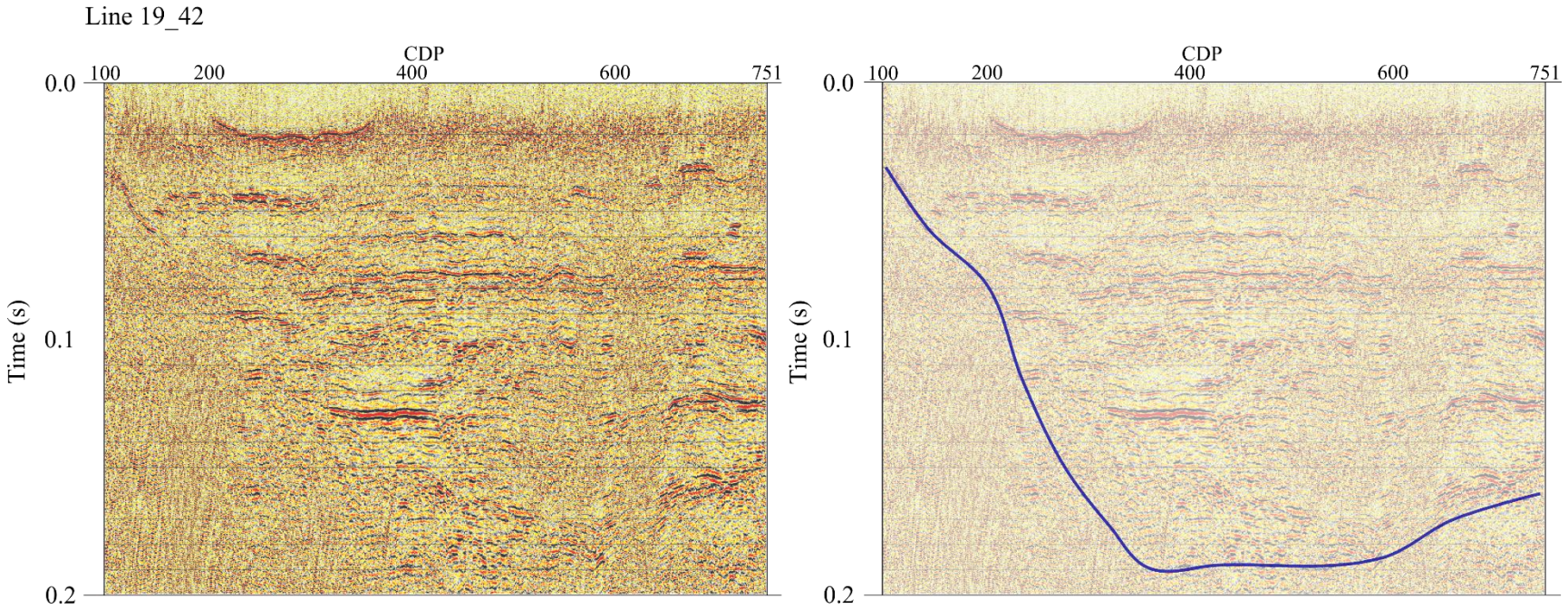

Figure 4.19: Basal reflection observed in Line 19_42, represented as a blue line.

4.7.1 Basal reflection model

A model of the basement surface was produced using the abundant basal reflections interpreted across the survey. Using the seismic analysis program Kingdom (from Market IHS)., basal horizons were manually selected across all the lines collected in 2019. Lines collected from 2016 and 2018 were also used and basement reflections were reselected under the same parameters as lines collected in 2019 to ensure consistency. Once all the basal reflections were selected, they were plotted as a two-way time surface, distinguished by a colour gradient. This grid interpolated between the selected reflections, inferring the basal surface between lines and in areas where wipeout was observed. The basal grid was then plotted using the VuPAK function in Kingdom, plotting the gridded layer as a three-dimensional surface (Figure 4.20).

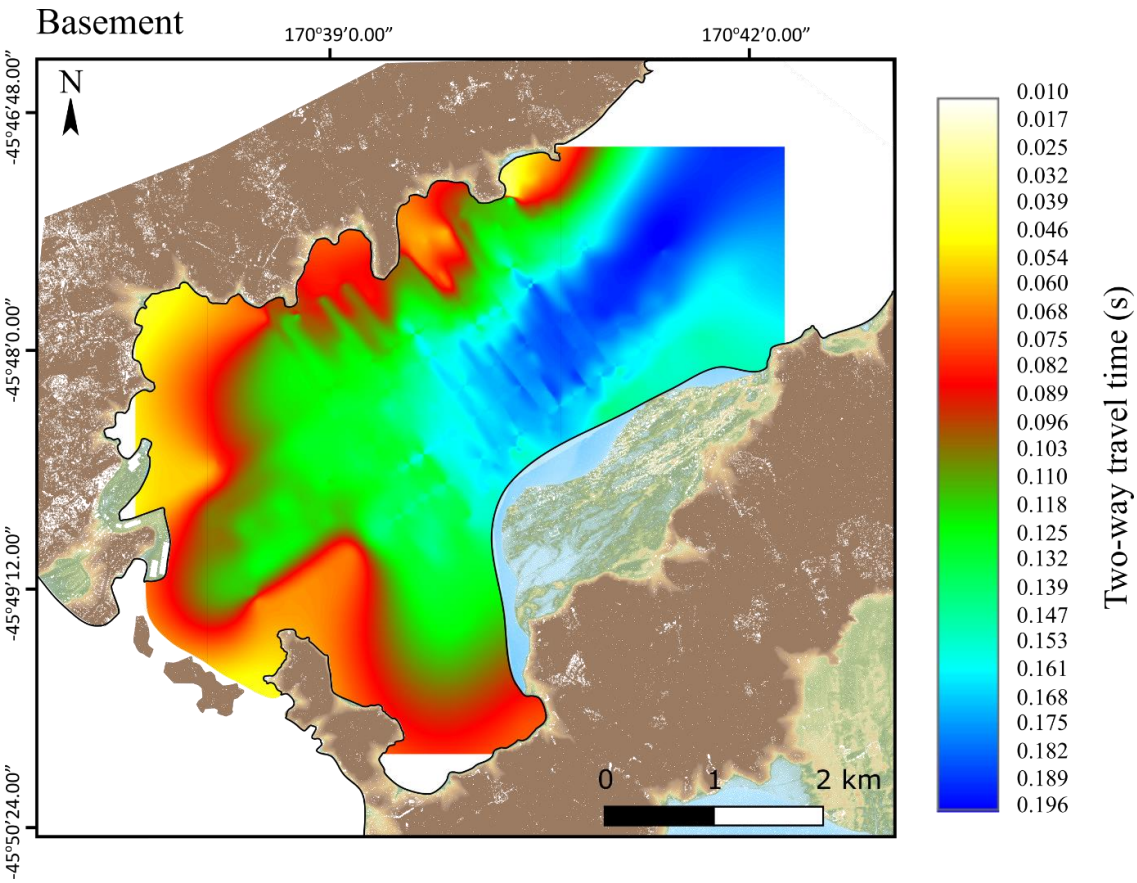

Figure 4.20: Two-dimensional basal reflection model, indicating the two-way time to the basement is shortest near in the southwest and longest in the northeast.

The colour gridded model indicates a considerable deepening of the basement from Port Chalmers (0.042 s) out towards Aramoana (0.169 s). The deepest basement is observed in the centre of the harbour indicated by a dark blue (0.196 s). This progresses to green, shallowing narrowly up towards Quarantine Island (Figure 4.20). The basement on the periphery of the harbour is shallower, probably a continuation of observed volcanic outcrops on land.

4.8 Sedimentary reflections

Within the sediment stratigraphy of the outer Otago Harbour, several distinct horizons were observed. Sedimentary horizons appear prominent reflections between different sediment units within the subsurface caused by changes in density and seismic velocity. Unlike the basal reflections, the sedimentary horizons in the harbour are typically planar, with regular appearances across multiple seismic lines. Using their reflection features and their depth (inferred from two-way travel time), five distinct horizons were identified and tracked throughout the subsurface (Table 4.4) (Figures 4.21 to 4.25). Due to the high density of seismic lines collected, time variations between horizons as they were tracked were minimal (Figures 4.21 to 4.25). Optimally, <0.02 s was used by both Fletcher (2016) and Rees (2018), which ensured consistency between data sets.

Each of the five identified stratigraphic horizons was assigned a label and easily identified colour. Starting from the shallowest horizon at the top of the sequence the colour yellow was assigned with the number 1 and the designation OH (outer harbour), giving the reflection an ID of 1OH for the yellow horizon. Subsequent horizon ID numbers with increasing depth are; 2OH(cyan), 3OH(green), 4OH(pink) and 5OH(black) (Table 4.4). The collection of the data was most limited in the shallowest horizon (1OH), where large areas were indistinguishable from the seafloor. The deepest interpreted horizon (5OH) was only present in the sections with the deepest basement, becoming more prevalent in lines further from the centre of the Dunedin Volcanic Group in proximity to Port Chalmers (Table 4.4). The most continuous horizons within the outer harbour were 2OH, 3OH and 4OH, as they were outside of the influence of the seafloor and not deep enough to be obscured by the basement.

Table 4.4: Summary table of characteristics of observed horizons.

Horizon	Colour	Time range (s)	Comments
1OH	Yellow	0.01-0.02	Shallowest; mostly planar; sometimes interferes with seafloor
2OH	Cyan	0.04	Mostly continuous and planar; observed in almost all lines
3OH	Green	0.06-0.08	Most observed horizon; largely planar and continuous
4OH	Pink	0.09-0.1	Predominantly planar; occurrences restricted to lines with deeper basal reflections; discontinuous and undulating when positioned near the basement
5OH	Black	0.11-0.13	Deepest horizon; least planar of horizons; undulating and discontinuous in occurrence; contours to basal reflection

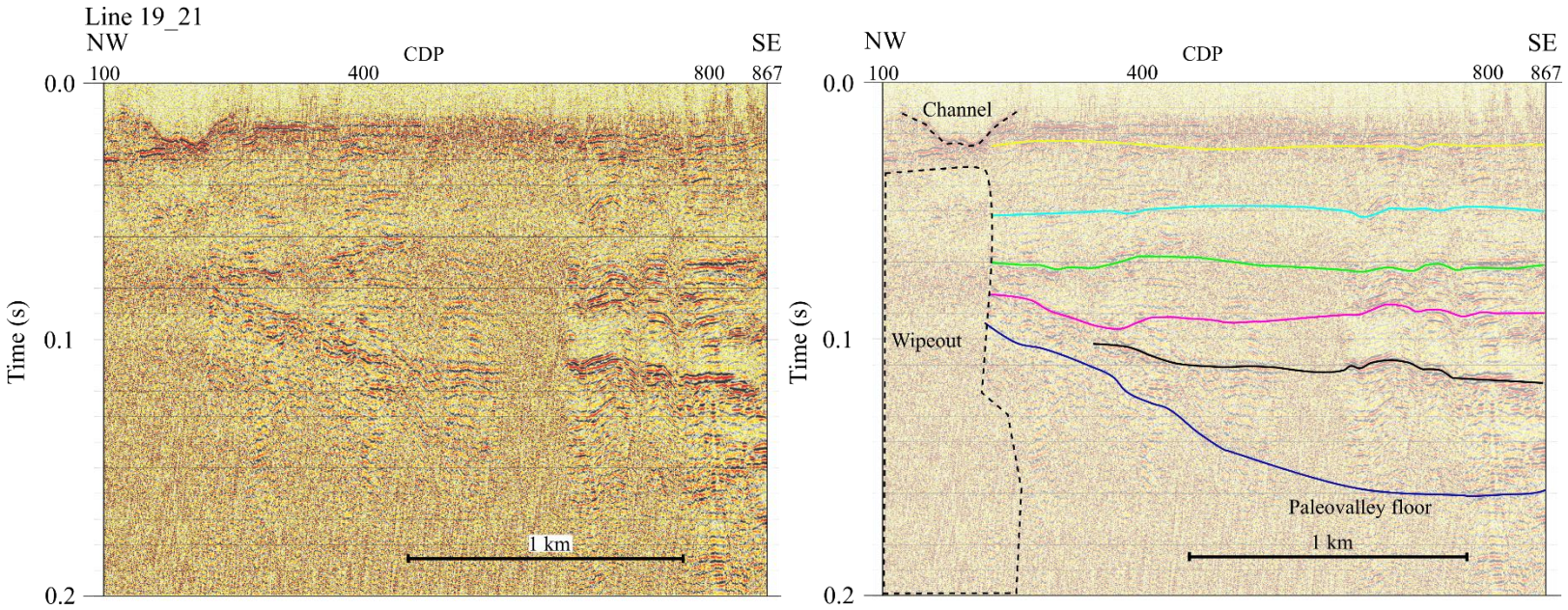

Figure 4.21: Seismic Line 19_21 with the uninterpreted cross-section on the left and identified sedimentary horizons on the right. Wipeout has occurred below the dredged channel obscuring the deeper horizons.

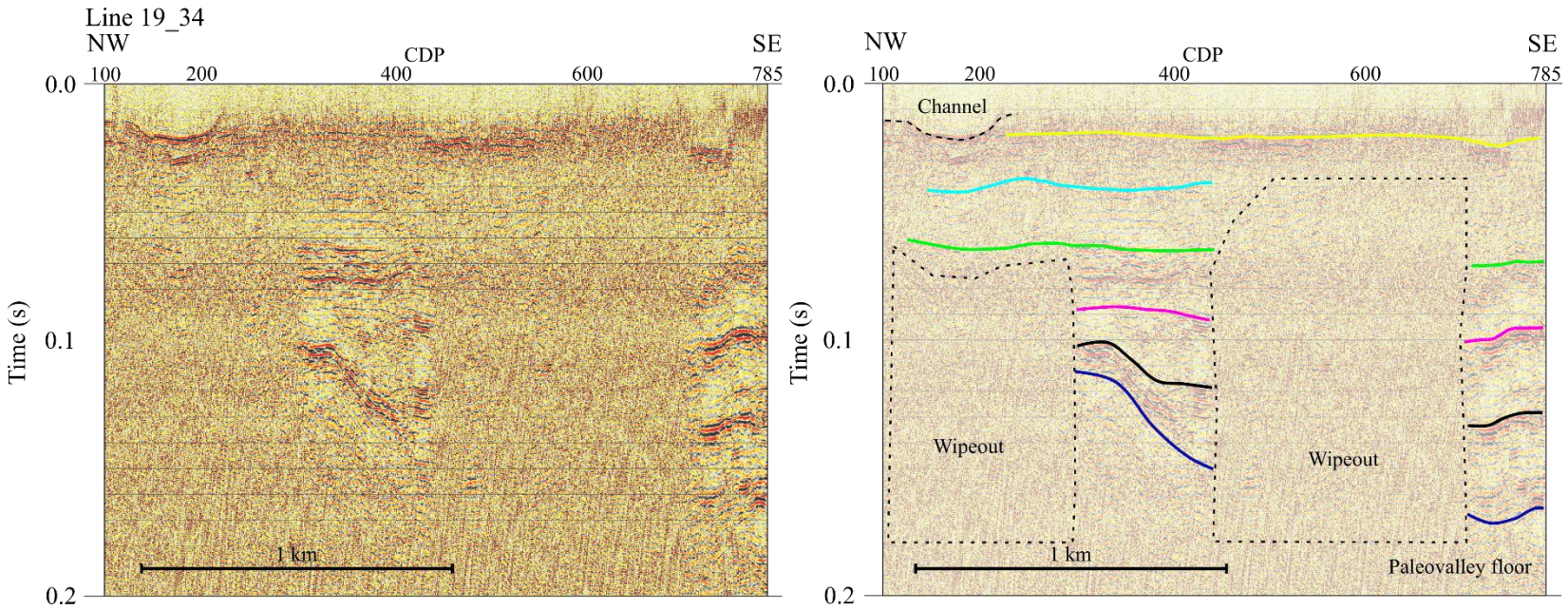

Figure 4.22: Seismic Line 19_34 with the uninterpreted cross-section on the left and identified sedimentary horizons on the right. Two areas have been affected by the presence of wipeout; however, all five of the horizons are partially present.

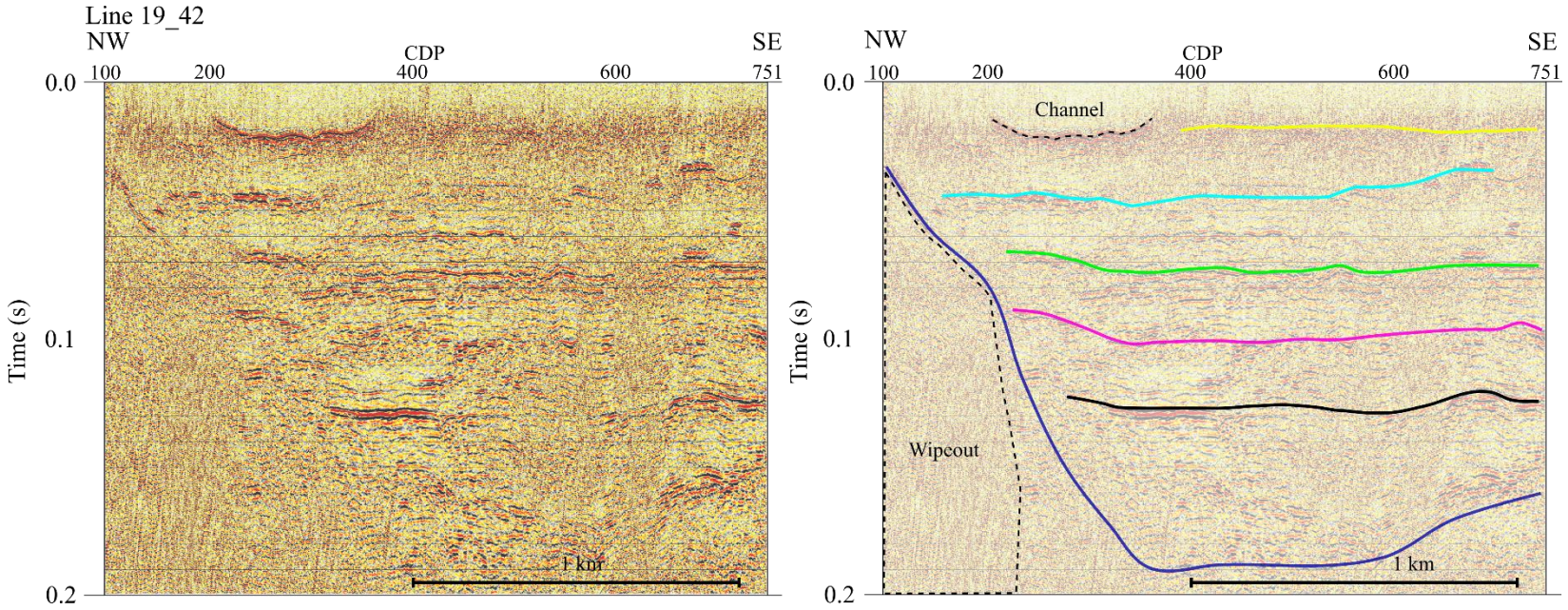

Figure 4.23: Seismic Line 19_42 with the uninterpreted cross-section on the left and identified sedimentary horizons on the right. Wipeout is present on the NW side of the cross-section.

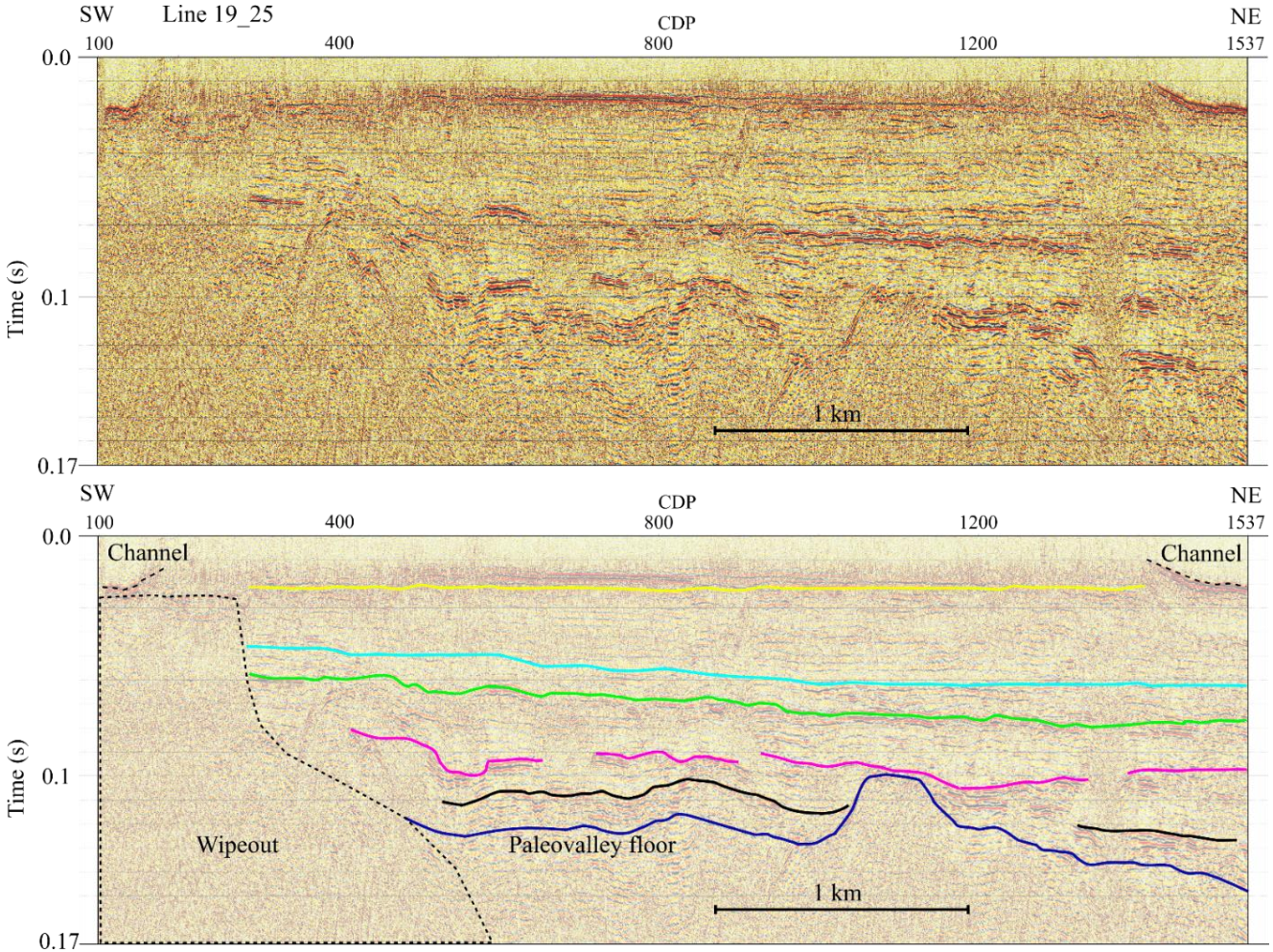

Figure 4.24: Seismic Line 19_25 with an uninterpreted cross-section on the left and identified sedimentary horizons on the right. The basal reflection is undulating and intersects 5OH. Both 4OH and 5OH are discontinuous. Wipeout has occurred on the southwest side of the line.

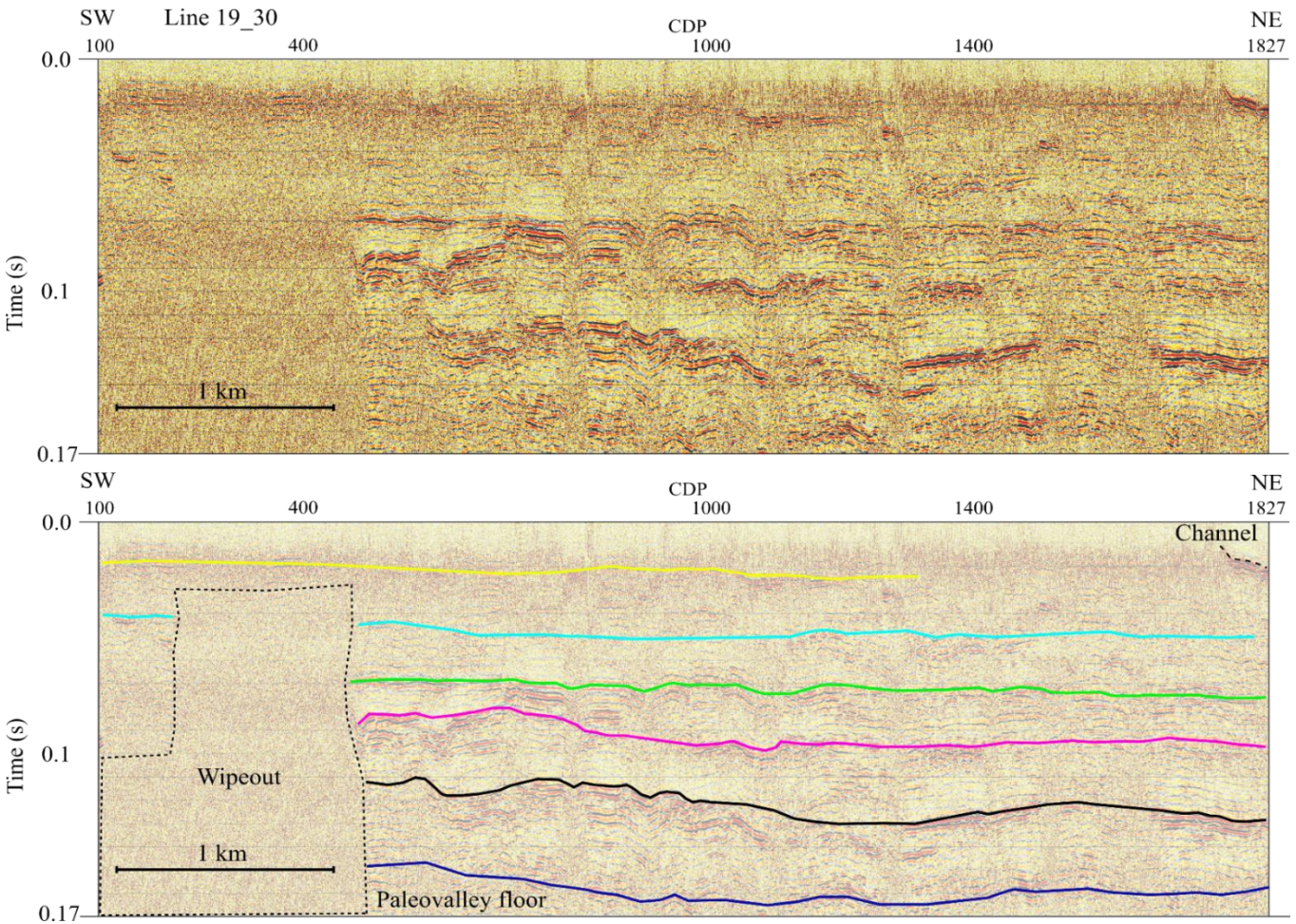

Figure 4.25: Seismic Line 19_30 with the uninterpreted cross-section on the left and identified sedimentary horizons on the right. Wipeout has obscured the southwest edge of the line. Horizons are predominantly continuous; however, 4OH and 5OH are undulating, unlike the more planar shallow horizons.

4.8.1 Horizon interpolation

As distinct sedimentary horizons were identified within the sedimentary record, their occurrences in adjacent lines allowed the orientation of the horizons to be interpolated and modelled. Coloured gridded layers were produced using the manually selected horizons. The grid function interpolates the area between lines to best represent the orientation of each horizon (Figures 4.26 to 4.30). This allowed each horizon to be compared to the basement to see how they dip, increase in travel time, or change in orientation, and to identify if any geomorphological features are present (Figures 4.26 to 4.30). Horizon generation can be implemented using a number of gridding algorithms available within Kingdom, each of which are suited for different data types or environments. Kingdom's Flex Gridding was selected to best represent the selected horizons. Flex Gridding works on two main criteria: first, it interpolates the surface of the grid close to or through the manually selected points, secondly it drapes the grid of the horizon across the manually selected points smoothing sharp and unrealistic areas. Both of these criteria act to provide the most realistic 3D interpretation of reflection surface through the subsurface.

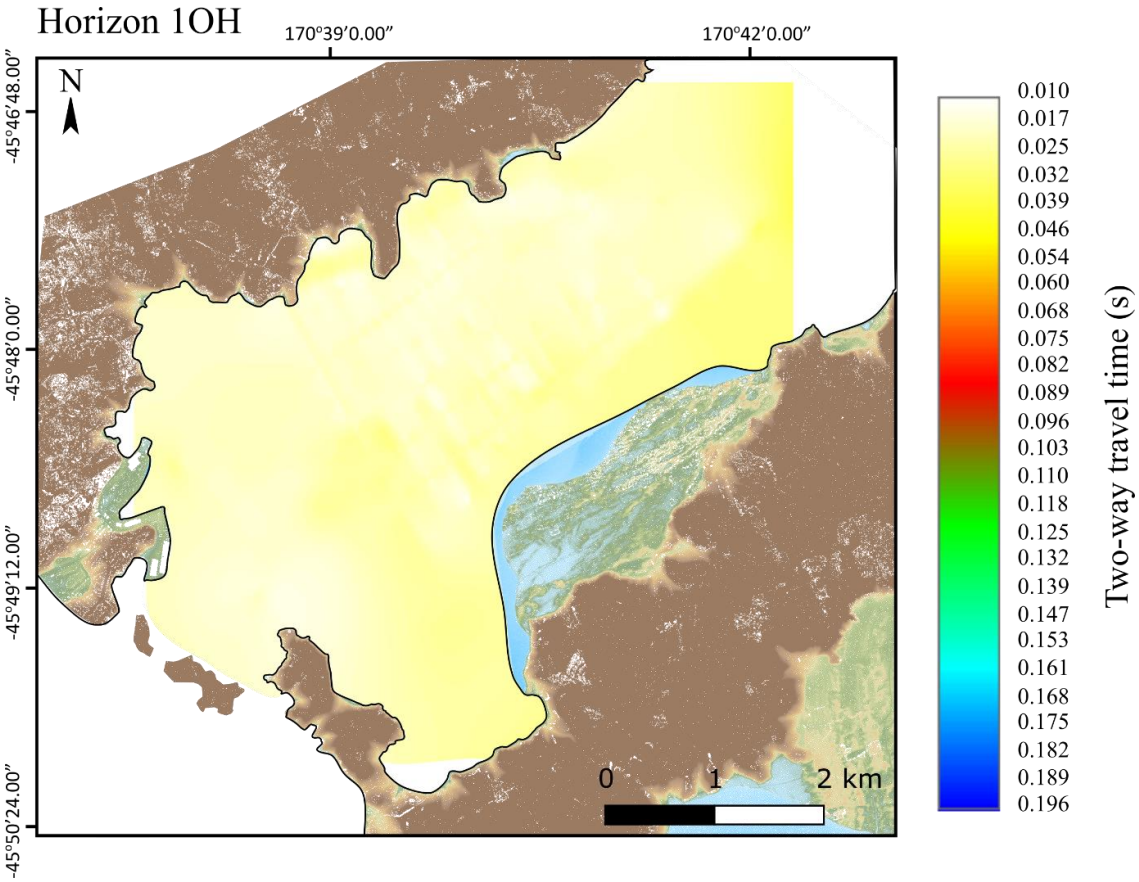

Figure 4.26: Gridded horizon map for horizon 1OH.

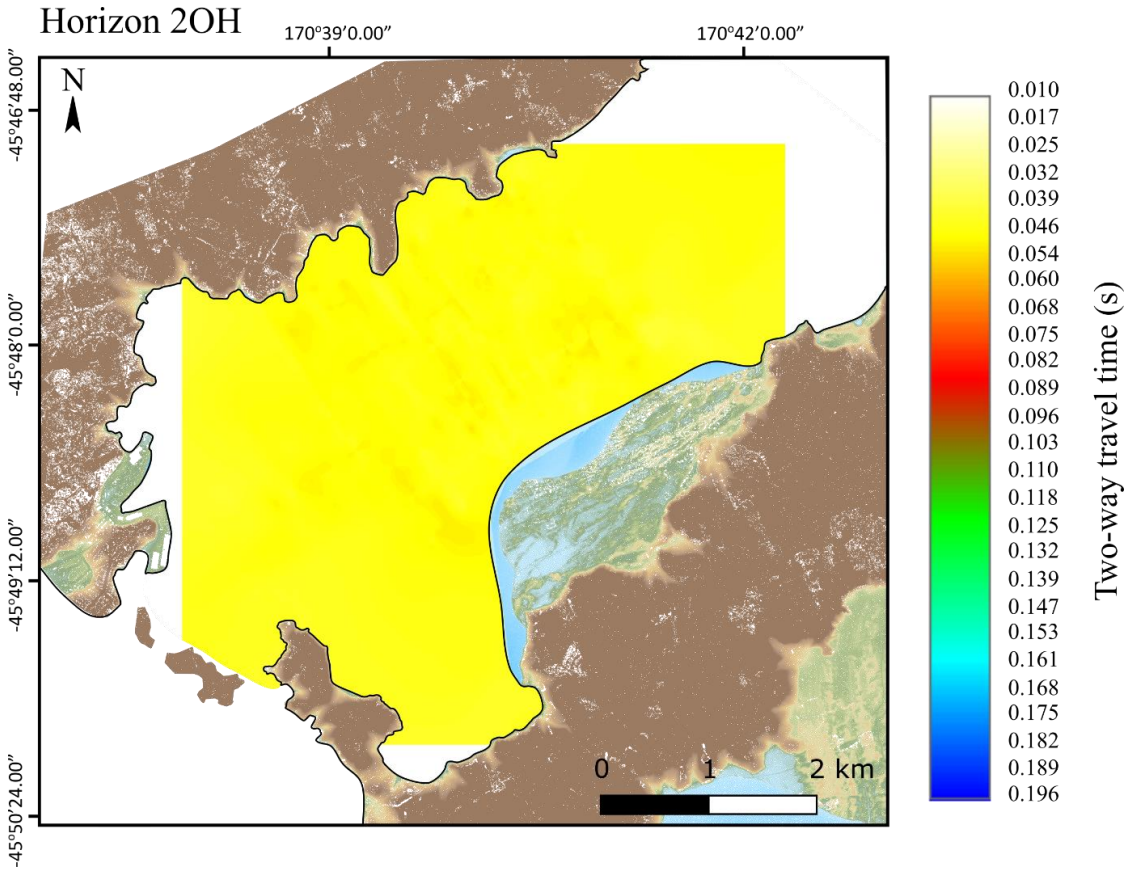

Figure 4.27: Gridded horizon map for horizon 2OH.

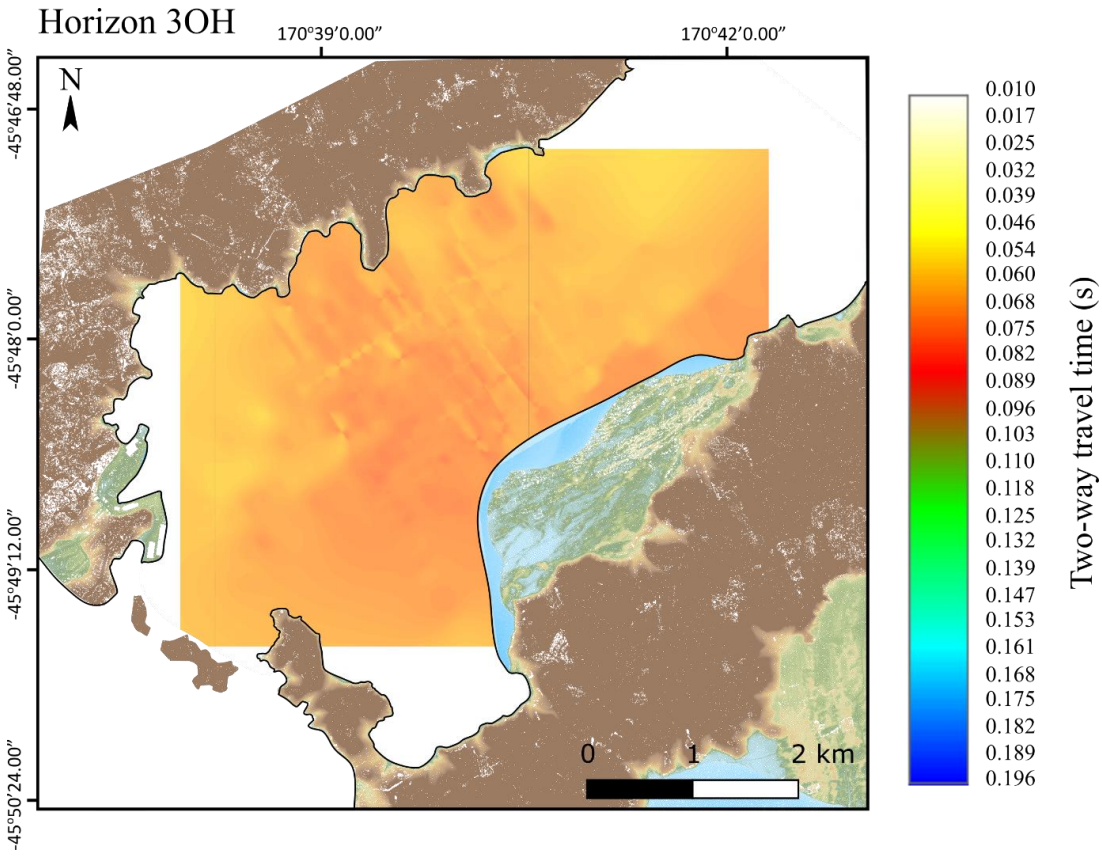

Figure 4.28: Gridded horizon map for horizon 3OH. Minor differences in two-way travel time to the horizon is observed between lines. This is illustrated as cross-hatched lines.

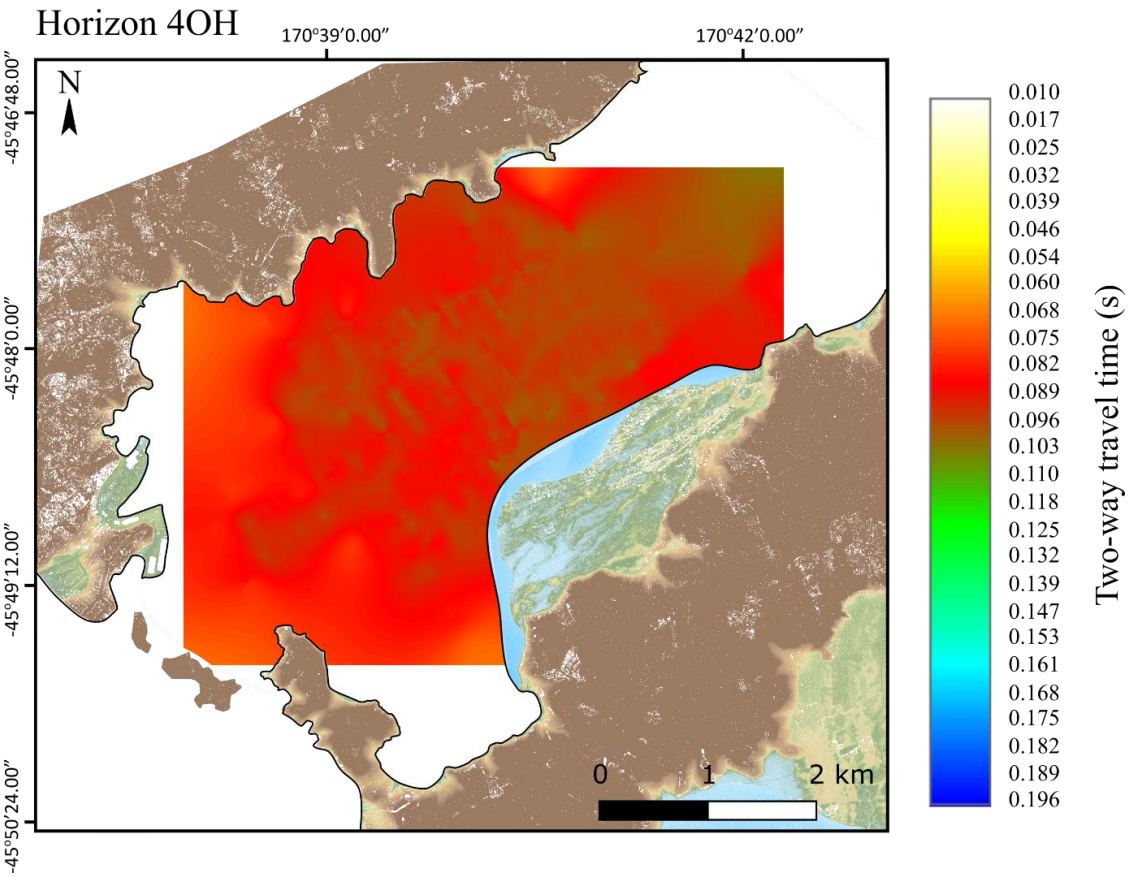

Figure 4.29: Gridded horizon map for horizon 4OH.

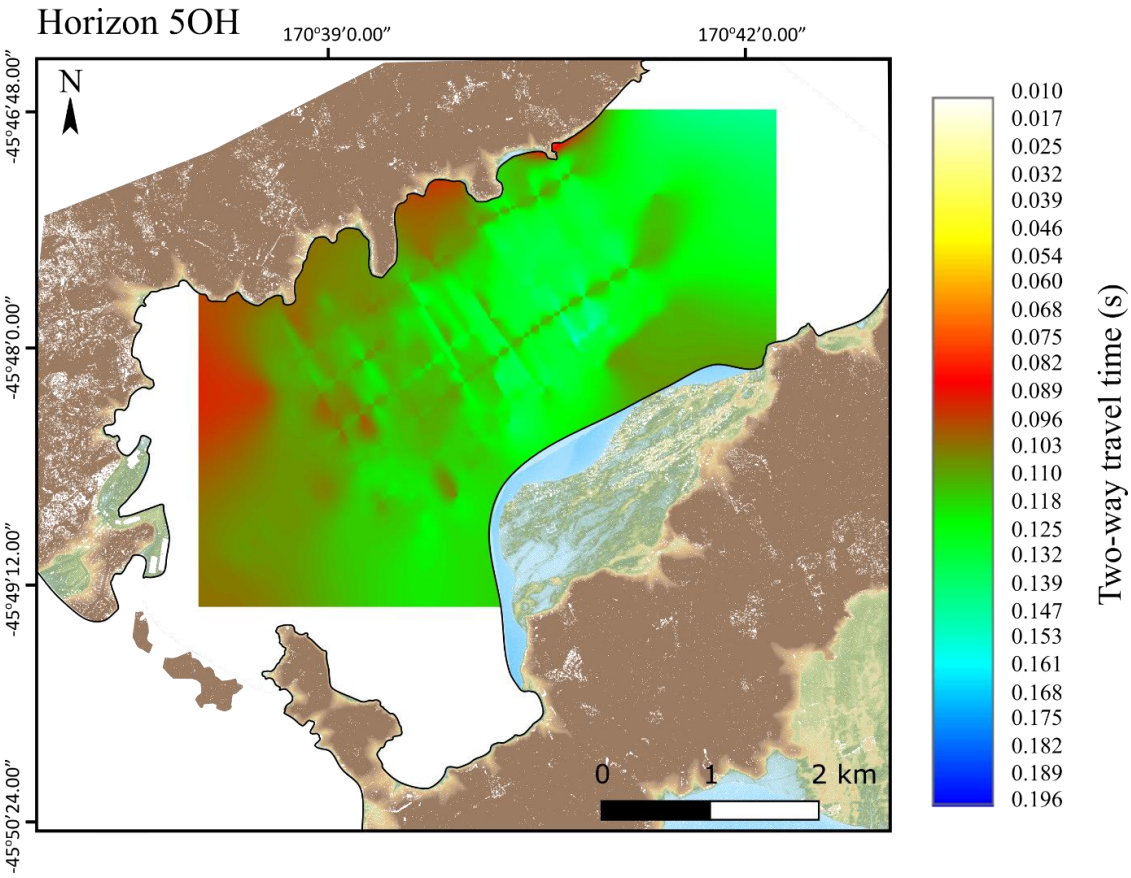

Figure 4.30: Gridded horizon map for horizon 5OH. Minor differences in two-way travel time to the horizon is observed between lines. This is illustrated as cross-hatched lines.

Chapter 5 Discussion

This investigation aims to improve our understanding of the history of sediment infill within Otago Harbour and Dunedin and explore its significance as a Holocene paleoclimate record. Otago Harbour provides a rare opportunity to observe near-shore highstand stratigraphic sequences within the sedimentary record. Near-shore highstand deposits like beaches, shore faces and estuary deposits are susceptible to erosion once sea level drops, so having a basin like the one found in Otago Harbour that acts to protect those nearshore sequences from erosion/removal is not really common around the world's ocean margins

This section discusses the infill history of the stratigraphy of South Dunedin from successive changes in sea level. The CE17/0106, Edgar Centre and NZ SeaRise cores coupled with previously collected gravity modelling and seismic data allowed have helped identify the southern drainage channel of Otago Harbour. It also addresses the paleovalley and sediment stratigraphy of the outer harbour through high-resolution seismic data. Geometric interpretations were made using velocity-to-depth calculations, placing depth constraints on the sedimentary horizons and the basement surface of the paleovalley.

5.1 Velocity-to-depth calculations

The vertical scale for seismic reflection data is primarily presented in two-way time (Yilmaz, 2001). This complicates geometric interpretations of subsurface geology as the acoustic velocity in the subsurface does not linearly increase, so two-way time is not representative of actual depth (Hamilton, 1963; Sidler & Holliger, 2010). Initially, during the processing stage, a stacking velocity model was produced. This was developed by individually testing average velocities on traces within a common depth point (CDP) gather to remove normal move out. To determine depths for the profiles, an interval velocity model was produced for two representative lines from the outer harbour. The interval velocity model was produced by converting the stacking velocity model into an interval velocity model using the GLOBE Claritas isovels "V(int)" function. The interval velocity model was smoothed manually, and selected velocities

were added below the basement reflection. The velocities were added as it was assumed that the basement velocity would be considerably higher than that found in the sedimentary packages above it; this would then help to improve the quality of the model and subsequent time-to-depth conversions (Figure 5.1).

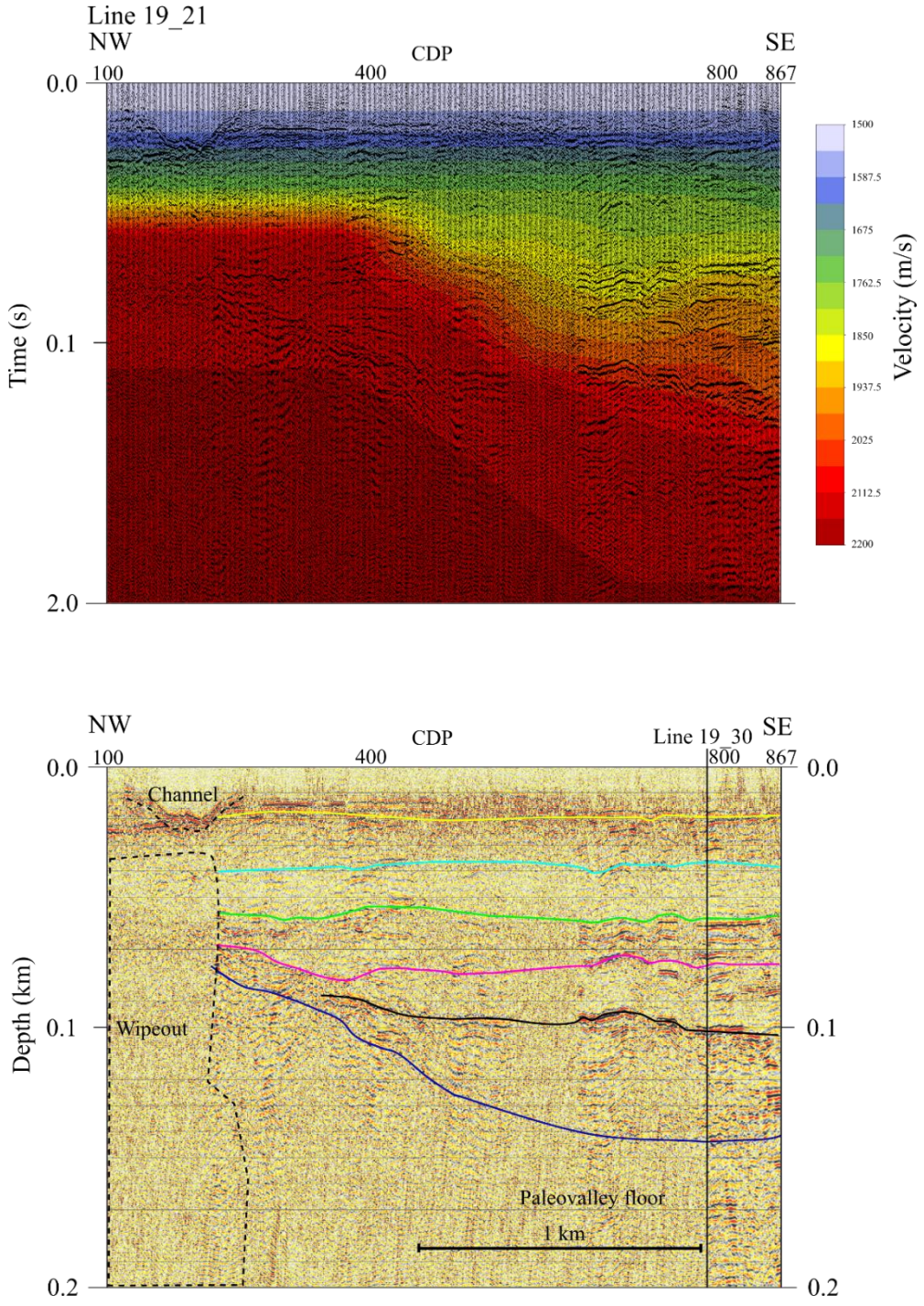

Figure 5.1: Line 19_21 velocity model plotted above the depth corrected profile below. Velocities are expressed in colour grade with light blue being lowest and red being highest. The point of intersection with line 19_30 is marked using a vertical black line.

The basement identified in line 19_30 deepens from approximately 125 mbsf in the southwest to 140 mbsf in the northeast (Figure 5.2). Between CDP 1100 and 1400, the basement reaches its deepest at almost 150 mbsf. This trough is punctuated by a high point in the basement suggesting two parallel paleochannels are present (Figure 5.2). Line 19_21 running perpendicular to Line 19_30 shows the depth of the observed paleovalley from the two-dimensional model (Figures 5.1 and 5.2). The observed basement starts at 80 mbsf in the northwest deepening to a total of 140 mbsf (Figure 5.1).

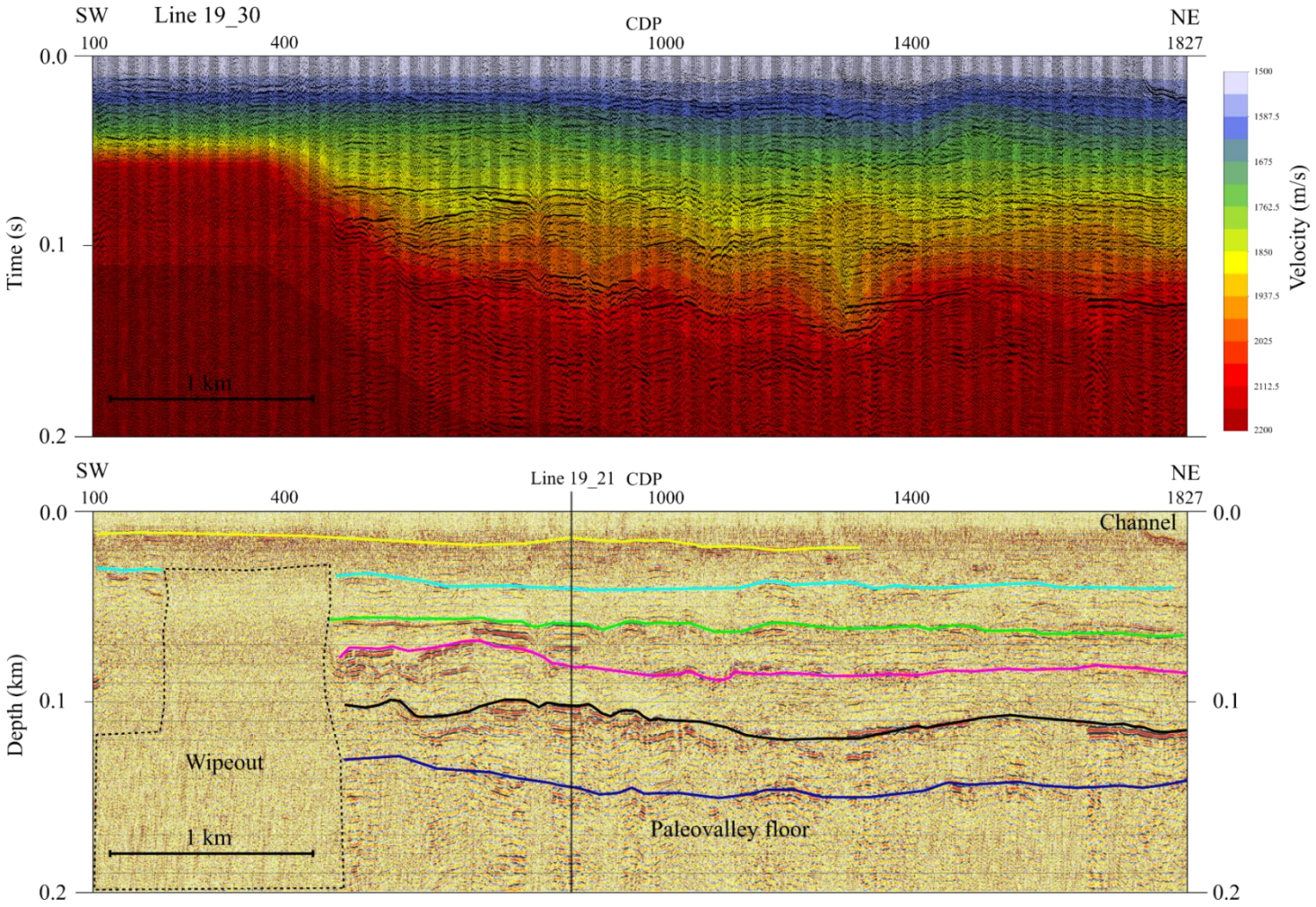

Figure 5.2: Line 19_30 velocity model plotted above the depth corrected profile below. Velocities are expressed in colour grade with light blue being lowest and red being highest.

5.2 Erosion from a central ridge

The idea that Otago Harbour initially formed through erosion from a central ridge was first proposed by Marshall (1906) and later investigated by Fletcher (2016) and Rees (2018). Under this model, the harbour formed from two rivers one flowing northeast towards Aramoana and one southwest towards St Kilda-from a central watershed at the centre of the Dunedin Volcano situated between Portobello and Port Chalmers (Figure 5.3). The rivers were possibly aligned along a fault running parallel to the Akatore Fault and other regional Otago faults, that focused runoff along a weakened surface. However, no direct evidence of such faulting has been observed (Fletcher, 2016). Observations of the morphology of the harbour by Marshall (1906) suggested its shape was probably formed through fluvial erosion along a fault-unlike Lyttleton and Akaroa harbours on the Banks Peninsula, the shapes of which were more influenced by erosion following the eruption pattern (Hampton, 2010; Marshall, 1906). The high-density network of high-resolution seismic lines recently collected on both the inner and outer harbour allowed constraints to be placed on the paleovalley erosional surface (Fletcher, 2016; Rees, 2018; Shears, 2009) (Figure 5.3).

The basement model produced from these lines (Figure 4.20) indicates that the basement is within metres of the surface at Quarantine and Goat islands, deepening to approximately 140 m with distance northeast along the harbour towards Aramoana. A central paleochannel is evident in the basement model aligned with Quarantine Island, extending northeast towards Aramoana. This indicates that when sea level was significantly lower in the past, a river fed from the surrounding catchment cutting through this basement surface, draining through the current-day harbour mouth. The basement depth of surrounding bays Portobello, Careys and Hamilton appear orientated towards this paleochannel, potentially acting as tributary river inputs into the larger channel system. The paleochannel is narrow (<500 m across) near Quarantine Island, widening to over 1 km as it progresses past Waipuna Bay (Figure 5.3).

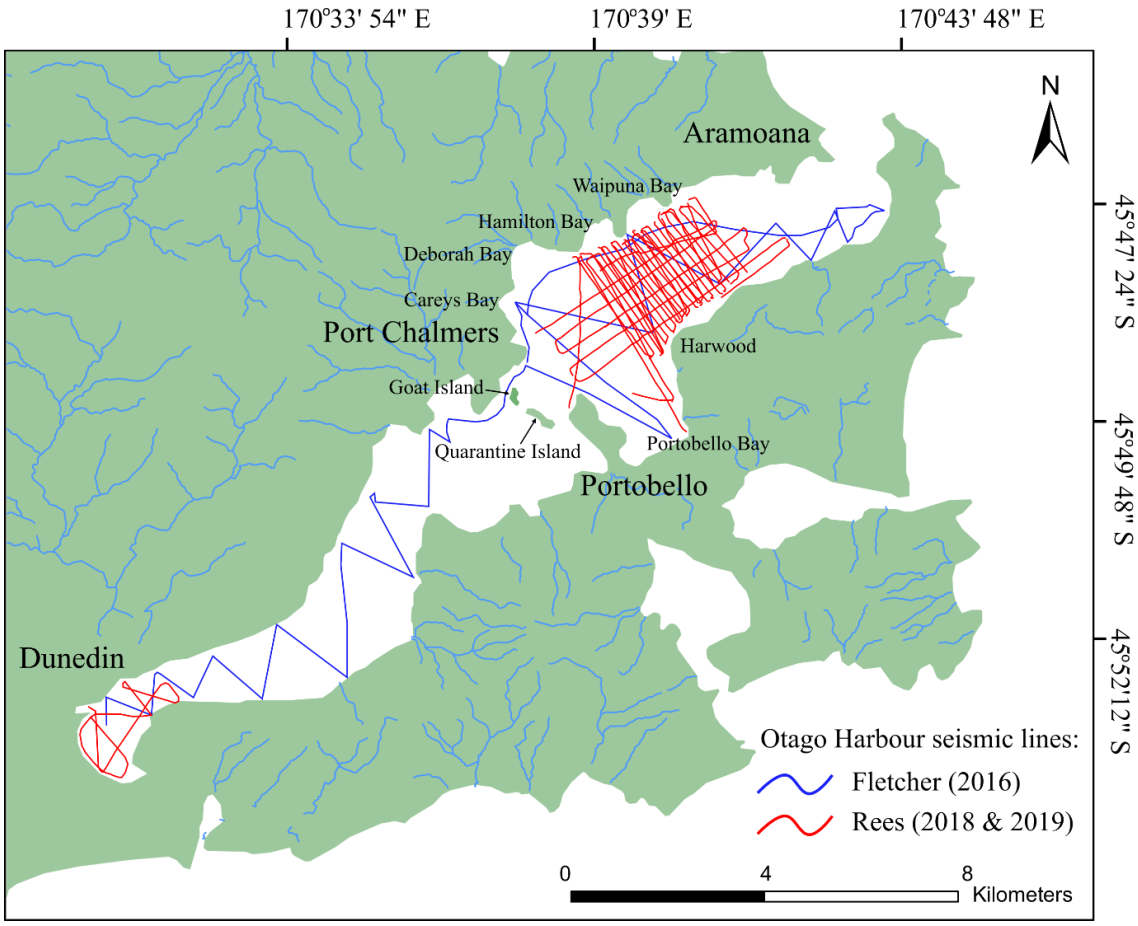

Figure 5.3: Location map of all lines collected in Otago Harbour by Fletcher (2016), Rees (2018 and 2019).

The coverage of seismic lines in the inner harbour is significantly less dense than in the outer harbour; however, lines collected by Rees (2018) indicate basement reflections close to Portsmouth Drive at 80-100 mbsf. Extensive gravity modelling in South Dunedin suggests that basement reaches a depth of 120 m (Sangster, 2019).

The gravity modelling, seismic reflection data and core records all indicate that the basement geology in South Dunedin is significantly deeper than at the centre of the Dunedin Volcanic Group at Portobello/Port Chalmers. The similar basement depths observed in both South Dunedin and the outer harbour towards Aramoana support the interpretation that infill progressed from both directions towards a central ridge. Evidence of faulting within the harbour could explain the orientation of erosion;

however, no evidence of faulting is seen in the planar bedding of the Quaternary sediments so faulting would have preceded the sediment infill.

5.3 Constraining the outer harbour paleovalley

Profiling of the outer harbour paleovalley by Shears (2009), Fletcher (2016) and Rees (2018) provided a basis for the lines collected in 2019. The high-density of lines collected in 2019 adds detail over previous surveys, aiming to fill in gaps and increase the accuracy of stratigraphic and structural modelling. Basal reflections were observed in each of the 42 lines collected; however, they were not always continuous and had to be interpolated in places (Figure 5.3 to 5.5). Much of the periphery of the model has inferred basement depths based on an extrapolation of the model from the already-shallowing basement. This creates unrealistic basement depths in the bays on the northeast side of the harbour where there are basement highpoints in the bays and basement low points between them; the opposite of what is expected (Figure 5.5).

The two-way time from the sea surface to the basal reflections varied across the survey area, typically being shorter at the margins of the harbour (between 0.032-0.082 s) and increasing towards the central axis of the harbour. Additionally, the basement reflection two-way times increase from approximately 0.054 s in the southwest to 0.196 s in the northeast (Figure 5.5). The main paleovalley has the same overall orientation as the current-day harbour and is fed by several smaller paleochannels, forming a concave valley floor (Shepherd & Schumm, 1976) (Figure 5.5). These paleochannels would have been fed from the surrounding topography funnelling water and sediment into the system (Nelson & Seminara, 2011). The main paleovalley aligns with the axis of the harbour towards Goat and Quarantine islands, the location of the probable central catchment (Fletcher, 2016). This main channel is fed on either side by two of the largest paleochannels, one from Portobello Bay and the other from Deborah Bay (Figure 5.4). The position of these two paleochannels suggests they were probably fed from the same catchment as the main paleovalley, with all feeding into the central channel (Figure 5.5).

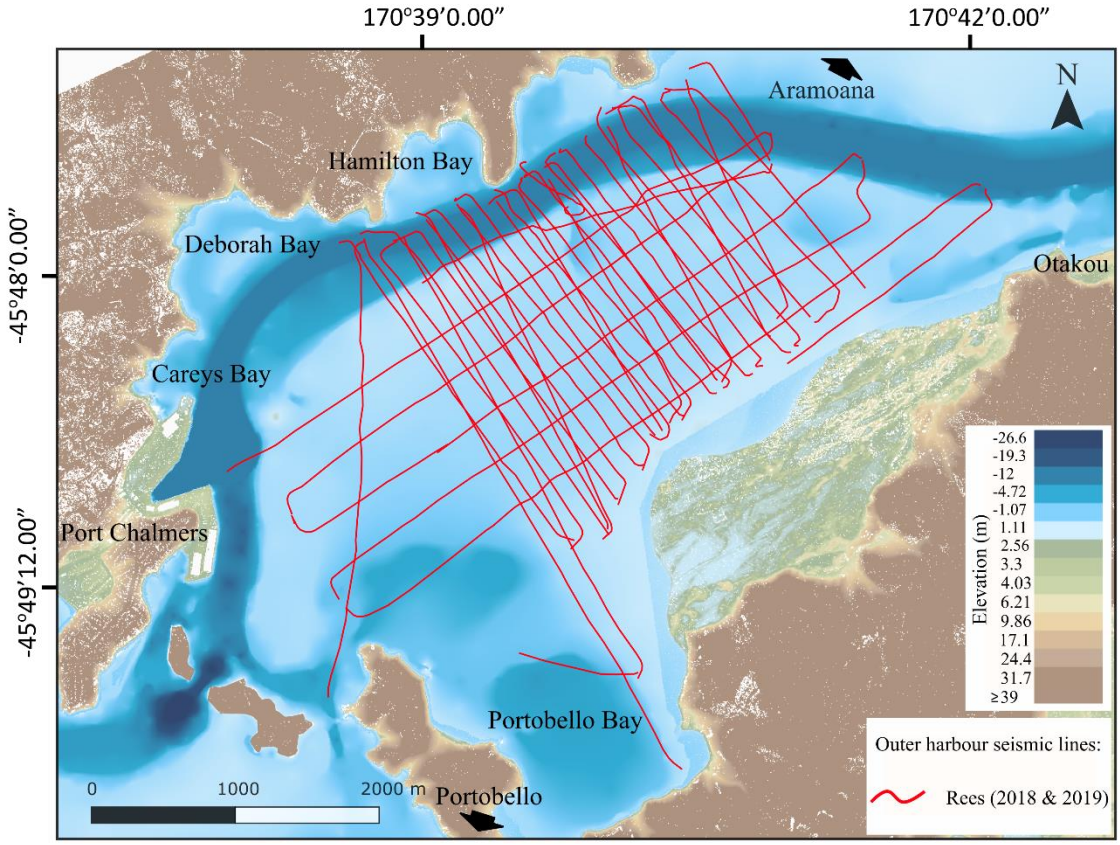

Figure 5.4: Location map of seismic lines used in the basement model. Most of the seismic profiles do not progress past the dredged channel in the northwest, resulting in the model interpolating past the line's extent. The bathymetry of the harbour ranges from <1 m (very pale blue) to approximately 20 m (dark blue).

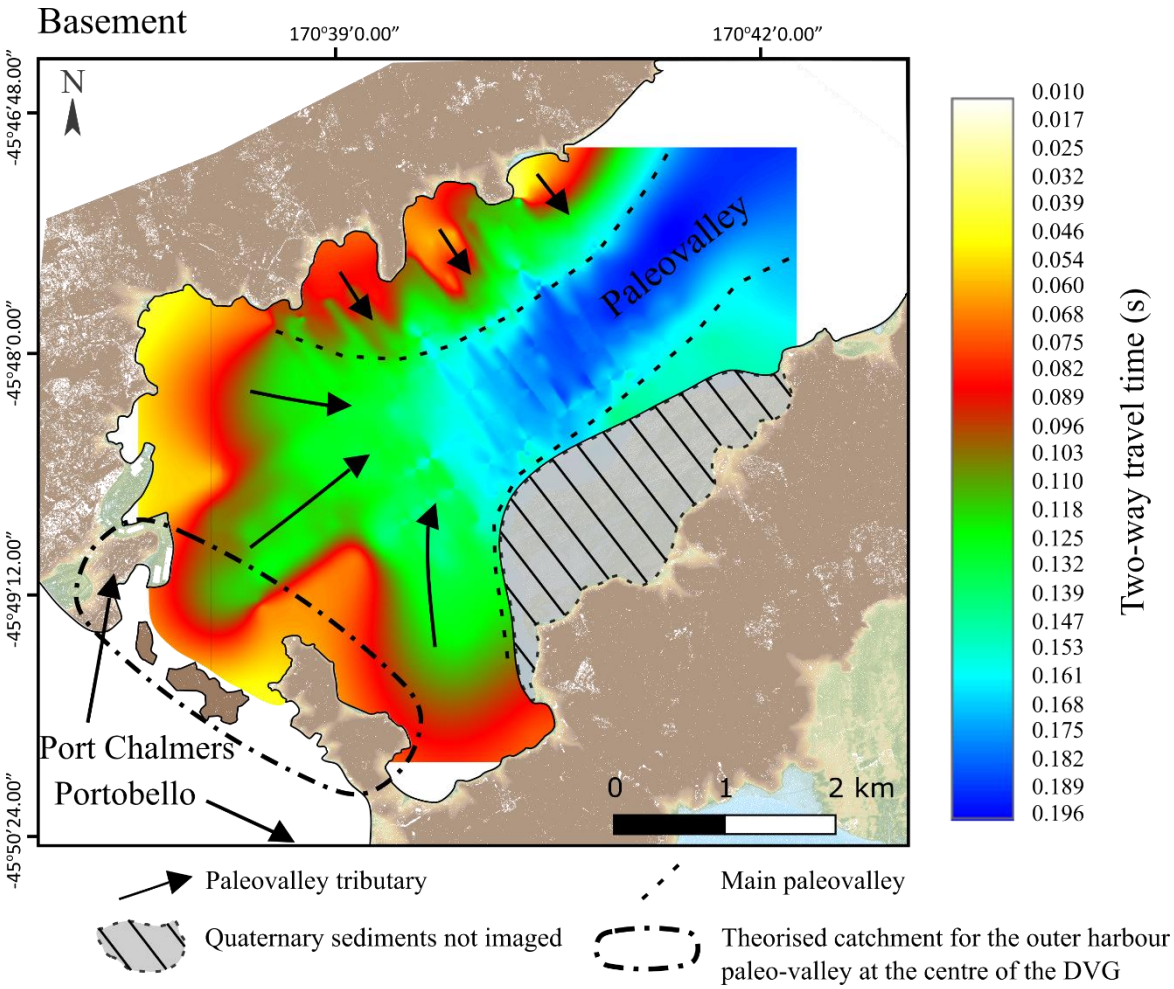

Figure 5.5: Interpolated basement two-way time model. The main paleovalley is indicated with contributing tributary paleochannels. The theorised catchment for the paleovalley is indicated at the centre of the DVG between Port Chalmers and Portobello.

5.4 Anthropogenic influence on sediments

Large tracts of the land currently occupied by central and South Dunedin were colonised via the reclamation of tidal estuarine/marsh environments (Glassey et al., 2003). The reclamation of coastal lands in Dunedin began in the mid-1800s by filling in the salt marsh and estuarine environments using any materials available, including harbour sand/silt as well as locally sourced rock and building materials. The anthropogenic influences on the sedimentary records can be quantified using pollution markers such as heavy metals like lead and arsenic (Molamohyeddin et al., 2017). Lead and arsenic counts were explored in the sediments of Dunedin as both could be

attributed to the industrialisation of Dunedin and subsequently used as chronostratigraphic markers in the sediment record (Liu et.al., 2012).

Pb/Inc has two major spikes in between comparatively low values, suggesting the introduction of lead into the environment was short-lived. The use of leaded petrol, which ceased in 1996, could be one of several likely sources of the comparatively high counts of lead in the upper 0.15 m of the CE17/0106 core. Lead contamination in the immediate subsurface via the use of leaded fuels has been investigated internationally, with health effects from lead contamination ultimately leading to legislation banning leaded fuels (MacKinnon et al., 2011). An additional significant contributor to the high counts of lead and also high arsenic would be the rapid industrialisation of Dunedin during the late 19th century as a result of the gold rush (Morris, 2008). For a short time following the 1860's gold rush, Dunedin was the most industrialised city in New Zealand, which brought industrial practices such as the burning of fossil fuels and manufacturing to the region, all probable sources of As and Pb.

Discerning the ultimate source of lead and arsenic in the South Dunedin environment was not possible as there were so many potential sources, as well as being untraceable due to the reworking of anthropogenic material; however, industrialisation in Dunedin is well documented, allowing the increase in Pb/Inc and As/Inc counts to place a chronostratigraphic constraint on the top 0.15 m of the recovered core. As the industrialisation of Dunedin began in the 1850s, we can infer a probable age of < 170 years BP at 1.15 m drilled depth (Morris, 2008) (Figure 4.12).

5.5 CE17/0106 infill history

The CE17/0106 core was differentiated into five distinct facies, the shallowest of which is anthropogenic in origin and the deepest of which is *in situ* volcanic material with three sedimentary facies in between (Figure 5.6).

The erosional paleovalley that contains the Quaternary sediments of Dunedin was previously modelled by Shears (2009), Lutter (2018) and Sangster (2019). Constraining the age of this paleovalley has been difficult, and relies on several assumptions, including a constant erosion rate for the volcano, as well as erosion only starting once

volcanism had ceased 11 Ma, and not during the 5 Myr period of volcanism. Fortunately, a dateable package of Dunedin sediments was recovered in core CE17/0106 punctuated by the volcanic basement. Radiocarbon dating has constrained the top 12.4 m of sediment at younger than 9049±43 Cal yr BP. This indicates that the sediments of CE17/0106 only constitute a fraction of the modelled time available for infill, further confirming that the core captures only the most recent of a series of erosion and infill events that have progressively filled the Dunedin paleovalley.

Multiple marine regressions and transgressions, related to cyclical glacial and interglacial periods, have controlled the shape and infill New Zealand's coastal environment (Carter, Carter and Johnson, 1986). Regional sea level curves can be used with dated cores to constrain where sea level was at a given time. Knowing the position of sea level at a time in the past can help infer the depositional environment in which sediments in the core record were deposited.

The errors in the three deepest dates overlap, suggesting these sediments were deposited over a short time. An abrupt and temporary change in sediment type was identified at 10.62-10.7 m separating the three deepest dates from the 7967±28 Cal yr BP age at 10.45 m. This change in lithology with the overlapping radiocarbon ages below suggests that this could mark a hiatus in sedimentation (Hiatus 2) where there is approximately 1000 years difference between the top of Hiatus 2 and the overlying unit (Figure 4.16). Reconstructions from Fiordland find that approximately 9000 ka, South Island sea level was approximately 10-20 m below current levels which would have left the sediments below Hiatus 2 exposed (Dlabola et al., 2015). During this time there would not be any accumulation space as sea level was significantly lower (Zorina, 2013). Marine transgression overtopped the lower hiatus (number two) approximately 8 ka, creating accommodation space for sediments to begin to infill. The infill was initially quick, depositing 4 mm/yr between 7967±28 Cal yr BP (10.45 m) and approximately 6700 Cal yr BP (5.25 m). Present mean sea level in Otago was reached at approximately 6700 BP and continued to increase to +1 m by 6000 BP (Clement et al., 2016). At 6700 BP accommodation space was still increasing slowly; however, the rate of accumulation began to slowly decrease from 3.3 mm/yr at 5.25 m to 0.7 mm/yr at 1.4 m as peak sea level is reached at 4 ka (+2 m) (Clement et al., 2016; Dlabola et al., 2015).

The Fiordland sea level curve from Dlabola et al (2015) is limited to the initial inundations of post-glacial marine transgression, losing resolution at approximately 7500 BP, after which the curve is comprised of other published global sea level curves. The sea level curve from Clement et al (2016) is comprised of dated estuarine shells and covers modelled sea level from 8 ka to present but lacks any older data points. The combination of the two curves allows the continuation of modelled sea level through the Holocene deposition of the CE17/0106 core.

Another hiatus, Hiatus 1, was placed at an abrupt change in lithology at 1.15 m, the boundary between F1 and F0 (Figure 4.16 and 5.6). Anthropogenic heavy metal contamination in the sediments provides a maximum age constraint of 170 yr at 1.15 m, which marks the start of industrialisation in Dunedin (Morris, 2008) (Figure 4.12). The absent 3653 yr between the top of F1 and the base of F0 presents a significant hiatus in sedimentation (Figure 4.16). F1 exhibits a larger mean grain size than F2, which included not only silts but very fine to fine sand, falling into group one of the grain size distribution graphs (Figure 4.3). The larger grain size coupled with an initially primarily lithogenic sediment source followed by an increase in marine biogenic sediment suggests an erosional contact at the top of F1 where any sediment deposited on top of this section is eroded or simply did not deposit as there wasn't any accommodation space left in the basin (Zorina, 2013) (Figure 5.6). Between 4 ka and present-day sea level gradually decreased, which reduced the accommodation space within the basin and probably resulted in the erosion of sediments deposited above current sea levels between 6-4 ka (Clement et al., 2016).

Both occurrences of F1 are interpreted as a salt marsh (which would provide the biogenic sediment) and surrounded by dunes (which would provide the lithogenic sediment), equivalent to the salt marsh seen in present-day Aramoana at the northern entrance to Otago Harbour (Meyers & Teranes, 2001; Nichols, 2009; Shears, 2009) (Figure 5.3).

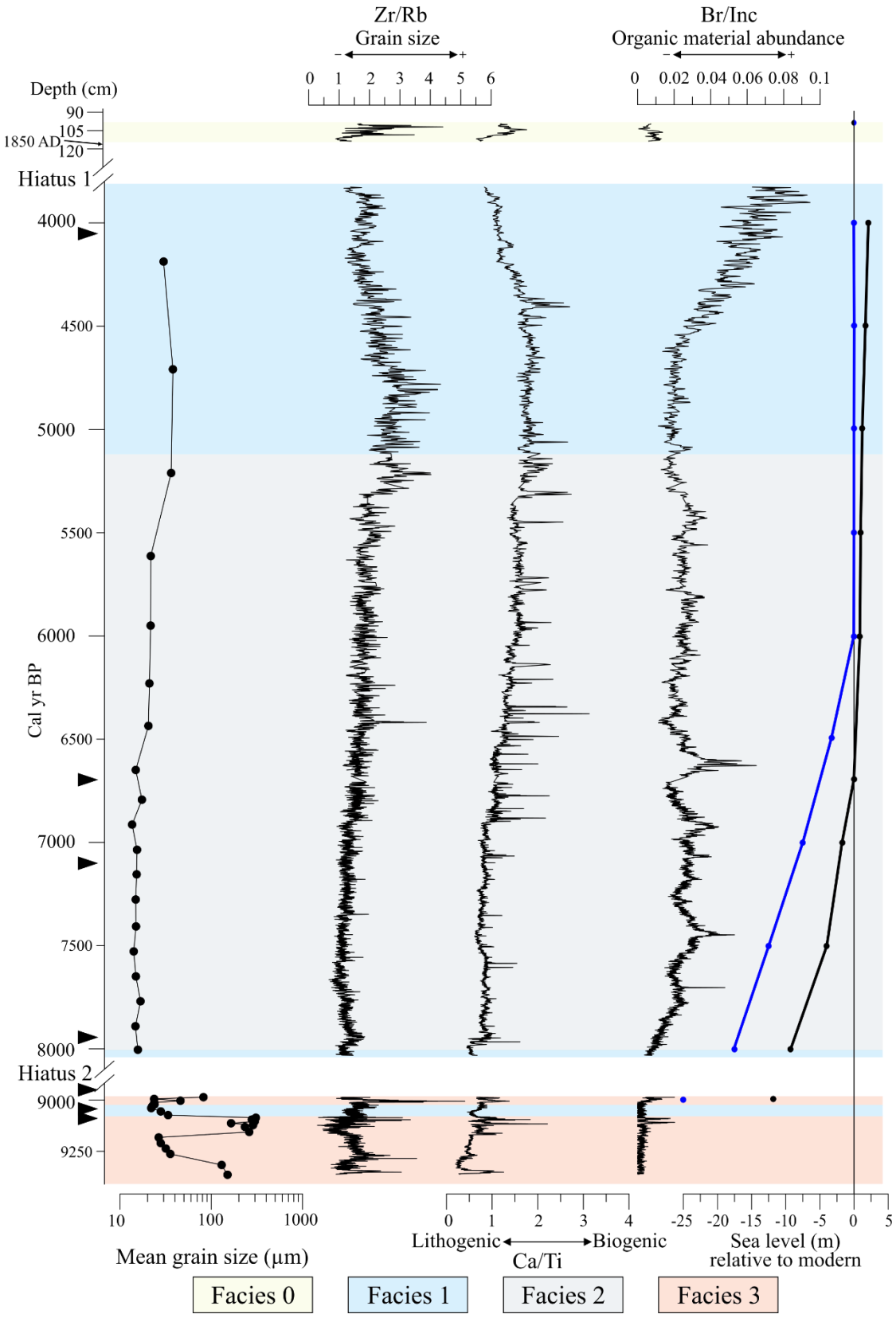

Figure 5.6: Grain size and XRF measurements plotted against the CE17/0106 age model , sea level curves adapted from Dlabola et al (2015) in blue and Clement et al (2016) in black. Radiocarbon samples are illustrated as black triangles on the age scale.

5.6 Southern paleovalley of Otago Harbour

The distribution of both the unconsolidated sediments of Dunedin and the basement rock observed across the NZ SeaRise cores was significantly different than theorised prior to drilling. Before 2019, few subsurface investigations were available to ground-truth geophysical interpretations of the geology beneath Dunedin. The tombolo that connects Otago Peninsula to the mainland consists of unconsolidated sediments, the thickness of which were poorly constrained (Glassey et al., 2003; Rees, 2018). The addition of the NZ SeaRise cores provides additional controls on the extent of the tombolo as well as indicating the probable location of the paleochannel that would have drained to the south in the past. Two cores, CE17/0106 and CE17/0107, collected at De Carle Park and Moana Rua Road respectively, terminated in basalt, at 13.3 m in core CE17/0106 and 16.2 m in core CE17/0107 (Figure 5.7 and 5.8). During initial logging of CE17/0106, the recovery of the weathered surface of the volcanic material was interpreted to mean that a volcanic boulder had been encountered; however, the recovery of similar volcanic material in core CE17/0107 suggests that both cores reached the basaltic basement of the Dunedin Volcanic Group (Figure 5.8).

The deepest of the NZ SeaRise cores (CE17/0105) was collected in Tonga Park. It reached a depth of 44.5 m and recovered volcanic material. From an interval spanning 18-23.5 m. However, unlike the basalt observed in the other cores, it consisted of heavily weathered and fractured volcanic clasts containing pebble-sized particles. The origin of this unit and whether it is *in situ* or was reworked post-eruption is still being debated by the researchers involved, but the evidence suggests that the sub-angular weathered volcanic material was likely sourced from a mass-wasting event from cliffs located to the west of Tonga Park. 21 m of unconsolidated sand, possibly weathered Caversham Sandstone, underlies this layer of volcanic material. However, the unconsolidated nature of the sand and the lack of basement recovery at 44.5 m at Tonga Park, contrasted with the shallow recovered basement at De Carle Park and Moana Rua Road, indicating that the paleochannel must have drained the harbour west of bedrock observations where the maximum sediment depth is >44.5 m. Edgar Centre core logs from Rees (2018) showed the basement at Portsmouth Drive was also >45.5 m, adding another constraint on the position of the paleochannel.

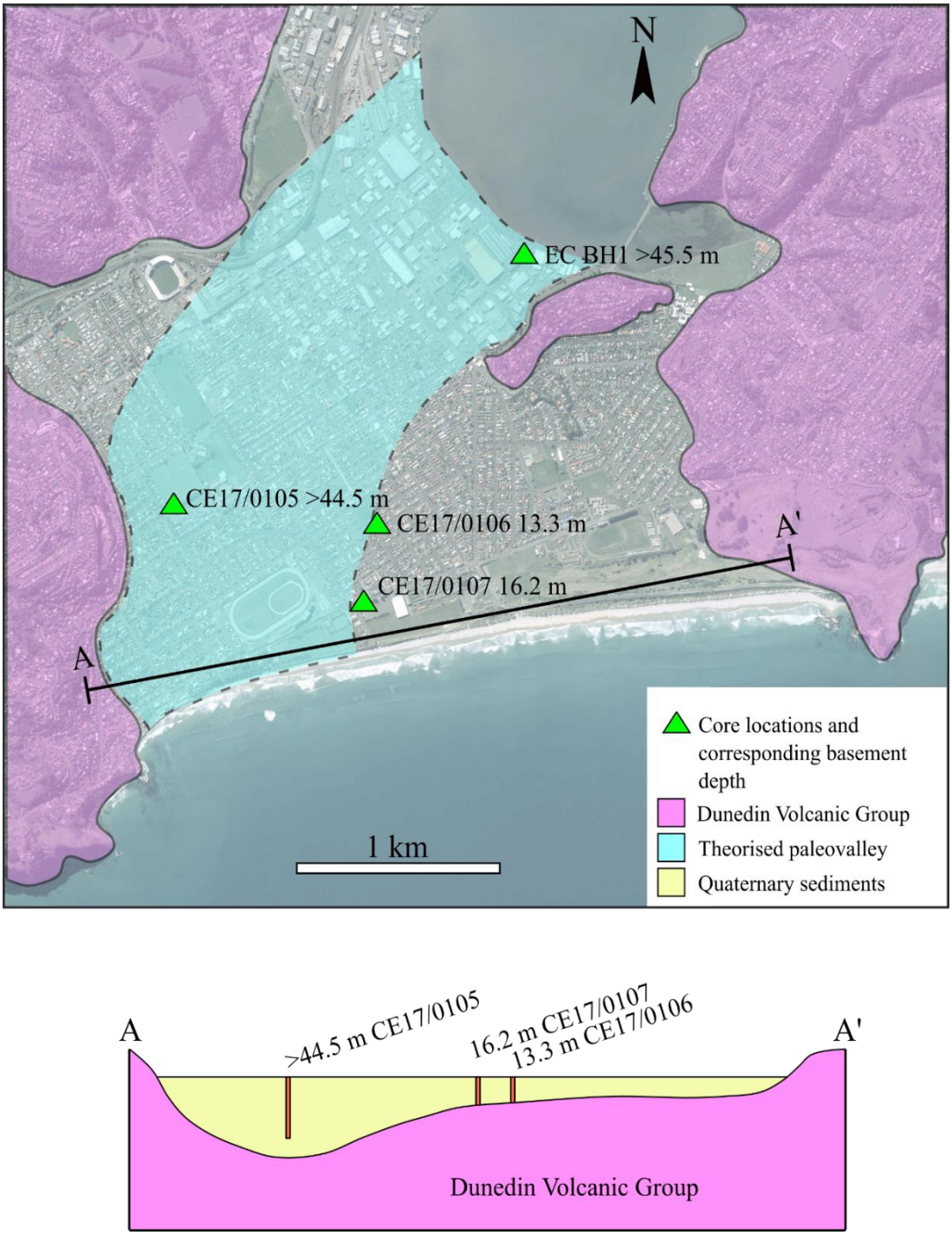

Figure 5.7: Dunedin basement map outlining the likely paleovalley's position through South Dunedin. Cores with observed basement depths are indicated on a cross-section spanning from St Clair in the west to Lawyers Head in the east. The basement is not observed in the deepest two cores but is thought to be part of the Dunedin Volcanic Group.

Figure 5.8: Generalised stratigraphic log of the NZ SeaRise and Edgar Centre cores.

Extensive gravity data collection and modelling has been undertaken in the Dunedin area by Shears (2009), and Lutter (2018), with remodelling by Sangster (2019). Two transects of interest collected at the harbourfront along Portsmouth Drive and along Victoria Road in St Clair have been used to infer likely basement profiles at the northeastern and southern extents of South Dunedin (Shears, 2009) (Figure 5.9). The transect along Portsmouth Drive indicates the deepest basement is between the Edgar Centre in the southeast and Birch Street in the north, between 60-79 m below mean sea

level (Figure 5.9). This generally agrees with a basement depth >45.5 m at the EC BH1 core site (Figure 5.7 and 5.8).

The southern transect heading from west to east along the St Clair and St Kilda dunes indicates the deepest basement (60-79 m) is located near Tahuna Park, 1.2 km northeast of the CE17/0107 core, which indicated basement at 16.2 m (Figure 5.8 and 5.9). With the revised model of South Dunedin basement, this measurement probably falls south of the basaltic flow observed in the CE17/0106 and CE17/0105 cores. The basement is indicated at 40-59 m from St Kilda to Tahuna Park, which with ground-truthing via the CE17/0107 core, indicates the deepest basement is probably between Moana Rua Road and St Clair (Shears, 2009).

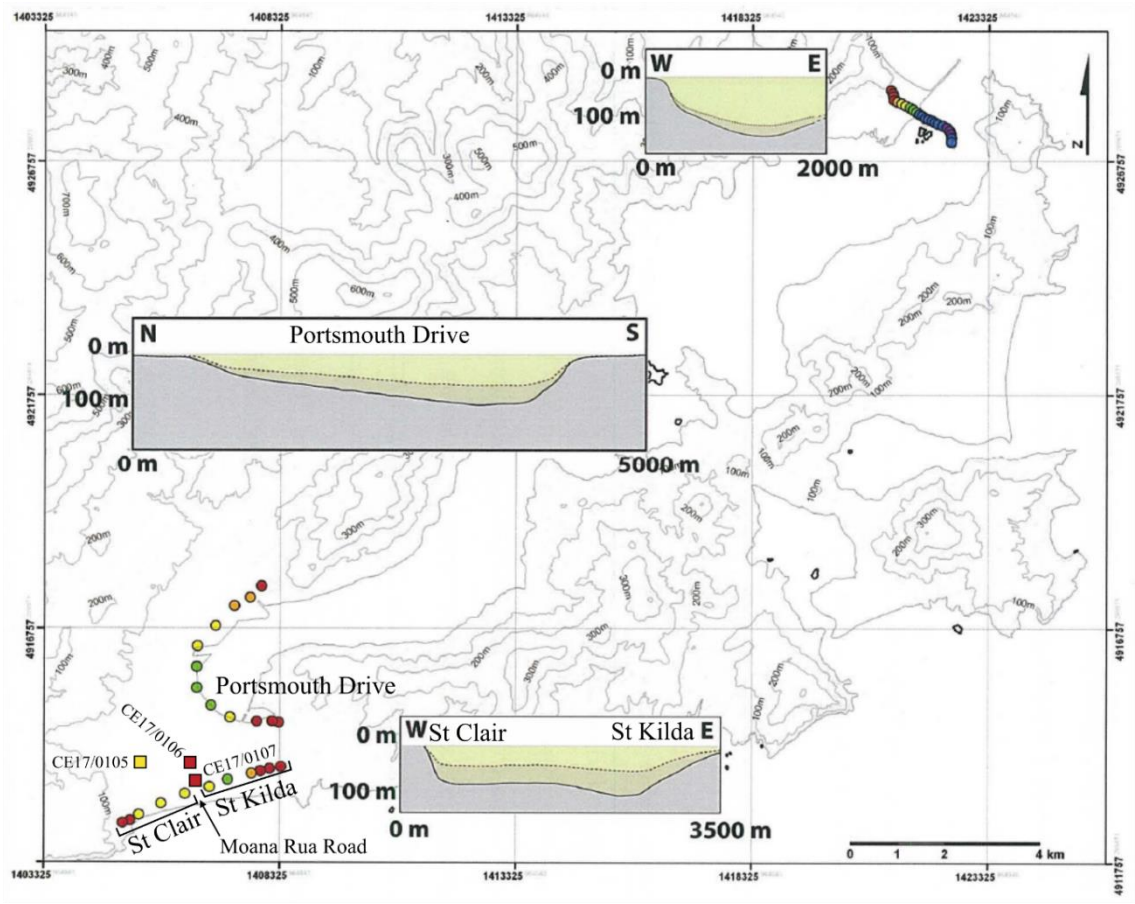

Figure 5.9: Gravity transect profiles adapted from Shears (2009). Profiles indicate modelled basement depths at the northeastern and southern extents of South Dunedin. Depths are presented as coloured dots; red is 0-19 m, orange is 20-39 m, yellow is 40-59 m, green is 60-79 m, blue is 80- 99m and purple is 100-119 m (Shears, 2009).

This interpretation is supported by Sangster's (2019) gravity depth contour map for South Dunedin. The gravity contours indicate the deepest basement in South Dunedin is located at Tonga Park (where CE17/0106 indicated >44.5 m basement), then it shallows to the south where the paleovalley probably drained between St Clair and Moana Rua Road (Lutter, 2018; Sangster, 2019) (Figures 5.9 and 5.10).

Although this paleovalley has not yet been cored at its deepest point, the newly collected cores coupled with extensive gravity modelling, indicate revised constraints on a southern paleo drainage channel for Otago Harbour. The new core record can now constrain the paleochannel to one-third of the area previously identified. These cores suggest the revised paleochannel location is between St Clair in the west and Moana Rua Road in the east (Figure 5.7 and 5.9).

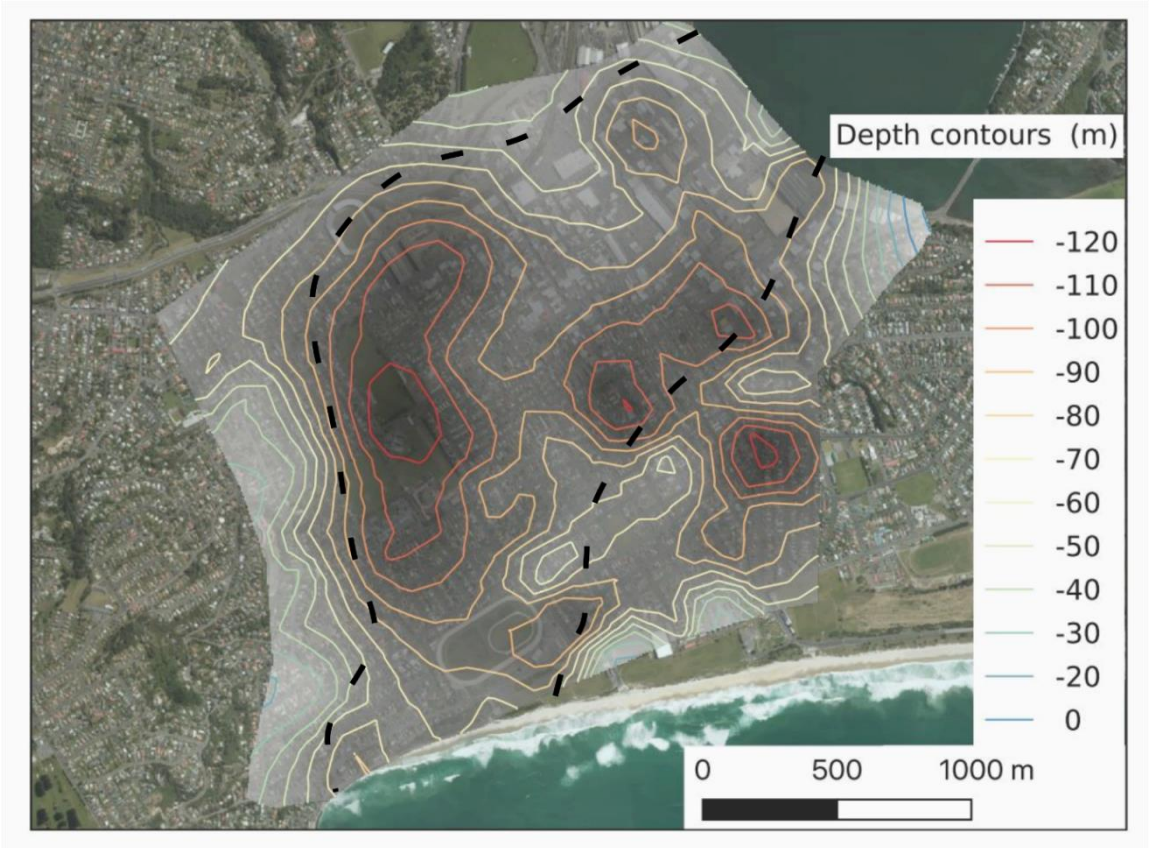

Figure 5.10: Three-dimensional gravity-depth contour map adapted from Sangster (2019). Gravity indicated depths of 120 m in Tonga Park shallowing south to the likely mouth of the southern harbour paleovalley. Probable paleovalley path is indicated by dashed lines.

5.7 Ground-truthing the Outer Harbour seismic stratigraphy

Several distinct horizons were identified in the high-density grid of seismic data collected in Otago Harbour. As discussed in section 4.8, sedimentary horizons could be identified in each of the 42 lines collected in 2019, matching horizons identified and interpreted from Fletcher (2016) and Rees (2018). These were selected using visual and spatial characteristics such as shape and two-way time which were all mapped in the seismic analysis software package Kingdom. Velocity-to-depth calculations for lines 19_30 and 19_21 indicate the shallowest prominent reflection observed across multiple surveys, 1OH (represented by a yellow line) varies in depth from approximately 15-20 mbsf (Fletcher, 2016; Rees, 2018; this thesis, section 4.8) (Figure 5.11). This reflection is interpreted to result from a lithologic change in the CE17/0106 core; a package of estuarine silts (F1) from 1.15 to 11.4 m is in sharp contact with an underlying 1.9 m section of fine to coarse sand (F3) (Figure 5.12). A similar package of sediments is observed in the EC BH1 core, with an upper interval of estuarine silts from 3.6- 18.4 m, underlain by 5.3 m section of fine to coarse sand (Figure 5.12). The significant density contrast related to these abrupt lithologic changes is consistent with the shallow 1OH reflection in the harbour seismic data (Sidler & Holliger, 2010) (Figure 5.11). The correlation of the sediment stratigraphy of Dunedin and the seismic reflection record provides a proof of concept for seismic imaging as a robust way of imaging the harbour.

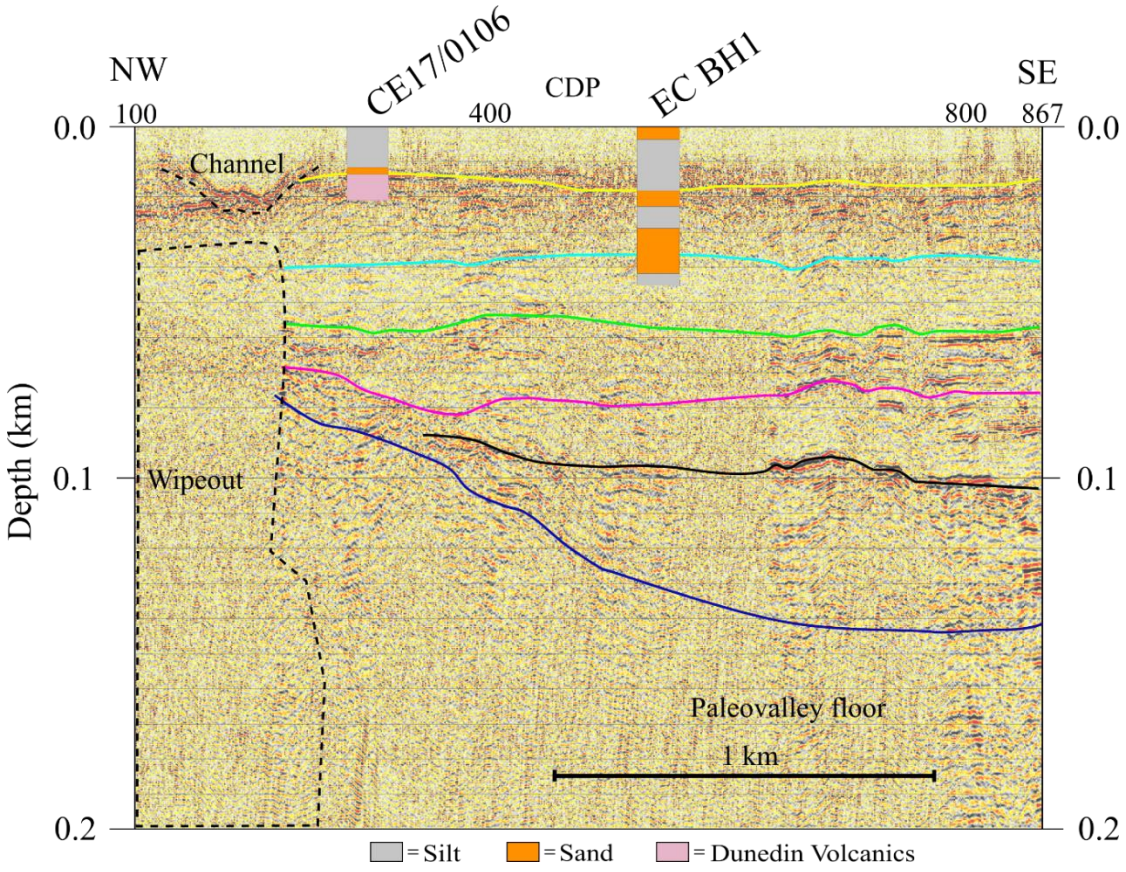

Figure 5.11: Cross-section of line 19_21. superimposed core logs illustrate the depth of changes in sediment and how they coincide with horizons observed in the outer harbour.

.

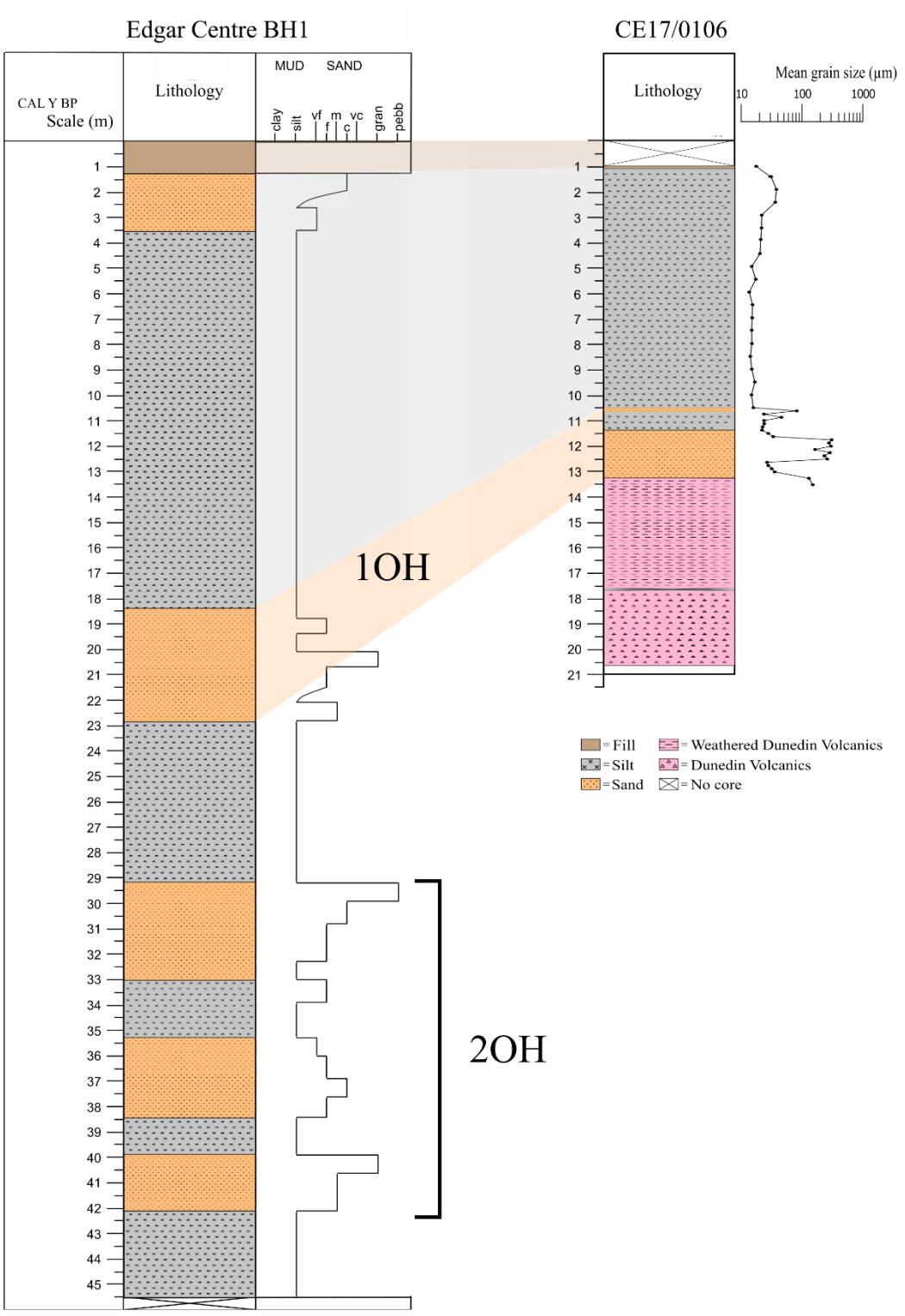

Figure 5.12: Core logs from the Edgar Centre and CE17/0106 with probable 1OH horizon.

5.8 Outer harbour infill characteristics

The five reflective horizons observed in the harbour represent laterally continuous erosional or depositional surfaces that probably correspond to past high stands (Spratt & Lisiecki, 2016). The upper three horizons (1OH, 2OH and 3OH) are largely continuous and planar, suggesting there was probably very little erosion or alteration to the horizons after deposition (Figure 5.13). The two deepest horizons, 4OH and 5OH, have a more undulating appearance, indicating probable reworking of the sediments and incision by paleochannels when sea level was lower, after the original planar deposition of the horizons (Fletcher, 2016; Nichols, 2009) (Figure 5.13). The presence of incised channels is further emphasised in the basal reflection where the deepest sector of the basement is bisected by a shallower ridge (Figure 5.13). On either side of the ridge, two largely concave reflections could be extensions of the same meandering paleochannel or two separate channels that were exploited at different times (Wakabayashi, 2013) (Figure 5.13).

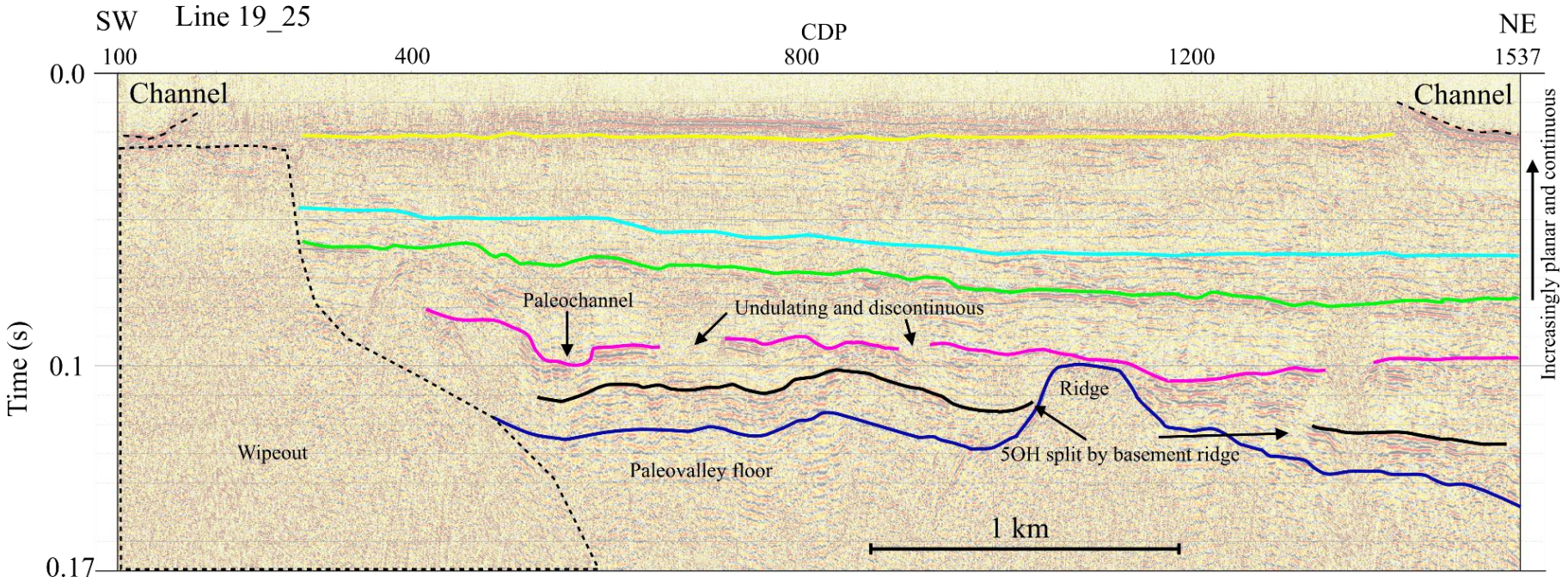

Figure 5.13: Line 19_25 seismic profile illustrating the increasing undulation of horizons with depth. The black horizon is punctuated by a ridge in the basal reflection.

5.9 Implications of characterising the Quaternary infill of Dunedin

Natural harbours like Otago Harbour can preserve extensive paleoclimate records, allowing the correlation of changes in lithology to global fluctuations in sea level (Smith et al., 2010).

A better understanding of the local Quaternary sediments and how they accumulated in low lying areas like South Dunedin, will help scientists and government agencies to plan remedial works when sea level inevitably rises to critical levels. Predicting the probable changes to coastal shorelines and the infrastructure that inhabits it is becoming more important than ever in paleoclimate research (Woodruff et al., 2013). Sea level is expected to increase in excess of 1 m by 2100; in South Dunedin's case, this will put a large area close to or below sea level (Morris, 2008).

The sediment of Otago Harbour is sourced primarily from longshore drift sediments from the south (Smith et al., 2010). This sediment formed the tombolo connecting Otago Peninsula and Dunedin, closing off the southern drainage of Otago Harbour (Lutter, 2018). The closure of the southern entrance to the harbour resulted in the formation of a low energy estuarine environment. As sea level begins to rise two main possibilities could occur to the sediments of Dunedin, driven by time and the relative abundance of sediment.

In the first scenario, as sea level rises, so too does the amount of accommodation space for sediments to accumulate, which could result in the South Dunedin landscape to returning (temporarily) to the predominantly estuarine and salt marsh environment observed in the CE17/0106 core before once again emerging as a coastal plain due to ongoing sedimentation sourced from longshore sediment transport (Figure 4.1). This outcome is dependent on the protective dune system of St Clair and St Kilda beaches being continually replenished by sediments sourced through longshore drift (Shears, 2009).

An alternate scenario based on a situation where there is an insufficient longshore sediment source would be the continued erosion of the South Dunedin tombolo, exposing the mainly estuarine/reclaimed sediments to inundation from the sea, and

causing significant damage to housing and infrastructure (Glassey et al., 2003). An example of a coastal setting with low sediment accumulation in New Zealand is Wellington Harbour. Sediment accumulation rates in Wellington Harbour have been stable since 5000 ka, and have only recently increased as a result of deforestation (Goff, 1997). One result of this low accumulation rate is that only minimal dredging of Wellington Harbour is needed to support shipping operations, unlike Otago Harbour, which requires regular dredging (Carter et al., 2003; Otago Regional Council, 2006).

The coastal beaches and estuaries of Otago Harbour would probably persist as sea level rose in Dunedin, provided accumulation rates remain high, unlike Wellington Harbour which with inundation would likely erode out the same coastal features (Carter et al., 2003; Morris, 2008). As sea level rises, the ocean will penetrate further inland, exacerbated by storm surge acting to further accelerate erosion (Morris, 2008; Warrick & Wigley, 1993). A rapid change in sea level expected by 2100, will likely have significant global impacts not only in cities with low lying lands in New Zealand, such as Dunedin but to coastal communities around the globe (Morris, 2008).

The collection, processing and analysis of shallow marine seismic reflection data in a harbour environment, has proved that such methods can successfully image the stratigraphy of a coastal basin infilled over a long period with highstand sediments. The resulting data have mapped a large shallow environment using high-resolution data. This provides methodological proof of concept that shallow-water seismic data can be used effectively to constrain other basins located in shallow water as a cost and time-effective alternative to drilling.

Radiocarbon dating of core CE17/0106 core demonstrates that the recovered sedimentary sequence was deposited during the Holocene. This package provides ground-truthing for the shallowest observed seismic horizon in the outer harbour (1OH), confirming that only the 1OH was deposited in the Holocene (Figure 4.16). The four deeper reflections observed in the outer harbour (2OH-5OH) are unconstrained by radiocarbon dating but must be older than Holocene in age; however, the similar reflection characteristics as 1OH suggest similar processes of formation. These four horizons are probably linked to glacially driven sea level fluctuations throughout the Quaternary, resulting in the gradual infill of Otago Harbour (Fletcher, 2016).

The Quaternary sediments of Dunedin provide a rare opportunity to observe near-shore highstand sedimentary sequences. Coastal environments deposited as a result of a sea level highstand often are not preserved within the geological record as they are easily eroded when exposed above sea level (Billeaud et al., 2007). These units, therefore, provide a unique opportunity to study past coastal environments established during relatively warm periods in the Earth's recent history.

5.10 Limitations and future work

In the future, an extensive harbour drilling and coring project based off Harwood, could provide a complete stratigraphic record through the harbour sediments and confirm the basement geology of the harbour (Figure 5.3). This drilling would not only be expensive but logistically difficult in the shallow mudflats, requiring a large number of environmental impacts to be considered. A full core to the basement could provide a complete stratigraphic record to ground-truth the seismic reflection data as well as providing P-wave velocities that could be used to more accurately calculate the relative depths of sedimentary horizons and basement mapped through the rest of Otago Harbour. Optical-stimulated luminescence dating coupled with additional radiocarbon dating of the upper portion of this sedimentary record could place more robust age constraints on the full infill history of Otago Harbour and other sedimentary units in the Dunedin Area.

A land-based seismic survey across South Dunedin with profiles running perpendicular to the theorised southwestern harbour channel could define the channel extent as well as help to identify any faults that may be present, particularly within sedimentary strata. This could also help to correlate the sediments observed across the NZ SeaRise and Edgar Centre cores.

Finally, revisiting both the Moana Rua Road and De Carle Park core sites and re-drilling into and below the basaltic flow observed in the NZ SeaRise cores, and into the underlying basement would conclusively determine whether Caversham Sandstone is present in this area (Figure 5.3). This could strengthen the interpretations of Caversham Sandstone at Tonga Park, definitively proving if the basement of Otago Harbour is Caversham Sandstone or part of the Dunedin Volcanic Group.

Chapter 6 Conclusion

This investigation into the sedimentation patterns found in the Quaternary deposits lying under Dunedin has produced a number of significant findings concerning past sea level variability and how that has resulted in the systematic infill of Dunedin's Quaternary sediment, as well as expanding on theories on the evolution of Otago Harbour proposed by previous researchers. This project aimed to combine geochemistry, radiocarbon dating and physical observations of core CE17/0106 with newly collected marine seismic data, supported by analyses of previously modelled gravity and marine seismic data, to produce enhanced understanding of the characteristics and processes forming the sediments of Dunedin and Otago Harbour.

A key result of this investigation was constraining both the basal geometry and infilling sedimentation patterns of the southern paleovalley that at one time would have drained Otago Harbour beneath South Dunedin. Prior gravity and marine seismic investigations identified the presence of the paleovalley; however, the NZ SeaRise cores collected in South Dunedin resolved the depth (or minimum depth) of the basement and the sediments that infilled at those locations. The NZ SeaRise cores, coupled with gravity modelling and marine seismic reflection data, have confidently placed constraints on the orientation and extent of this southern drainage of Otago Harbour.

Another major result of this investigation was constraining basement geometry and using this to indicate the erosion history and key boundary conditions for the infill of the basin. The lack of observed basement in the CE17/0105 (Tonga Park) and the Edgar Centre cores in South Dunedin indicate that basement is significantly deeper there than where it outcrops at Quarantine and Goat islands near Port Chalmers. This basin geometry, from the seismic data in the outer harbour, suggests that the harbour formed as a result of erosion from two main river systems, flowing in opposite directions away from a central catchment situated at the centre of the Dunedin volcano between Port Chalmers and Portobello. The depth of the paleovalleys illustrates the controls that sea level has on erosion. As sea level dropped it increased the influence of fluvial erosion on the basement of the harbour, which began to infill as sea level rose.

Based on these new data, the most recent episode of rapid sediment infill in South Dunedin is attributed to sea level transgression over the last 9 ka, during which time the region in the vicinity of the CE17/0106 core underwent three major lithological changes, producing five distinct facies. The entire core was deposited in the last 9048.5±42 Cal yr BP on top of an *in situ* basaltic flow >11 Ma in age. The age of the sediments, as well as the depth of sedimentary features, is consistent with regional sea level curves, showing that the sediment package that makes up the CE17/0106 core only constitutes a fraction of the modelled infill time. Further, this suggests that the core recovered only the most recent in a series of Quaternary erosion and infill events that have progressively produced the sedimentary sequence, identified using geophysical techniques, beneath Dunedin and Otago Harbour.

The high-density collection of seismic data in the outer harbour has constrained five regional horizons that could be mapped across the Quaternary basin infill. The shallower horizons are planar and continuous, becoming more undulating and discontinuous with depth. Where the basement is shallower (adjacent to Port Chalmers) the deeper horizons are less evident; these deeper horizons become more evident as the basement deepens towards the northeast. The two deepest horizons (4OH and 5OH) and the basement reflection show evidence of channelling, where a river has eroded material between highstand events.

The improved understanding and constraints that this project and previous seismic and gravity work have placed on the sediments of the harbour and South Dunedin, will have an ongoing impact on how policymakers and other stakeholders (e.g., the Dunedin City Council, Otago Regional Council, and Port Otago) manage the local environment and resources. The newly identified depth of basement at De Carle Park and Moana Rua Road was significantly shallower than anticipated; this could have significant implications in future development in this area (e.g., the depth to a solid volcanic basement upon which to build is less than 16.2 m). Finally, using radiocarbon dating and correlation to horizons observed in harbour seismic images, I have constrained the infill of the harbour through successive changes in sea level through the Quaternary.

This investigation has revised our understanding of the sediments of Dunedin and Otago Harbour, establishing a foundation for future investigation to ground-truth these theories with additional drilling.

Chapter 7 Appendix

A. Original CE17/0106 core log produced by GNS Science

B. CE17/0106 core photos

C. CE17/0106 secondary core log

D. CE17/0106 Itrax XRF and Mastersizer grain size data

E. Outer harbour job control system (JCS) file

F. 2019 outer harbour processed seismic lines

G. Portable Kingdom project file

References

Allen, J. M. (1974). Port Chalmers Breccia and adjacent early flows of the Dunedin volcanic complex at Port Chalmers. *New Zealand Journal of Geology and Geophysics*, *17*(1), 209–223. https://doi.org/10.1080/00288306.1974.10427997

Baxter, R. J. M. (2019). Petrogenesis , eruption and emplacement of the volcanic rocks at Otapahi , Otago Peninsula . *Unpublished MSc Thesis, University of Otago*, 169.

Benson, W. N., & Turner, F. J. (1989). Comparative Composition-Variation Diagrams for the Cenozoic Igneous Rocks of New Zealand with Determinations of the Optic Axial Angles of the Pyroxenes and Olivines Contained Therein. *Mineralogical Notes from the University of Otago, New Zealand*.

Billeaud, I., Tessier, B., Lesueur, P., & Caline, B. (2007). Preservation potential of highstand coastal sedimentary bodies in a macrotidal basin : Example from the. *Sedimentary Geology*, *202*, 754–775. https://doi.org/10.1016/j.sedgeo.2007.09.002

Blott, S. J., & Pye, K. (2001). GRADISTAT: A grain size distribution and statistics package ffor the analysis of unconsolidated sediments. *Earth Surface Processes and Landforms*, *1248*, 1237–1248.

Boggs, S. (2006). *Principles of SEDIMENTOLOGY and STRATIGRAPHY*. (P. Lynch, Ed.) (4th ed). New Jersey: PEARSON, Prentice Hall.

Bull, W. B., & Cooper, A. F. (1986). Uplifted marine terraces along the alpine fault, new zealand. *Science (New York, N.Y.)*, *234*(i), 1225–1228. https://doi.org/10.1126/science.234.4781.1225

Carteer, R. ., Carter, L., & Johnson, D. P. (1986). Submergent shorelines in the SW Pacific: evidence for an episodic post-glacial transgression. *Sedimentology*, *33*(5), 629–649. https://doi.org/10.1111/j.1365-3091.1986.tb01967.x

Carter, D., Hedley, S., & Clarke, B. (2003). Port dredging and the resource management act 1991: the Centreport experience. *Coasts & Ports Australasian Conference 2003*, *2000*(61), 1–11.

Carter, L. (2010). A budget for modern - Holocene sediment on the South Otago continental shelf A budget for modern-Holocene sediment on the South Otago continental shelf. *Marine and Freshwater Research*, *8330*. https://doi.org/10.1080/00288330.1986.9516187

Chong, J., & Ni, S. (2009). Near surface velocity and QS structure of the Quaternary sediment in Bohai basin, China. *Earthquake Science*, *22*(5), 451–458. https://doi.org/10.1007/s11589-009-0451-1

Clement, A. J. H., Whitehouse, P. L., & Sloss, C. R. (2016). An examination of spatial variability in the timing and magnitude of Holocene relative sea-level changes in the New Zealand archipelago. *Quaternary Science Reviews*, *131*, 73–101.

Coombs, D S, White, A. J. R., & Hamilton, D. (1960). Age relations of the Dunedin volcanic complex and some paleogeographic implications. *New Zealand Journal of Geology and Geophysics*, *3*(2), 325–336. https://doi.org/10.1080/00288306.1960.10423605

Coombs, Douglas S, Adams, C. J., Roser, B. P., & Reay, A. (2010). Geochronology and geochemistry of the Dunedin Volcanic Group , eastern Otago , New Zealand. *New Zealand Journal of Geology and Geophysics*, *8306*. https://doi.org/10.1080/00288300809509860

Croudace, I. W., & Rothwell, R. G. (2015). *Micro-XRF Studies of Sediment Cores: Applications of a non-destructive tool for the environmental sciences*. *Developments in Paleoenvironmental Research* (Vol. 17). https://doi.org/10.1007/978-94-017-9849-5

Davies, S. J., Lamb, H. F., & Roberts, S. J. (2015). Micro-XRF Studies of Sediment Cores. In *Micro-XRF Studies of Sediment Cores: Applications of a non-destructive tool for the environmental sciences* (Vol. 17). https://doi.org/10.1007/978-94-017-9849-5

Dlabola, E. K., Wilson, G. S., Gorman, A. R., Riesselman, C. R., & Moy, C. M. (2015). A post-glacial relative sea-level curve from Fiordland, New Zealand. *Global and Planetary Change*, *131*, 104–114. https://doi.org/10.1016/j.gloplacha.2015.05.010

Fletcher, P. T. (2016). The Geological Evolution of Otago Harbour: A High-Resolution Seismic Reflection Study. *Unpublished BSc(Hons) Thesis, University of Otago*.

Frank, M. (2016). Brittle faulting and fluid flow in basement rocks of coastal Otago (South Island , New Zealand). *Unpublished MSc Thesis, University of Otago*, 129.

Glassey, P., Barrell, D., Forsyth, J., & Macleod, R. (2003). The geology of Dunedin, New Zealand, and the management of geological hazards. *Quaternary International*, *103*, 23–40. https://doi.org/10.1016/S1040-6182(02)00139-8

Goff, J. . (1997). A chronology of natural and anthropogenic influences on coastal sedimentation, New Zealand. *Marine Geology*, *3227*(97).

Gray, D. R., & Foster, D. A. (2004). Ar / 39 Ar thermochronologic constraints on deformation , metamorphism and cooling / exhumation of a Mesozoic accretionary wedge , Otago Schist , New Zealand. *TECTONOPHYSICS*, *385*, 181–210. https://doi.org/10.1016/j.tecto.2004.05.001

Haldorsen, J. B. U., Miller, D. E., & Walsh, J. J. (1994). Multichannel Wiener deconvolution of vertical seismic profiles. *Geophysics*, *59*(10), 1500–1511. https://doi.org/10.1190/1.1443540

Hamilton, E. L. (1963). Sediment Sound Velocity Measurements Made In Situ from Bathyscaph Trieste. *Journal of Geophysical Research*, *68*, 5991–5998.

Hampton, S. J. (2010). Growth, Structure and Evolution of the Lyttelton Volcanic Complex, Banks Peninsula, New Zealand. *Unpublished PhD Thesis, University of Canterbury*, 330.

Han, F. X., Sun, J. G., & Wang, K. (2012). The influence of sea water velocity variation on seismic traveltimes, ray paths, and amplitude. *Applied Geophysics*, *9*(3), 319–325. https://doi.org/10.1007/s11770-012-0344-2

Hepp, D. A., Mörz, T., & Grützner, J. (2006). Pliocene glacial cyclicity in a deep-sea sediment drift (Antarctic Peninsula Pacific Margin). *Palaeogeography, Palaeoclimatology, Palaeoecology*, *231*(1–2), 181–198. https://doi.org/10.1016/j.palaeo.2005.07.030

Hogg, A. G., Hua, Q., Blackwell, P. G., Niu, M., Buck, C. E., Guilderson, T. P., … Zimmerman, S. R. H. (2013). SHCal13 Southern Hemisphere Calibration, 0–50,000 Years cal BP. *Radiocarbon*, *55*(4), 1889–1903. https://doi.org/10.2458/azu_js_rc.55.16783

Ingram, W. C., Meyers, S. R., Brunner, C. A., & Martens, C. S. (2010). Late Pleistocene-Holocene sedimentation surrounding an active seafloor gas-hydrate and cold-seep field on the Northern Gulf of Mexico Slope. *Marine Geology*, *278*(1–4), 43–53. https://doi.org/10.1016/j.margeo.2010.09.002

Kamp, P. J. J., & Tippett, J. M. (1993). Dynamics of Pacific plate crust in the South Island (New Zealand) zone of oblique continent-continent convergence. *Journal of Geophysical Research*, *98*(B9), 16105. https://doi.org/10.1029/93JB01091

Kim, D. C., Lee, G. H., Seo, Y. K., Kim, G. Y., Kim, S. Y., Kim, J. C., … Wilkens, R. (2004). Distribution and acoustic characteristics of shallow gas in the Korea Strait shelf mud off SE Korea. *Marine Georesources and Geotechnology*, *22*(1–2), 21–31. https://doi.org/10.1080/10641190490466928

Landis, C. A., Campbell, H. J., Begg, J. G., Mildenhall, D. C., Paterson, A. M., & Trewick, S. A. (2008). The waipounamu erosion surface: Questioning the antiquity of the New Zealand land surface and terrestrial fauna and flora. *Geological Magazine*, *145*(2), 173–197. https://doi.org/10.1017/S0016756807004268

Libby, W. F. (1961). Radiocarbon dating. *Science*, *133*(3453), 621–629. https://doi.org/10.1126/science.133.3453.621

Liu, E., Shen, J., Yang, X., & Zhang, E. (2012). Spatial distribution and human contamination quantification of trace metals and phosphorus in the sediments of Chaohu Lake, a eutrophic shallow lake, China. *Environmental Monitoring and Assessment*, *184*(4), 2105–2118. https://doi.org/10.1007/s10661-011-2103-x

Liu, L., Chen, J., Ji, J., Chen, Y., & Balsam, W. (2006). Variation of Zr/Rb ratios in the Chinese loess deposits during the past 1.8 Myr and its implication for the change of East Asian monsoon intensity. *Geochemistry, Geophysics, Geosystems*, 1–9. https://doi.org/10.1029/2005GC001188

Löwemark, L., Chen, H. F., Yang, T. N., Kylander, M., Yu, E. F., Hsu, Y. W., … Jarvis, S. (2011). Normalizing XRF-scanner data: A cautionary note on the interpretation of high-resolution records from organic-rich lakes. *Journal of Asian Earth Sciences*, *40*(6), 1250–1256. https://doi.org/10.1016/j.jseaes.2010.06.002

Lutter, T. J. (2018). 3D Gravitational Inversion Modelling of the South Dunedin Sub Basin , Otago , New Zealand. *Unpublished MSc Thesis, University of Otago*.

MacKinnon, G., MacKenzie, A. B., Cook, G. T., Pulford, I. D., Duncan, H. J., & Scott, E. M. (2011). Spatial and temporal variations in Pb concentrations and isotopic composition in road dust, farmland soil and vegetation in proximity to roads since cessation of use of leaded petrol in the UK. *Science of the Total Environment*, *409*(23), 5010–5019. https://doi.org/10.1016/j.scitotenv.2011.08.010

Marshall, P. (1906). The Geology of Dunedin (New Zealand). *Quarterly Journal of the Geological Society*, *62*, 381–424. https://doi.org/10.1017/CBO9781107415324.004

Martin, U. (2000). Eruptions and deposition of volcaniclastic rocks in the Dunedin Volcanic Complex , Otago Peninsula , New Zealand. *Unpublished PhD Thesis, University of Otago*.

Mcdougall, I., & Coombs, D. S. (2012). Potassium-argon ages for the Dunedin volcano and outlying volcanics. *New Zealand Journal of Geology and Geophysics*, *8306*. https://doi.org/10.1080/00288306.1973.10431451

McKellar, I. C., Liggett, K. A., Mutch, A. R., Ryan, G., & Hyslop, K. J. (1990). Southwest Dunedin urban area. *New Zealand Geological Survey, Dept. of Scientific and Industrial Research.*

Meyers, P. A., & Teranes, J. L. (2001). Sediment Organic Matter. *Physical and Geochemical Methods, Vol. 2*(Tracking Environmental Change Using Lake Sediments), 239–269. https://doi.org/10.1007/0-306-47670-3_9

Minjie, W., Hongbo, Z., Xin, X. I. E., Daidu, F. A. N., Shouye, Y., Quanhong, Z., & Ke, W. (2011). A 600-year flood history in the Yangtze River drainage : Comparison between a subaqueous delta and historical records. *Chinese Science Bulletin*, *56*(2), 188–195. https://doi.org/10.1007/s11434-010-4212-2

Molamohyeddin, N., Ghafourian, H., & Sadatipour, S. M. (2017). Contamination assessment of mercury, lead, cadmium and arsenic in surface sediments of Chabahar Bay. *Marine Pollution Bulletin*, *124*(1), 521–525. https://doi.org/10.1016/j.marpolbul.2017.07.035

Morris, K. E. (2008). Sea Level Rise : An Assessment of Risk , South Dunedin , New Zealand. *Unpublished MSc Thesis, University of Otago*.

Mortimer, N. (2004). New Zealand's geological foundations. *Gondwana Research*, *7*(1), 261–272. https://doi.org/10.1016/S1342-937X(05)70324-5

Nelson, P. A., & Seminara, G. (2011). Modeling the evolution of bedrock channel shape with erosion from saltating bed load. *Geophysical Research Letters*, *38*(17), 1–5. https://doi.org/10.1029/2011GL048628

Nichols, G. (2009). *Sedimentology and Stratigraphy* (2nd ed). Wiley-Blackwell.

Otago Regional Council. (2006). *Otago Harbour Reserves Management Plan*. Dunedin. Retrieved from https://www.dunedin.govt.nz/council/policies,-plans-and-strategies/plans/otago-harbour-reserves-management-plan

Price, R. C., & Chappell, B. W. (1975). Fractional crystallisation and the petrology of Dunedin volcano. *Contributions to Mineralogy and Petrology*, *53*(3), 157–182. https://doi.org/10.1007/BF00372602

Rees, O. W. (2018). Seismic characterisation of Otago Harbour sediments tied to a carbon-dated core record. *Unpublished BSc(Hons) Thesis, University of Otago*.

Reichgelt, T., Kennedy, E. M., Jones, W. A., Jones, D. T., & Lee, D. E. (2016). Contrasting palaeoenvironments of the mid / late Miocene Dunedin Volcano , southern New Zealand : Climate or topography ? *Palaeogeography, Palaeoclimatology, Palaeoecology*, *441*, 696–703. https://doi.org/10.1016/j.palaeo.2015.10.029

Reilly, W. I. (1972). Gravitational expression of the dunedin volcano. *New Zealand Journal of Geology and Geophysics*, *15*(1), 16–21. https://doi.org/10.1080/00288306.1972.10423943

Rothwell, R. G., & Croudace, I. W. (2015). Micro-XRF Core Scanning in Palaeolimnology: Recent Developments. In *Micro-XRF Studies of Sediment Cores: Applications of a non-destructive tool for the environmental sciences* (Vol. 17, pp. 25–35). https://doi.org/10.1007/978-94-017-9849-5

Sangster, C. (2019). Dunedin rock and roll : 3D shear wave velocity modelling for seismic hazard analysis . *Unpublished MSc Thesis, University of Otago*.

Scott, J. M., Pontesilli, A., Brenna, M., White, J. D. L., Giacalone, E., Palin, J. M., & le Roux, P. J. (2020). The Dunedin Volcanic Group and a revised model for Zealandia's alkaline intraplate volcanism. *New Zealand Journal of Geology and Geophysics*, *0*(0), 1–20. https://doi.org/10.1080/00288306.2019.1707695

Shears, A. (2009). Characterisation of the sediment budget of Otago Harbour: a geophysical and sedimentological study. *Unpublished MSc Thesis, University of Otago*.

Shepherd, R. G., & Schumm, S. A. (1976). Experimental study of river incision. *Bulletin of the Geological Society of America*, *87*(2), 320.

Sheriff, R. E. (1994). Encyclopedic Ditionary of Exploration Geophysics (Third). *Society of Exploration Geophysicists.*

Sidler, R., & Holliger, K. (2010). Seismic reflectivity of the sediment-covered seafloor: Effects of velocity gradients and fine-scale layering. *Geophysical Journal International*, *181*(1), 521–531.

Smith, A. M., Wood, A. C. L., Liddy, M. F. A., Shears, A. E., & Fraser, C. I. (2010). Human impacts in an urban port: The carbonate budget, Otago Harbour, New Zealand. *Estuarine, Coastal and Shelf Science*, *90*(2), 73–79.

Spratt, R. M., & Lisiecki, L. E. (2016). A Late Pleistocene sea level stack. *Climate of the Past*, 1079–1092.

Strogen, D. P., Bland, K. J., Nicol, A., & King, P. R. (2014). Paleogeography of the Taranaki Basin region during the latest Eocene-Early Miocene and implications for the total drowning of Zealandia. *New Zealand Journal of Geology and Geophysics*, *57*(2), 110–127.

Turnbull, I. M., Mortimer, N., Craw, D., & Mortimer, N. (2010). Textural zones in the Haast Schist — a reappraisal. *New Zealand Journal of Geology and Geophysics*, 171–183.

Wakabayashi, J. (2013). Paleochannels , stream incision , erosion , topographic evolution , and alternative explanations of paleoaltimetry , Sierra Nevada , California, (2), 191–215.

Warrick, R. ., & Wigley, E. . (1993). Climate and sea level change: observations, projections and implications, *5*(3), 424.

Waters, J. M., & Craw, D. (2006). Goodbye Gondwana? New Zealand Biogeography, Geology, and the Problem of Circularity. *Systematic Biology*, *55*(2), 351–356.

Woodruff, J. D., Irish, J. L., & Camargo, S. J. (2013). Coastal flooding by tropical cyclones and sea-level rise. *Nature*, 44–45. https://doi.org/10.1038/nature12855

Yilmaz, O. (2001). SEISMIC DATA ANALYSIS, Processing, Inversion, and Interpretation of Seismc Data. *Society of Exploration Geophysicists*.

Zorina, S. O. (2013). The sediment accommodation space and sedimentary successions in platformal basins: mechanisms of formation. *Geology*, 672–675.